KI in der diagnostischen CT-Bildgebung

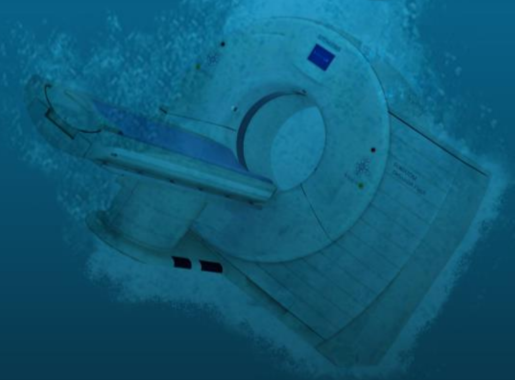

Marc Kachelrieß

German Cancer Research Center (DKFZ)

Heidelberg, Germany

www.dkfz.de/ct

DEUTSCHES KREBSFORSCHUNGSZENTRUM IN DER HELMHOLTZ-GEMEINSCHAFT

Fully Connected Neural Network

- Each layer fully connects to previous layer
- Difficult to train (many parameters in *W* and *b*)
- Spatial relations not necessarily preserved

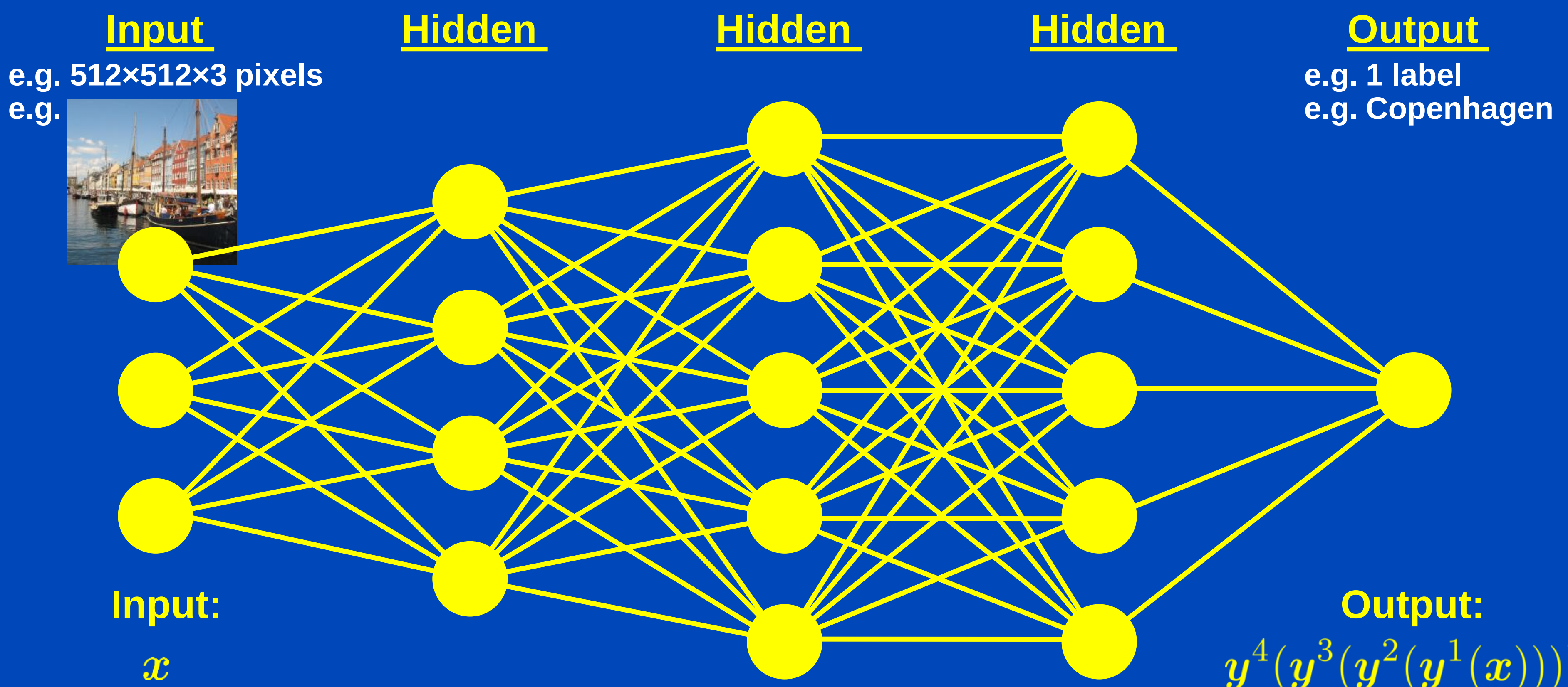

$$\boldsymbol{y}(\boldsymbol{x}) = \boldsymbol{f}(\boldsymbol{W}\cdot\boldsymbol{x}+\boldsymbol{b}) \text{ with } \boldsymbol{f}(\boldsymbol{x}) = \big(f(x_1), f(x_2), \ldots\big) \text{ point-wise scalar, e.g. } f(x) = x \vee 0 = \mathrm{ReLU}$$

Convolutional Neural Network (CNN)

- Replace dense *W* in $y(x) = f(W \cdot x + b)$ by a sparse matrix *W* with sparsity being of convolutional type.
- CNNs consist (mainly) of convolutional layers.
- Convolutional layers are not fully connected.
- Convolutional layers are connected by small, say 3×3, convolution kernels whose entries need to be found by training.
- CNNs preserve spatial relations to some extent.

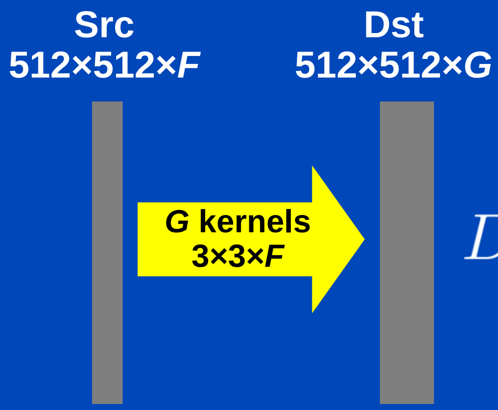

$$D_{i,j,g} = \sum_f S_{i,j,f} * K^g_{i,j,f} = \sum_{a,b,f} S_{i-a,j-b,f} K^g_{a,b,f}$$

Attention: No convolution in depth direction!

Here, a 2D example is shown. Conv layers also exist in 3D and higher dimensions.

U-Net[1]

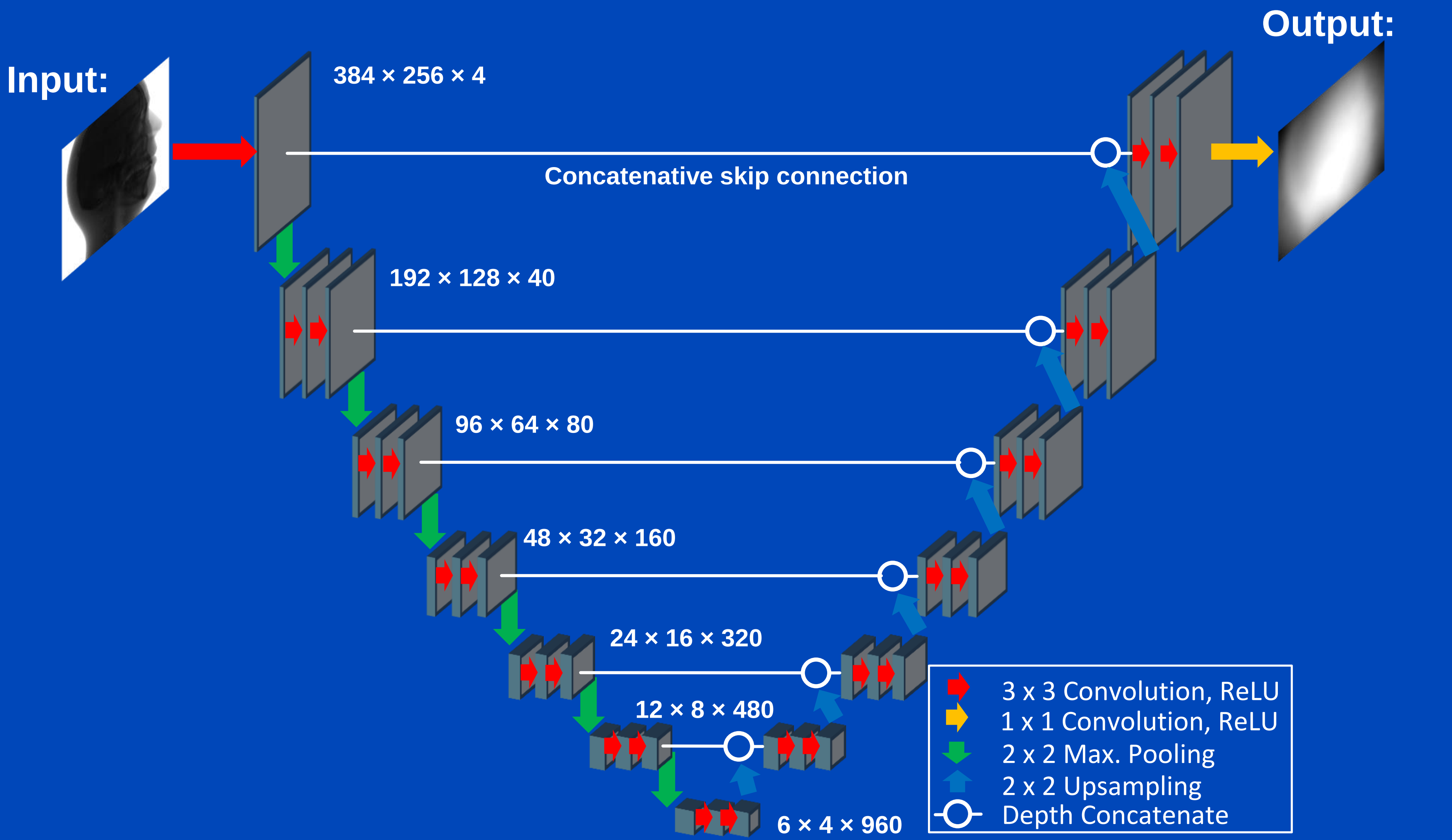

[1] O. Ronneberger, P. Fischer, and T. Brox. U-net: Convolutional networks for biomedical image segmentation. Proc. MICCAI:234-241, 2015.

dkfz.

Generative Adversarial Network[1] (GAN)

- Useful, if no direct ground truth (GT) is available, the training data are unpaired, unsupervised learning

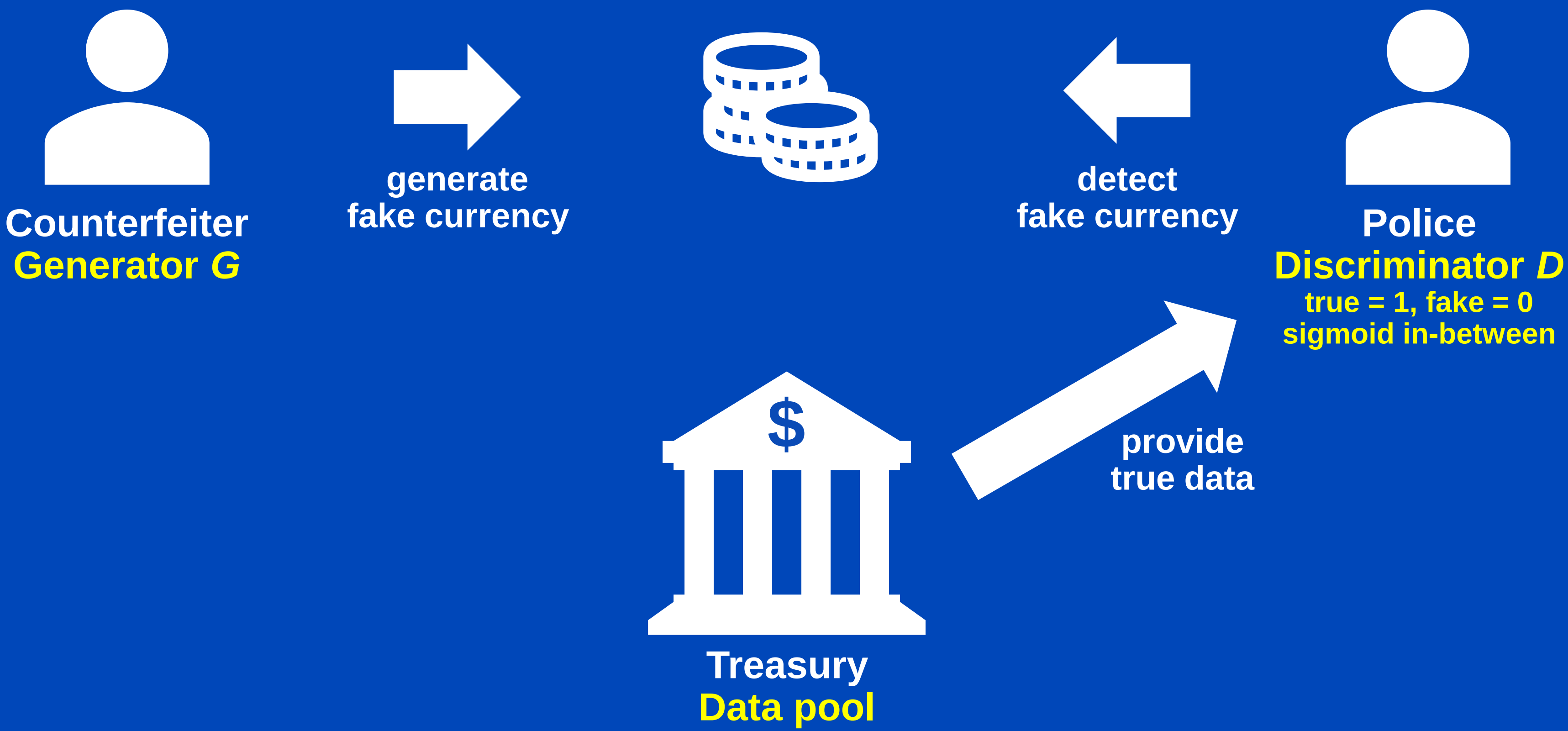

[1] I. Goodfellow et al. Generative Adversarial Nets, arXiv 2014

Generative Adversarial Network (GAN)

- **Typical loss function and minimax game:**

$$\min_G \max_D L(D,G) := \mathrm{E}_x \ln\big(1 - D(G(x))\big) + \mathrm{E}_y \ln D(y)$$

- **Conditional GAN[1]**
  - **Conditional GANs sample the generator input *x* not from a uniform distribution but from a conditional distribution, e.g. noisy CT images.**
  - **Need some measure to ensure similarity to input distribution (e.g. pixelwise loss added to the minimax loss function)**
- **Cycle GAN[2]**
  - **Two GANs ($X \rightarrow Y$ and $Y \rightarrow X$)**
  - **Demand cyclic consistency, i.e. $x = G_X(G_Y(x))$ and $y = G_Y(G_X(x))$**

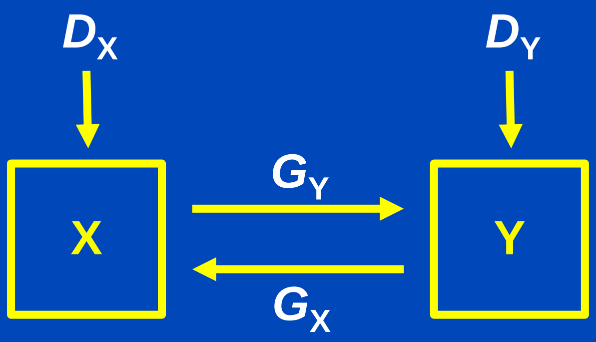

[1]Isola et al. 2017
[2]Zhu et al., 2017

Resolution Improvement Example

- 2D U-net to converts 5 mm thick images into 1 mm ones.
- E.g. to "replace a scanning protocol for a 1 mm slice with a 5 mm protocol"

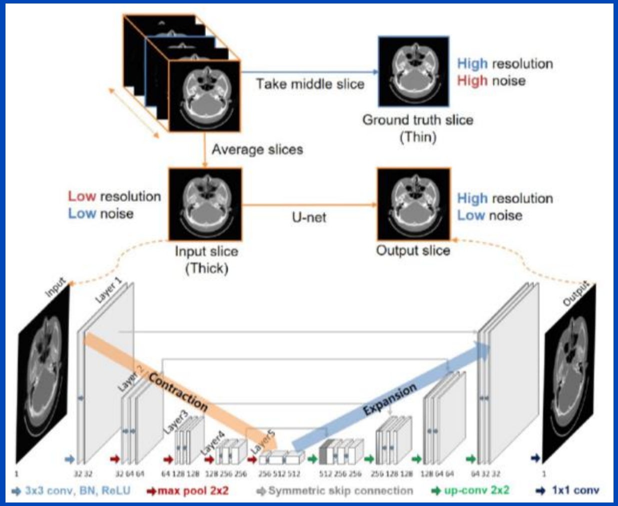

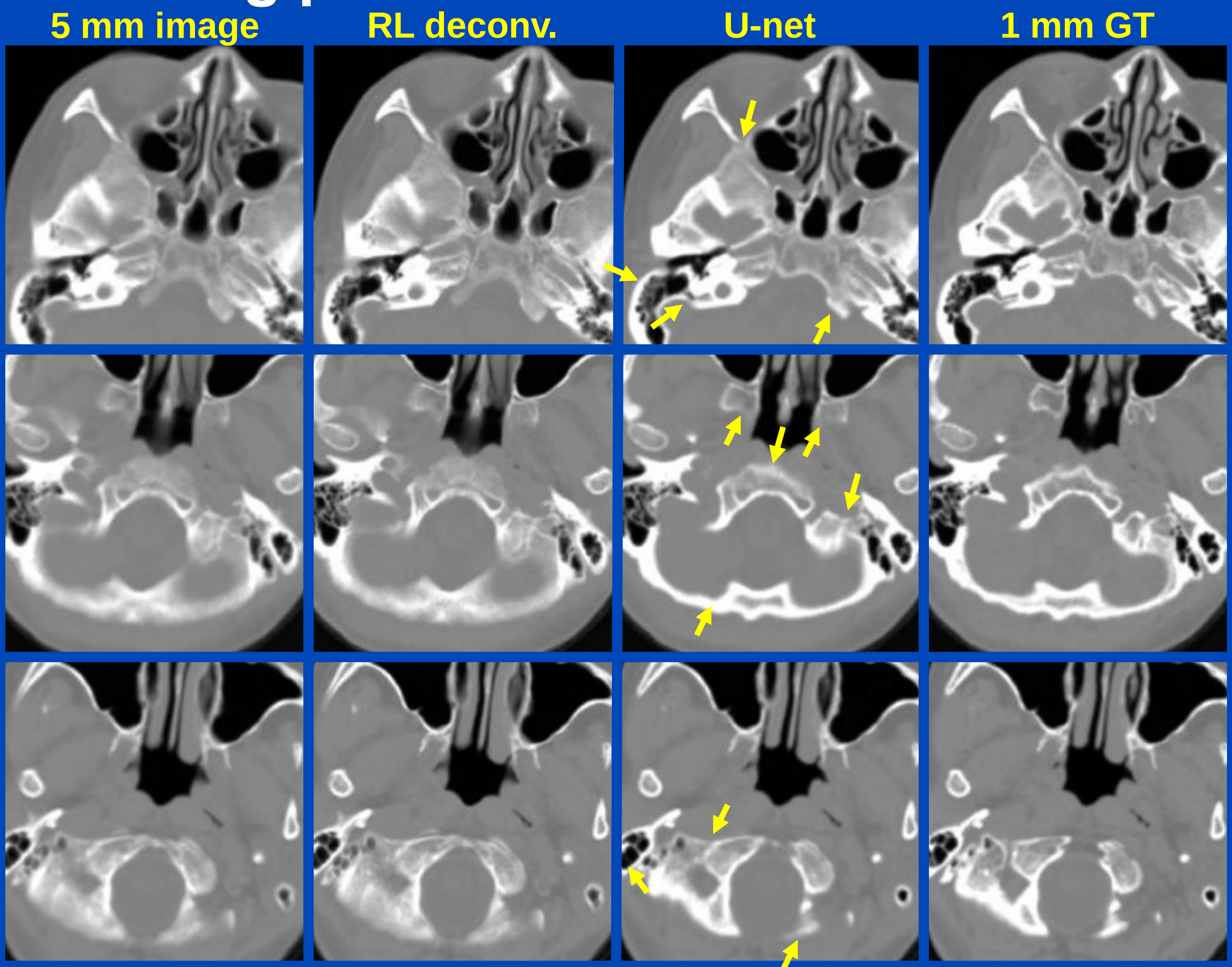

Junyoung Park, Donghwi Hwang, Kyeong Yun Kim, Seung Kwan Kang, Yu Kyeong Kim and Jae Sung Lee. Computed tomography super-resolution using deep convolutional neural network. Phys. Med. Biol. 63: 145011, 2018

Canon PIQE

- Precise IQ Engine (PIQE).
- Trained on data from Canon's Precision high spatial resolution CT
- Converts images from Canon's standard spatial resolution scanners (e.g. Aquilion ONE / PRISM edition) to look like high spatial resolution images.

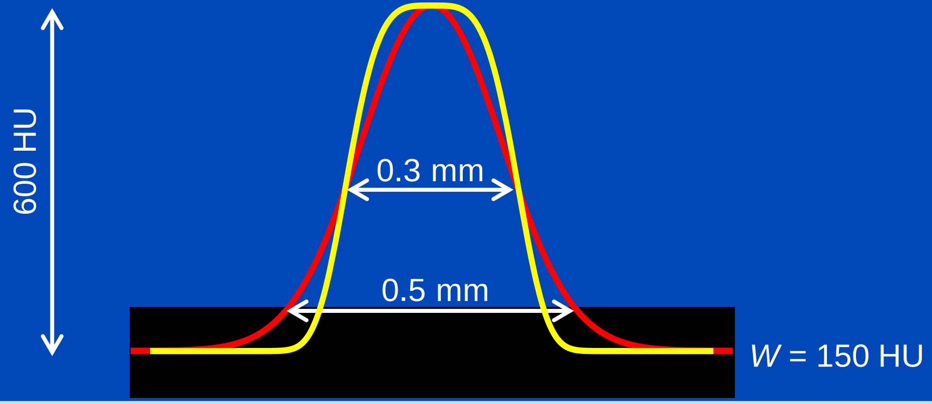

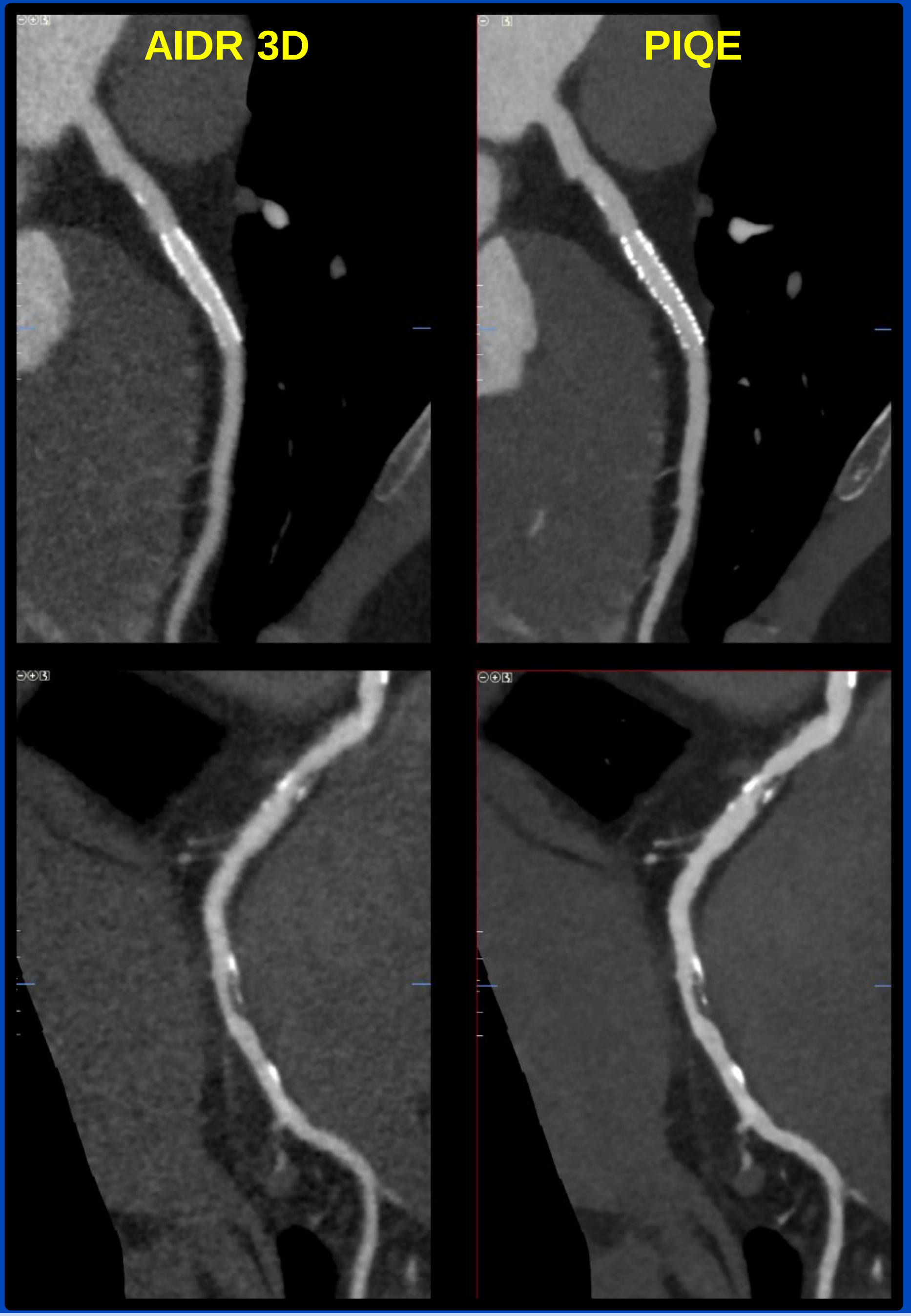

Sparse View Restoration Example

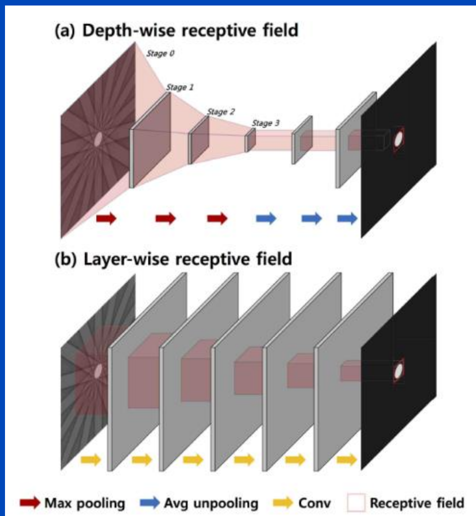

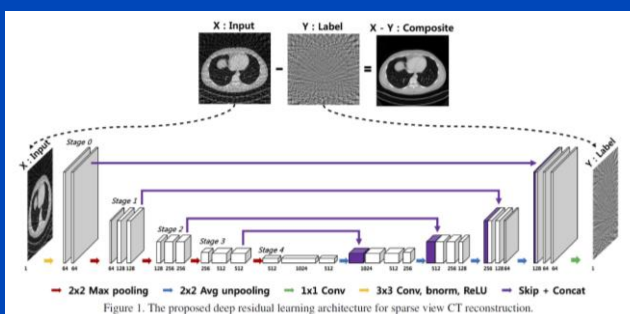

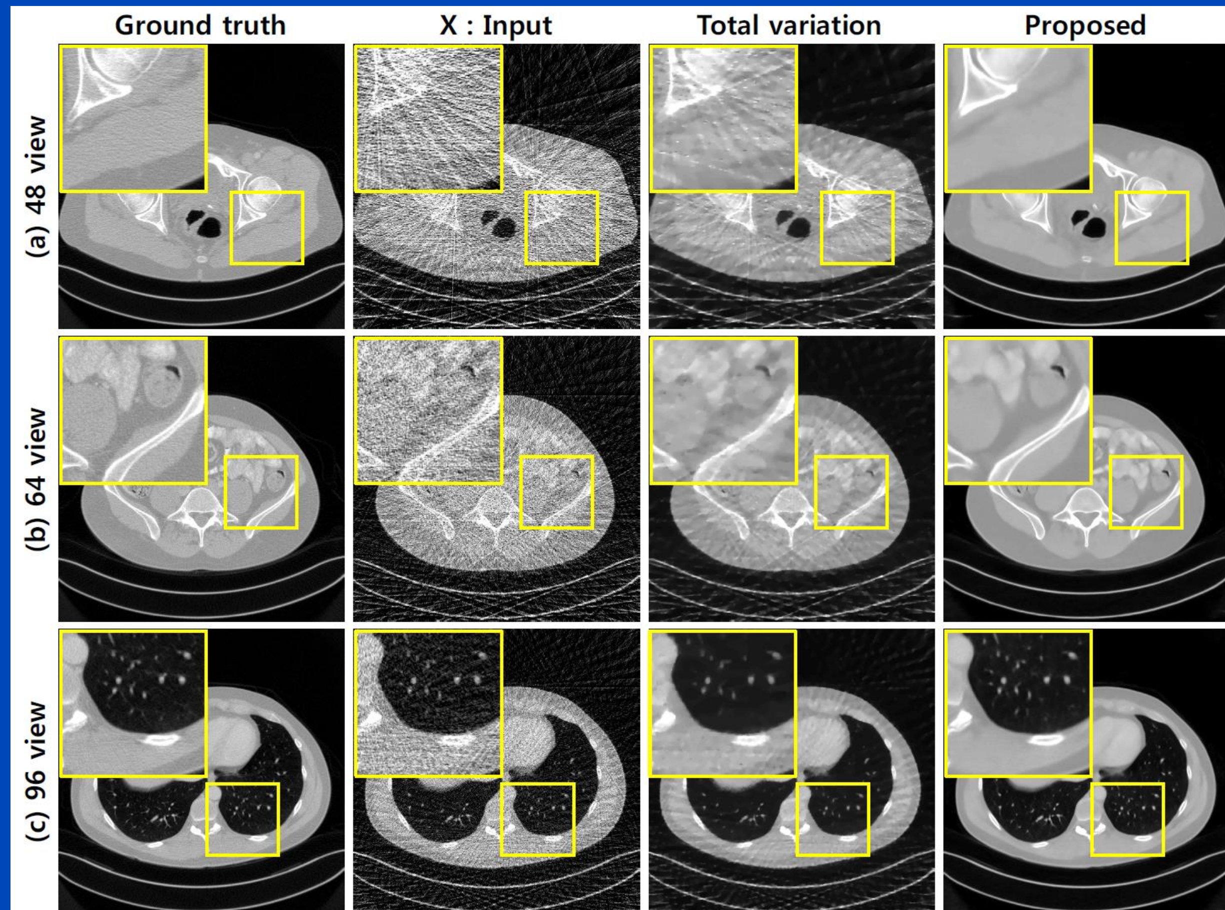

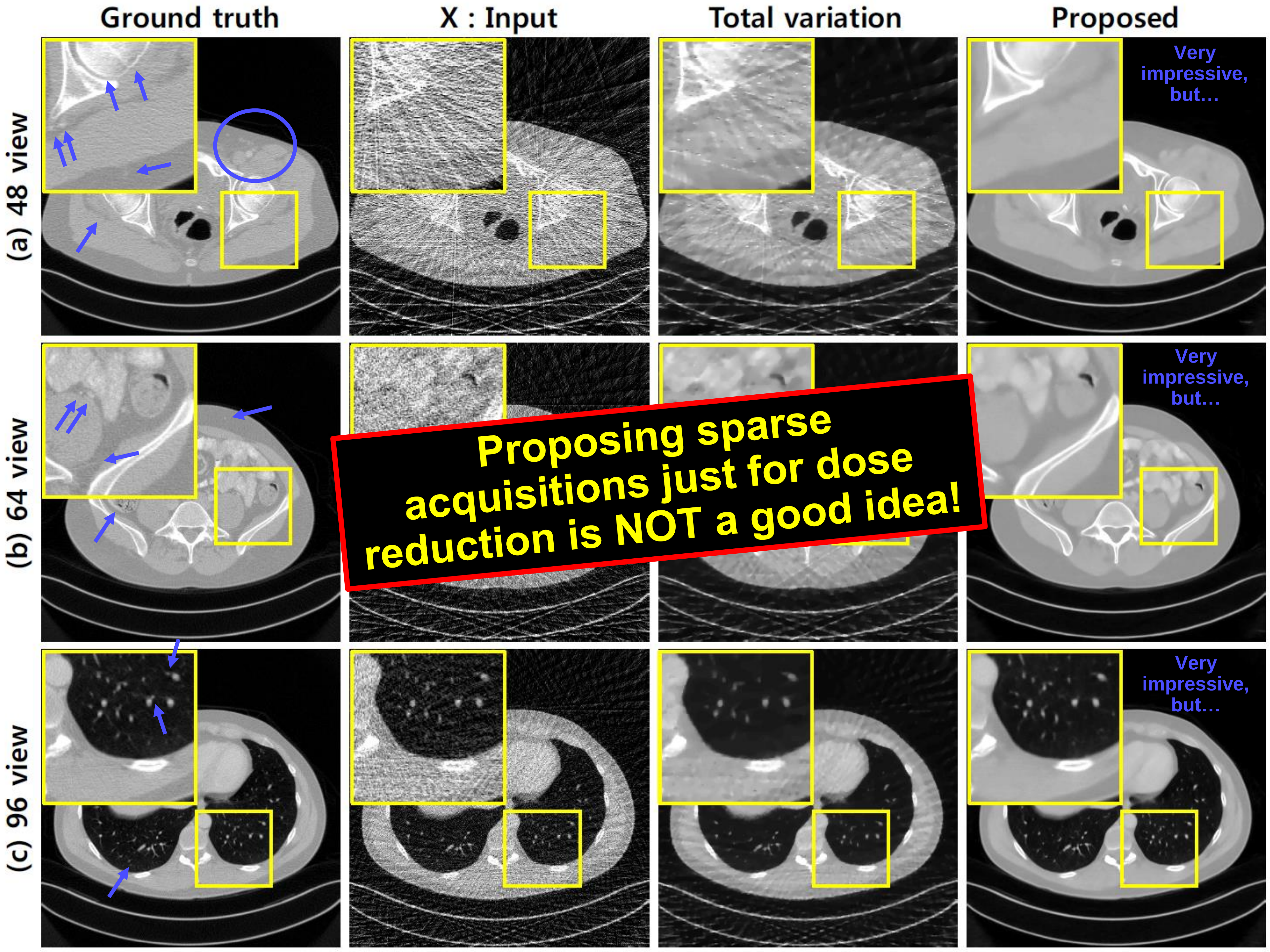

Ground truth
X : Input
Total variation
Proposed
(a) 48 view
(b) 64 view
(c) 96 view
Very impressive, but…
Very impressive, but…
Very impressive, but…
Proposing sparse acquisitions just for dose reduction is NOT a good idea!

Noise Reduction

Noise Removal Example 2

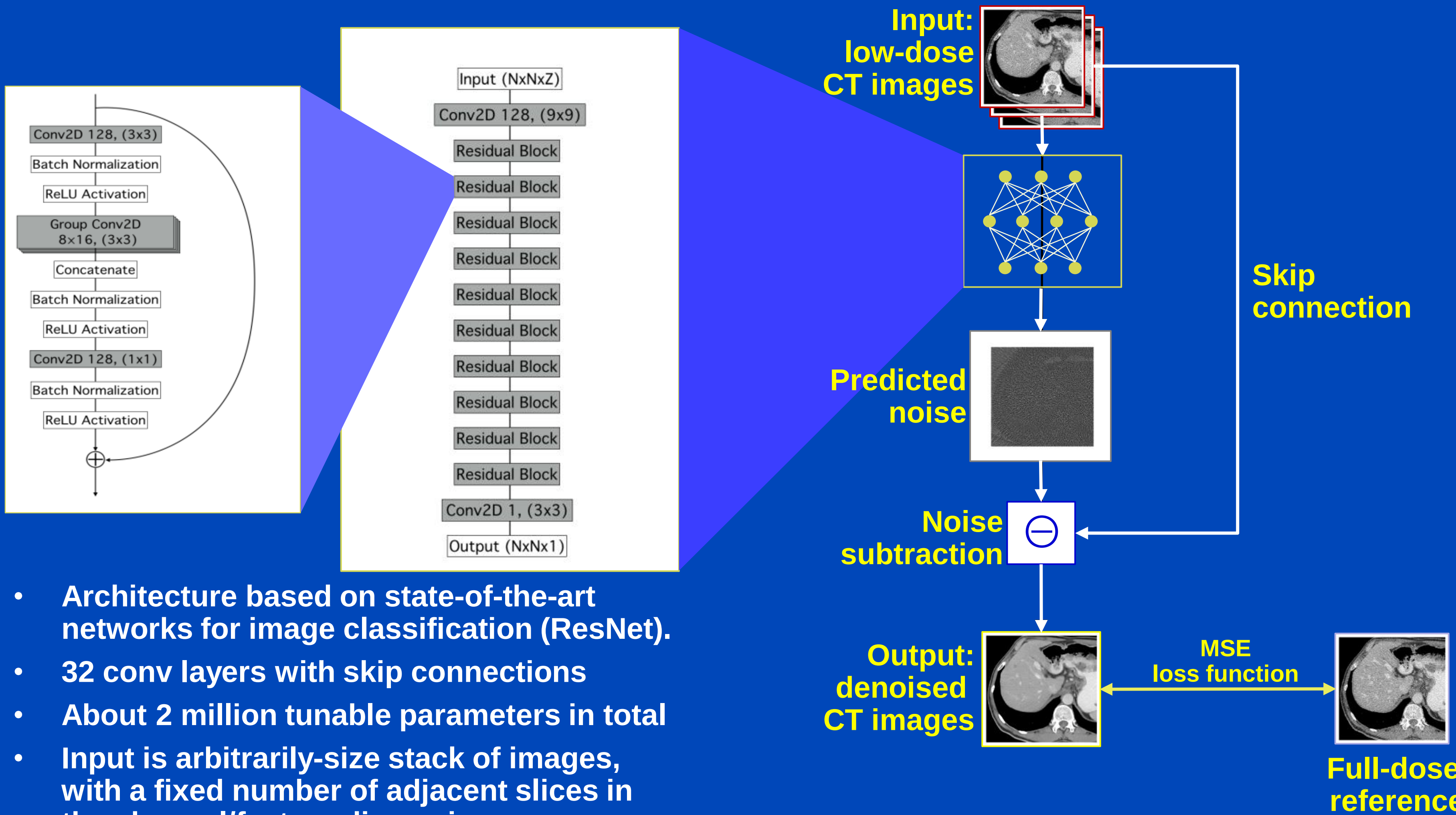

- Architecture based on state-of-the-art networks for image classification (ResNet).
- 32 conv layers with skip connections
- About 2 million tunable parameters in total
- Input is arbitrarily-size stack of images, with a fixed number of adjacent slices in the channel/feature dimension.

Andrew D. Missert, Shuai Leng, Lifeng Yu, and Cynthia H. McCollough. Noise Subtraction for Low-Dose CT Images Using a Deep Convolutional Neural Network. Proceedings of the 5th CT-Meeting: 399-402, 2018.

dkfz.

Noise Removal Example 2

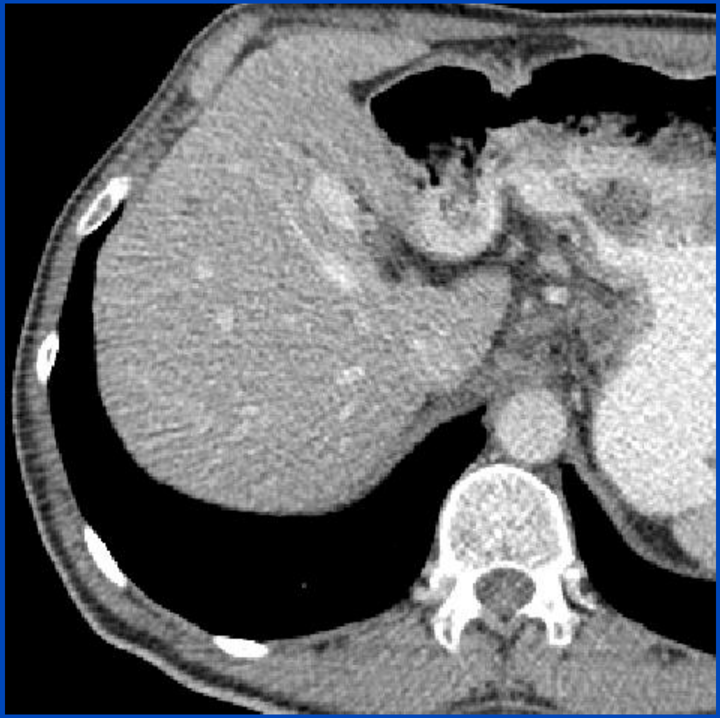

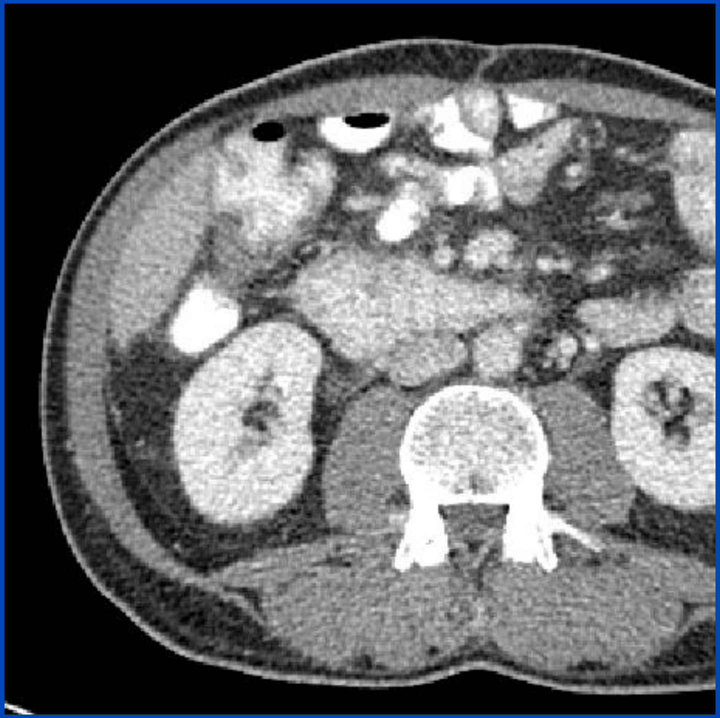

Low dose images (1/4 of full dose)

Andrew D. Missert, Shuai Leng, Lifeng Yu, and Cynthia H. McCollough. Noise Subtraction for Low-Dose CT Images Using a Deep Convolutional Neural Network. Proceedings of the 5th CT-Meeting: 399-402, 2018.

Noise Removal Example 2

Denoised low dose

Noise Removal Example 2

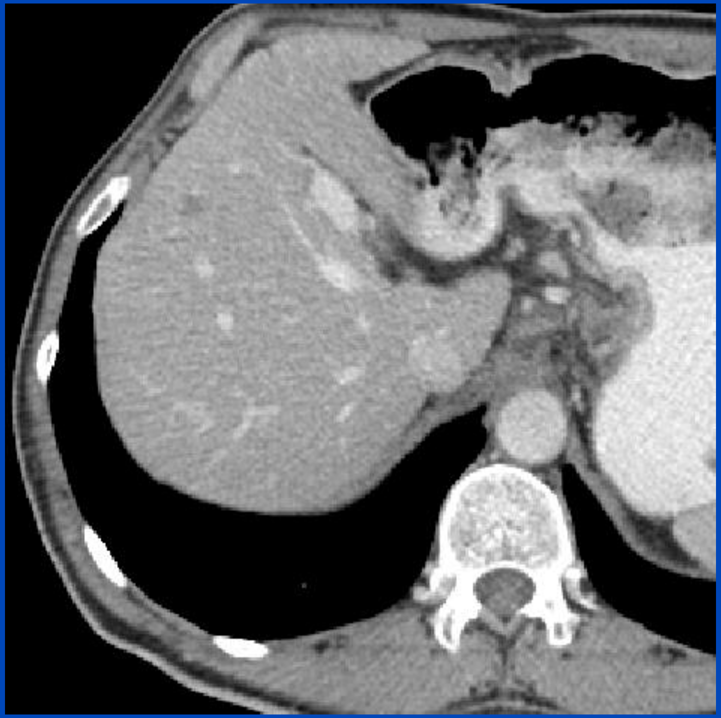

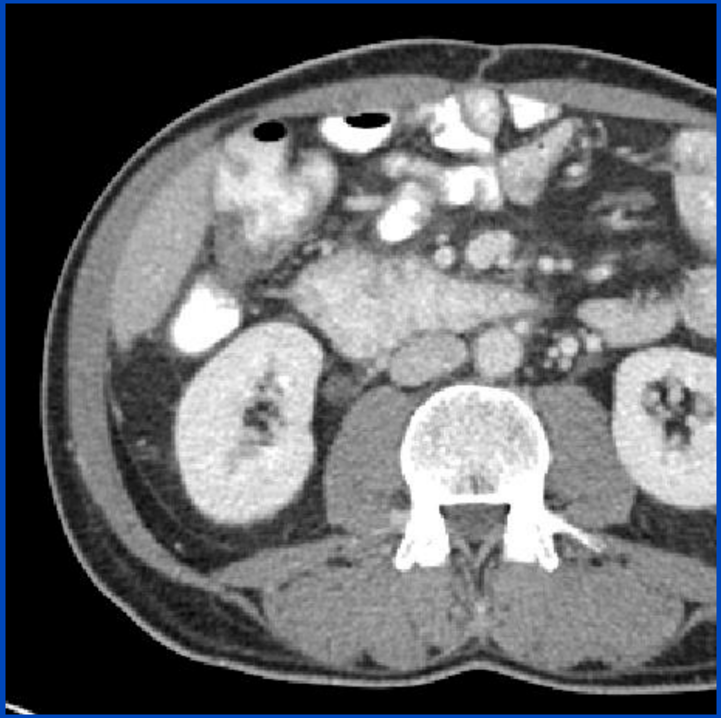

Full dose

Andrew D. Missert, Shuai Leng, Lifeng Yu, and Cynthia H. McCollough. Noise Subtraction for Low-Dose CT Images Using a Deep Convolutional Neural Network. Proceedings of the 5th CT-Meeting: 399-402, 2018.

Noise Removal Example 2

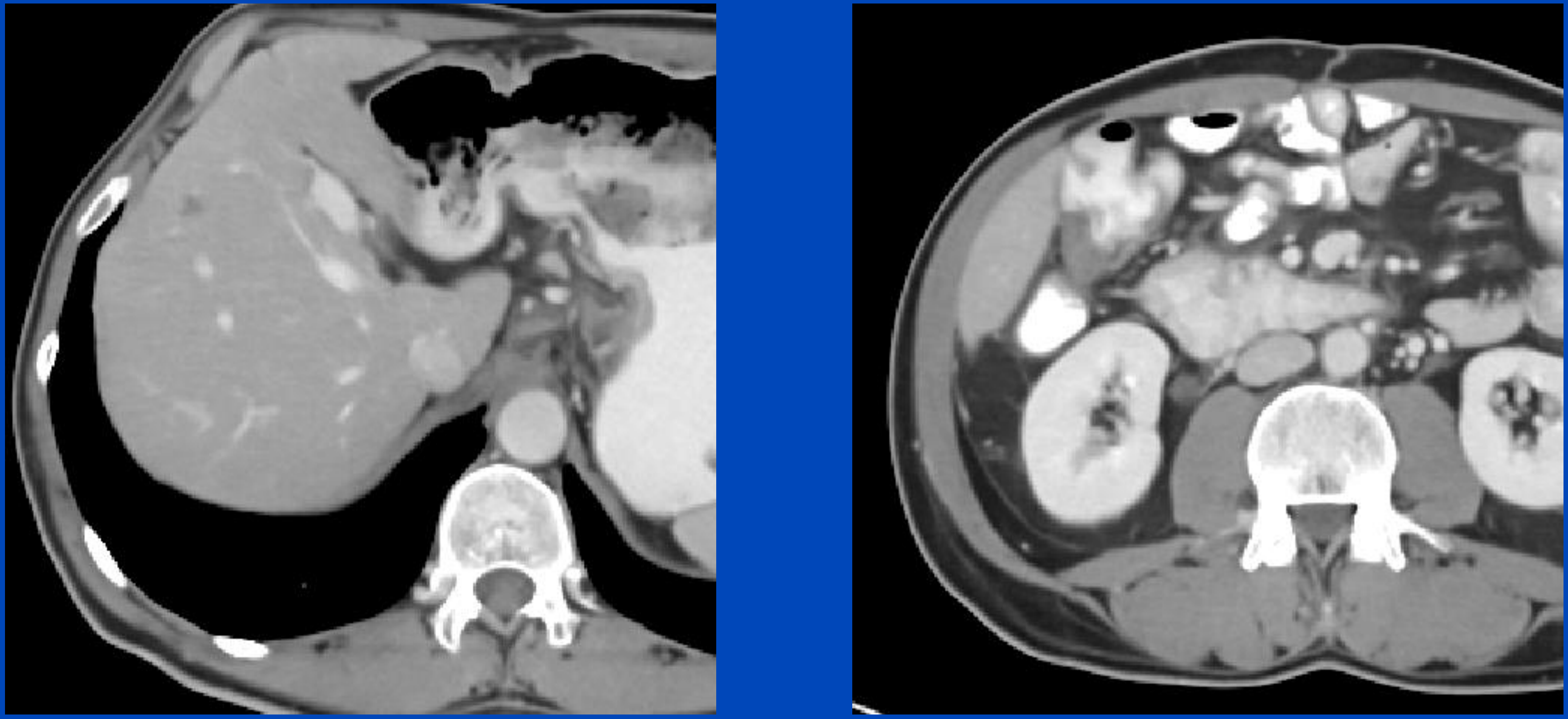

Denoised full dose

Noise Removal Example 3

- Task: Reduce noise from low dose CT images.
- A conditional generative adversarial networks (GAN) is used
- Generator *G*:
  - 3D CNN that operates on small cardiac CT sub volumes
  - Seven 3×3×3 convolutional layers yielding a receptive field of 15×15×15 voxels for each destination voxel
  - Depths (features) from 32 to 128
  - Batch norm only in the hidden layers
  - Subtracting skip connection
- Discriminator *D*:
  - Sees either routine dose image or a generator-denoised low dose image
  - Two 3×3×3 layers followed by several 3×3 layers with varying strides
  - Feedback from *D* prevents smoothing.
- Training:
  - Unenhanced (why?) patient data acquired with Philips Briliance iCT 256 at 120 kV.
  - Two scans (why?) per patient, one with 0.2 mSv and one with 0.9 mSv effective dose.

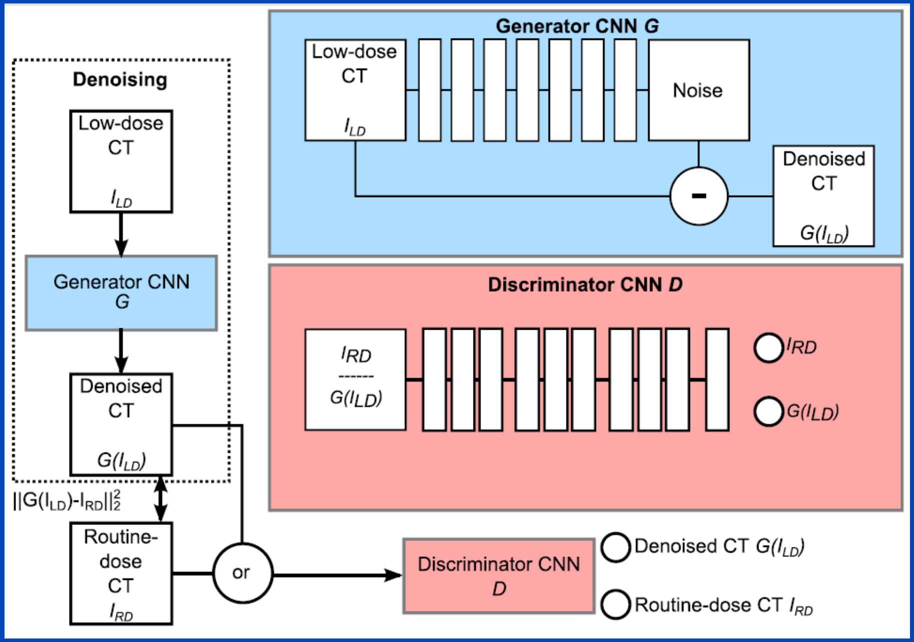

J. Wolterink, T. Leiner, M. Viergever, and I. Išgum. Generative Adversarial Networks for Noise Reduction in Low-Dose CT. IEEE TMI 36(12):2536-2544, Dec. 2017.

Noise Removal Example 3

- ***G***$_1$ **and** ***G***$_2$ **include supervised learning and thus perform only with phantom measurements.**
- ***G***$_3$ **is unsupervised.**
- ***G***$_3$ **is said to generate images with a more similar appearance to the routine-dose CT. Feedback from the discriminator** ***D*** **prevents smoothing the image.**

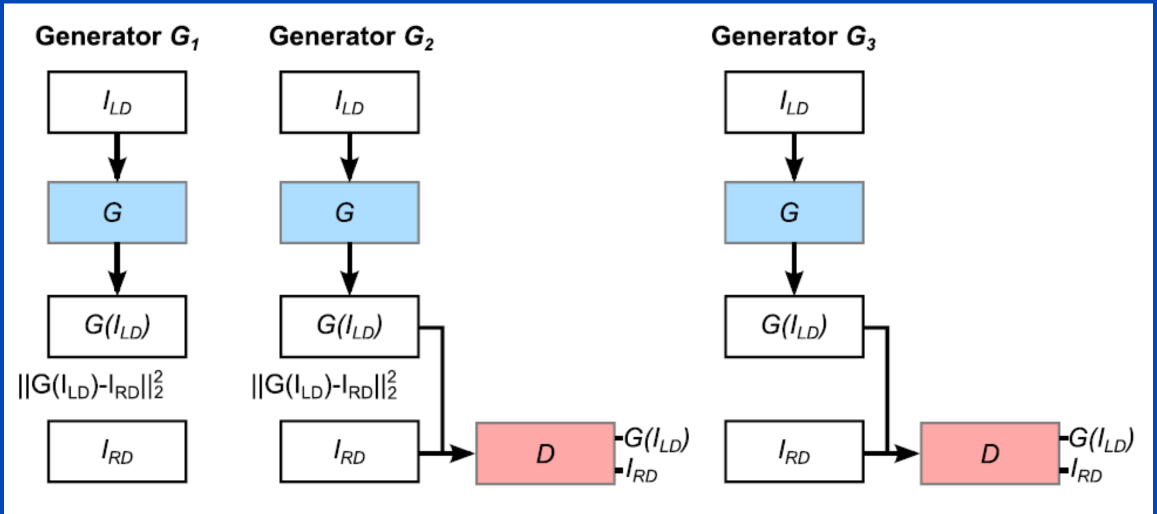

J. Wolterink, T. Leiner, M. Viergever, and I. Išgum. Generative Adversarial Networks for Noise Reduction in Low-Dose CT. IEEE TMI 36(12):2536-2544, Dec. 2017.

dkfz.

Noise Removal Example 3

Low dose image (0.2 mSv)

J. Wolterink, T. Leiner, M. Viergever, and I. Išgum. Generative Adversarial Networks for Noise Reduction in Low-Dose CT. IEEE TMI 36(12):2536-2544, Dec. 2017.

Noise Removal Example 3

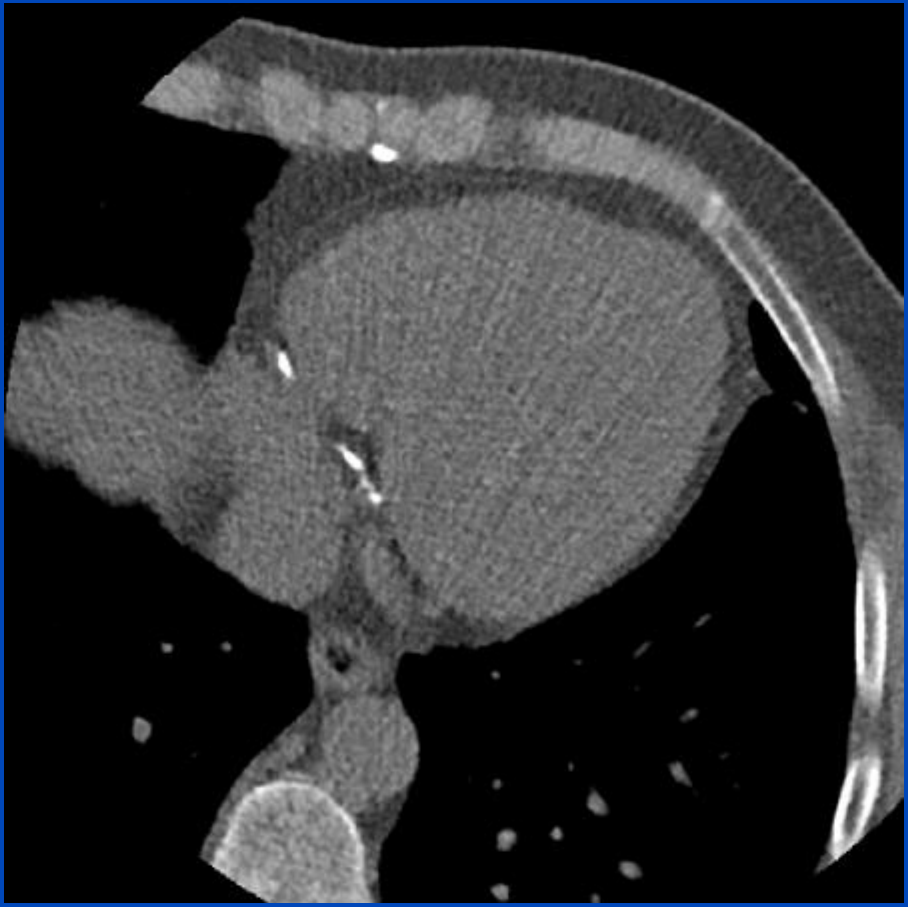

iDose level 3 reconstruction (0.2 mSv)

J. Wolterink, T. Leiner, M. Viergever, and I. Išgum. Generative Adversarial Networks for Noise Reduction in Low-Dose CT. IEEE TMI 36(12):2536-2544, Dec. 2017.

Noise Removal Example 3

Denoised low dose image (0.2 mSv)

J. Wolterink, T. Leiner, M. Viergever, and I. Išgum. Generative Adversarial Networks for Noise Reduction in Low-Dose CT. IEEE TMI 36(12):2536-2544, Dec. 2017.

Noise Removal Example 3

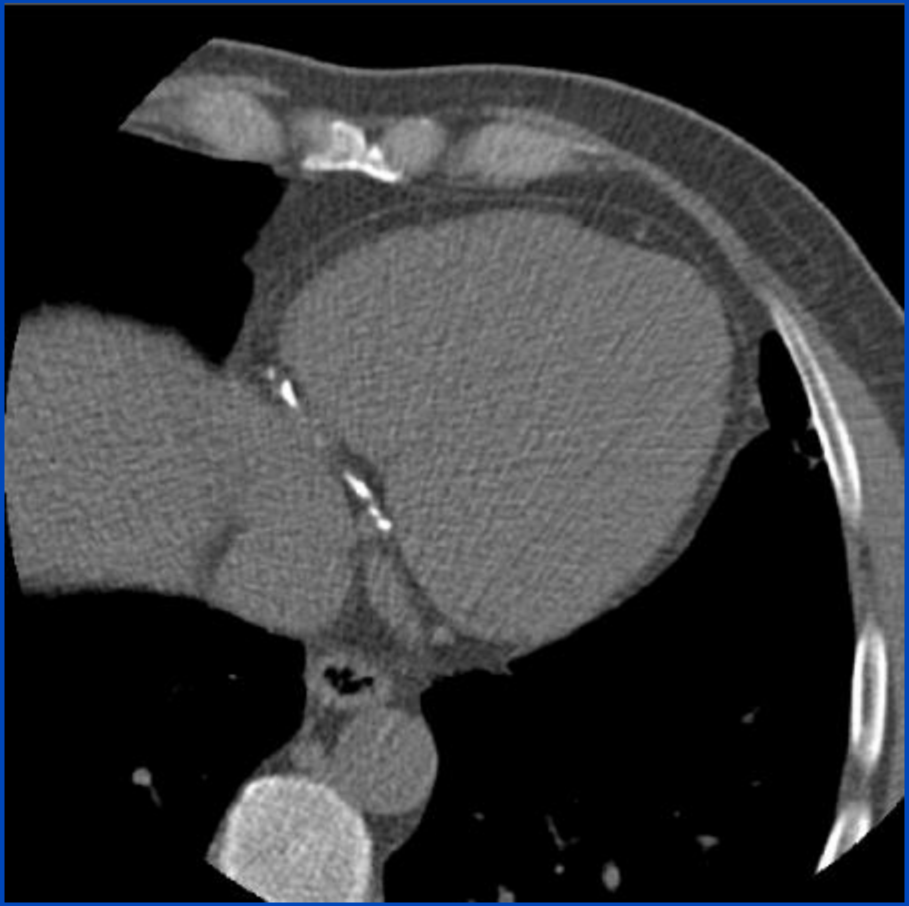

Normal dose image (0.9 mSv)

J. Wolterink, T. Leiner, M. Viergever, and I. Išgum. Generative Adversarial Networks for Noise Reduction in Low-Dose CT. IEEE TMI 36(12):2536-2544, Dec. 2017.

Noise Removal Example 4

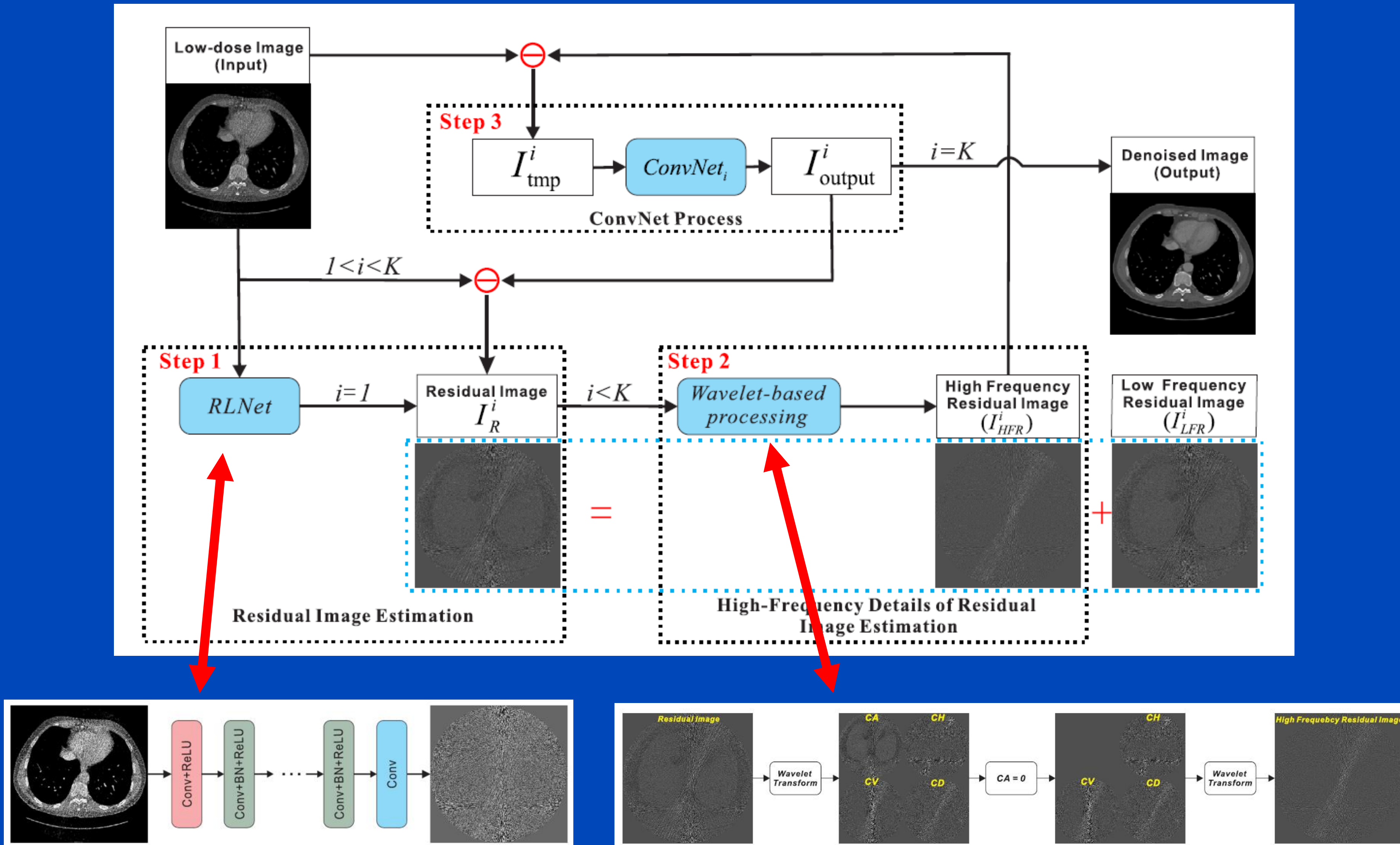

Y. Wang et al. Iterative quality enhancement via residual-artifact learning networks for low-dose CT.
Phys. Med. Biol. 63:215004, 2018.

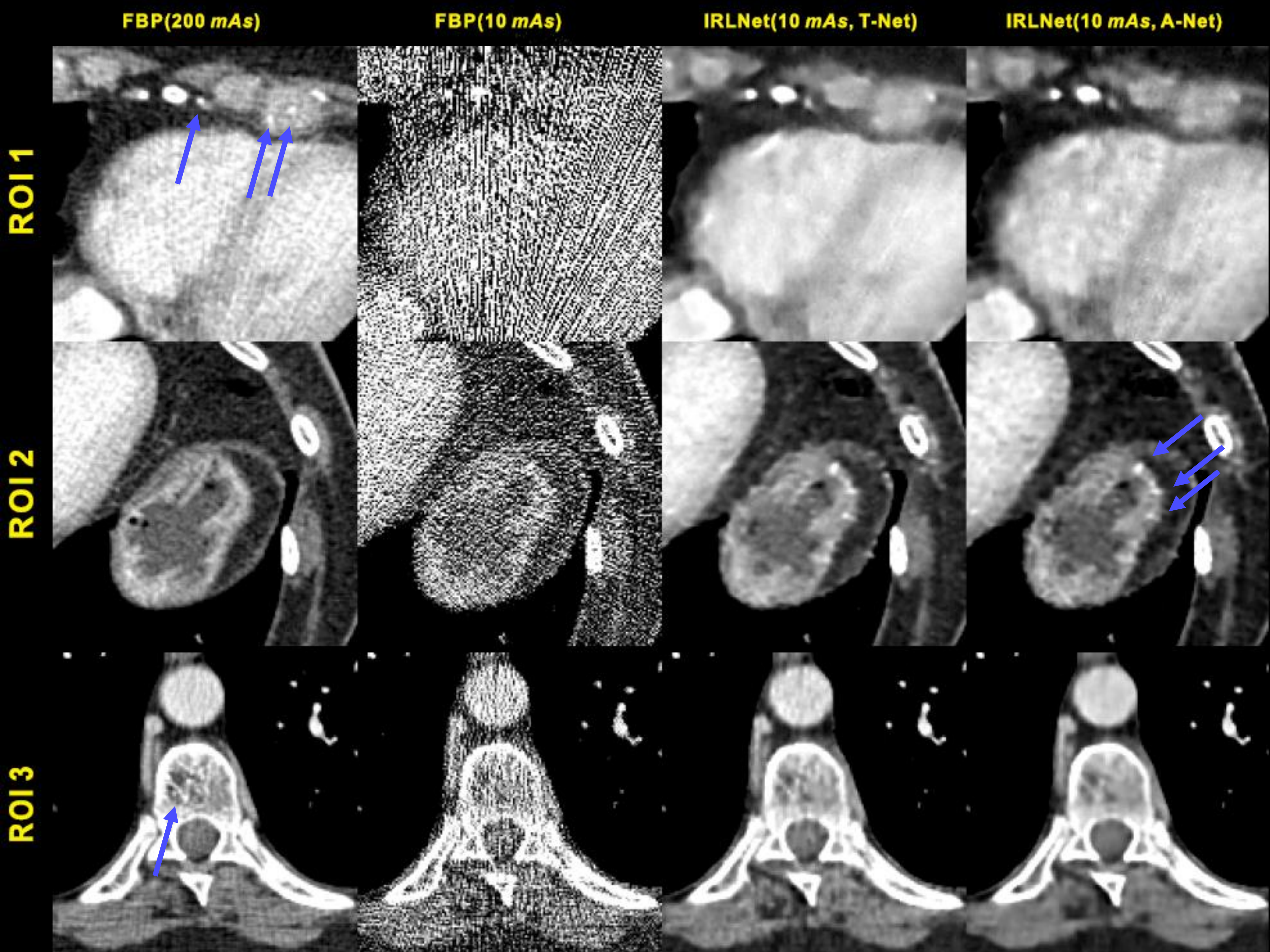

FBP(200 mAs)
FBP(10 mAs)
IRLNet(10 mAs, T-Net)
IRLNet(10 mAs, A-Net)
ROI 1
ROI 2
ROI 3

Noise Removal: Canon‘s AiCE

- Advanced intelligent Clear-IQ Engine (AiCE)
- Trained to restore low-dose CT data to match the properties of FIRST, the model-based IR of Canon.
- FIRST is applied to high-dose CT images to obtain a high fidelity training target

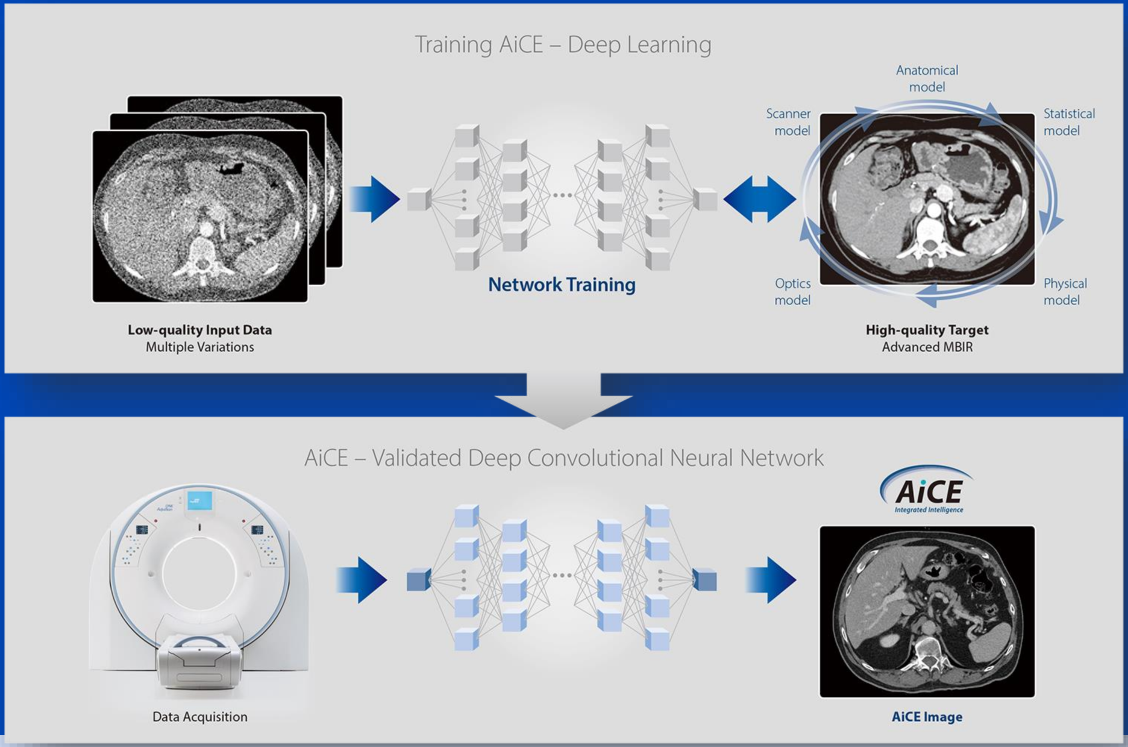

K. Boedeker. AiCE Deep Learning Reconstruction: Bringing the Power of Ultra High Resolution CT to Routine Imaging. Whitepaper, Canon, 2019.

dkfz.

U = 100 kV
CTDI = 0.6 mGy
DLP = 24.7 mGy·cm
D_{eff} = 0.35 mSv

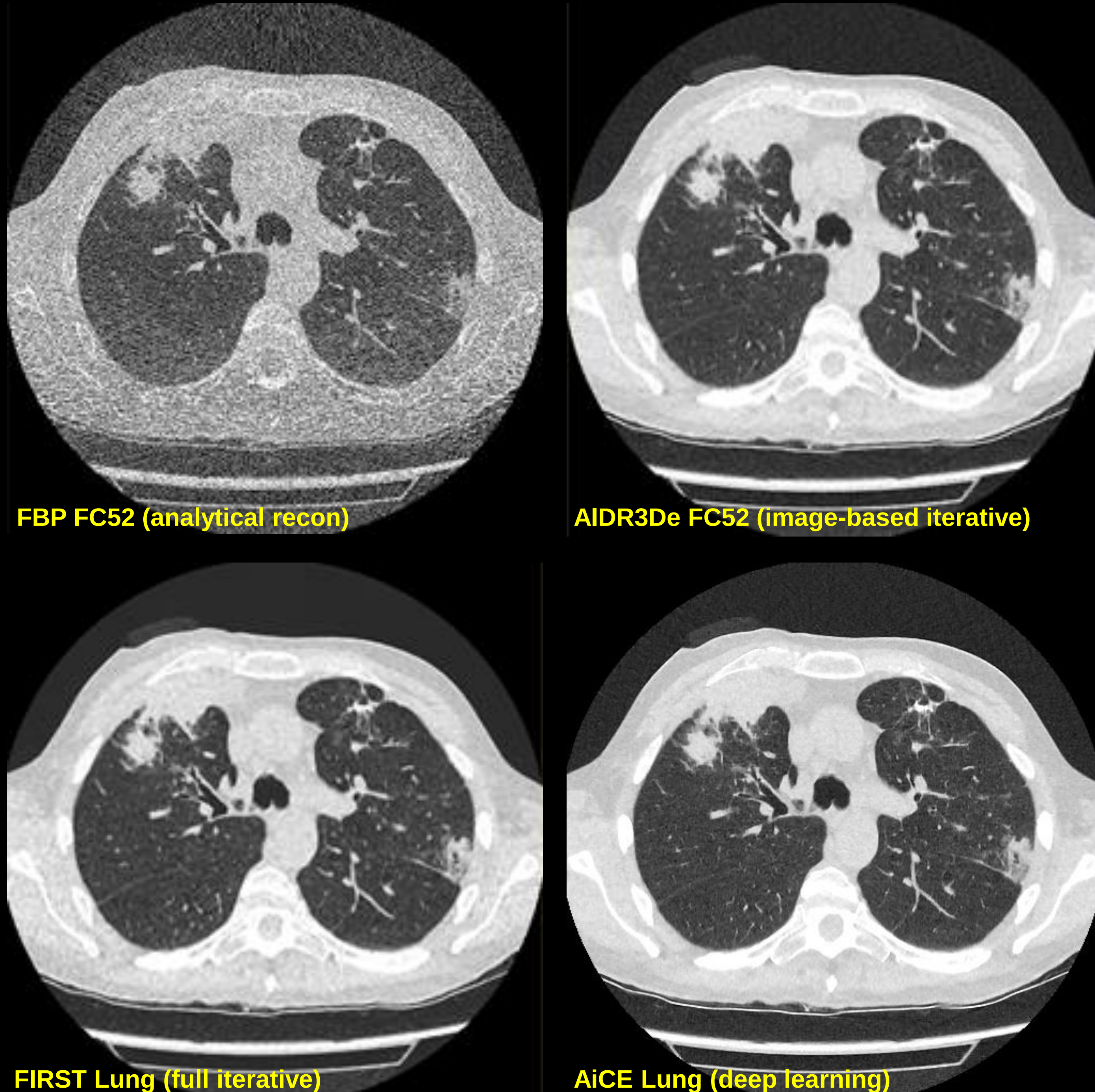

Courtesy of
Radboudumc,
the Netherlands

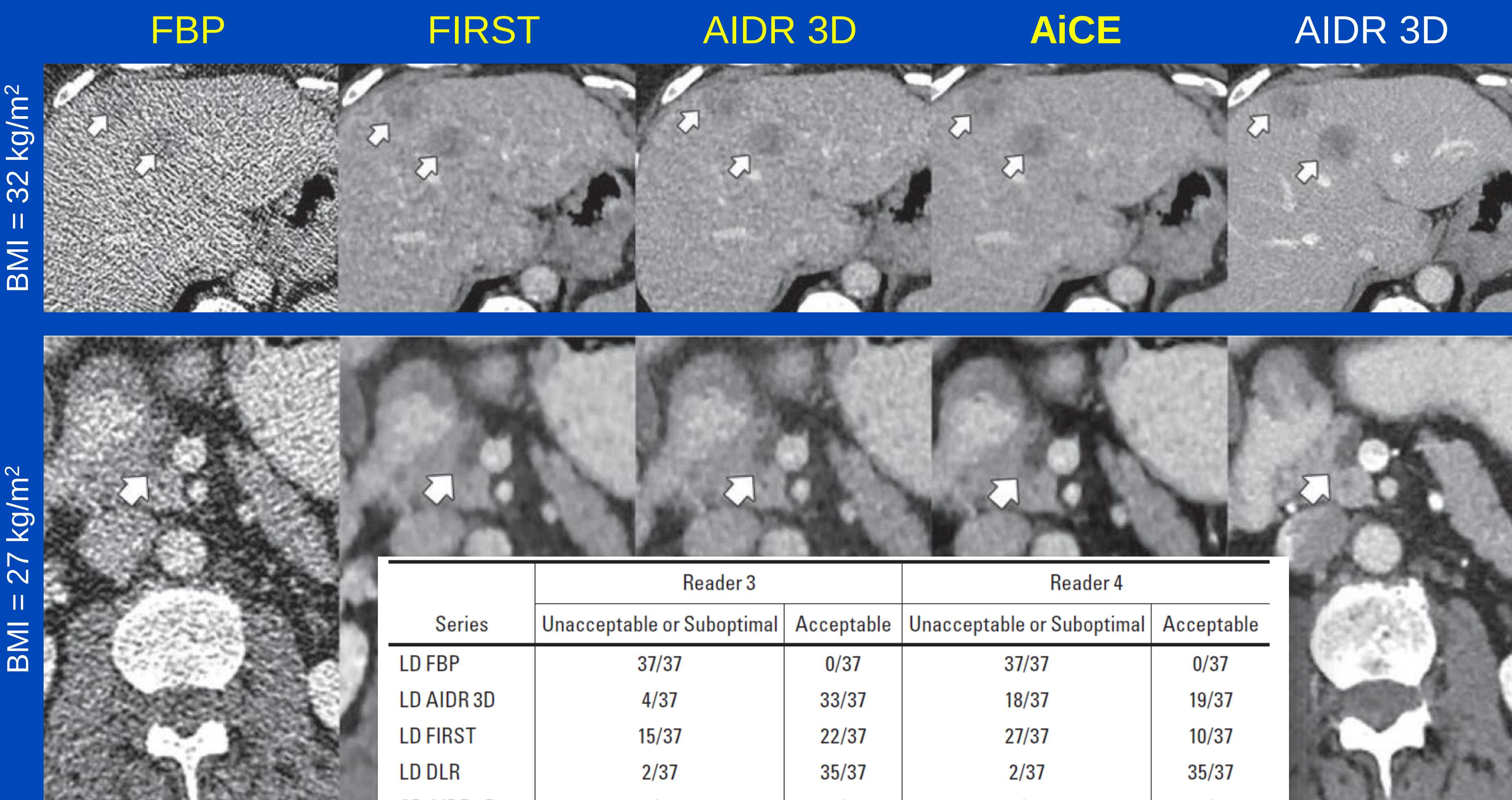

Series	Reader 3		Reader 4	
	Unacceptable or Suboptimal	Acceptable	Unacceptable or Suboptimal	Acceptable
LD FBP	37/37	0/37	37/37	0/37
LD AIDR 3D	4/37	33/37	18/37	19/37
LD FIRST	15/37	22/37	27/37	10/37
LD DLR	2/37	35/37	2/37	35/37
SD AIDR 3D	0/37	37/37	0/37	37/37

Low Dose CT
2 mGy CTDI (top)
3 mGy CTDI (bottom)

Standard Dose CT
19 mGy CTDI (top)
18 mGy CTDI (bottom)

Singh et al., Image Quality and Lesion Detection on Deep Learning Reconstruction and Iterative Reconstruction of Submillisievert Chest and Abdominal CT. AJR 214:566-573, March 2020

Noise Reduction: GE's True Fidelity

- Based on a deep CNN
- Trained to restore low-dose CT data to match the properties of high quality FBP datasets.
- Said to preserve noise texture and NPS

The 20 cm water phantom (GE Healthcare, WI, US) was scanned on Revolution CT with two CTDIvol levels: 4.9mGy and 15.1mGy, and 2.5 mm thick images were reconstructed using FBP, ASiR-V 100% and DLIR-H (Fig. 11a). ASiR-V 100% and DLIR-H were selected for the highest potential visible change in image texture relative to the FBP reference at higher dose, for a challenging setup to compare the impact of the iterative reconstruction and deep-learning technologies on image appearance. The normalized NPS curves (Fig. 11b) show that images of low-dose DLIR have the same NPS characteristics as the images of high-dose FBP, whereas iterative reconstruction produces results that are clearly different.

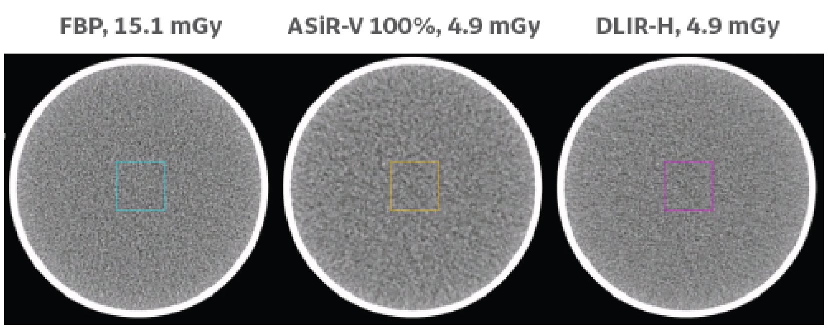

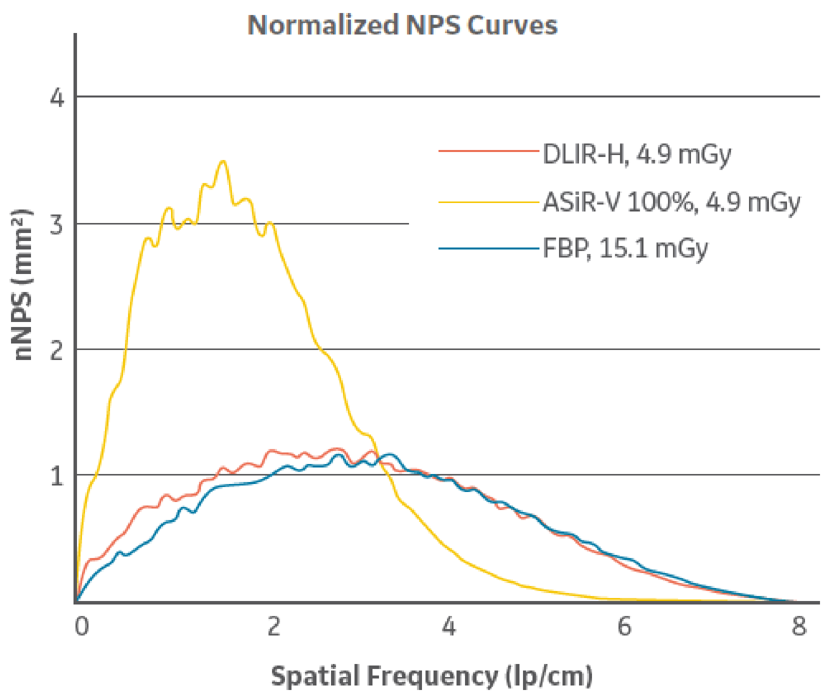

FBP

ASIR V 50%

True Fidelity

Courtesy of GE Healthcare

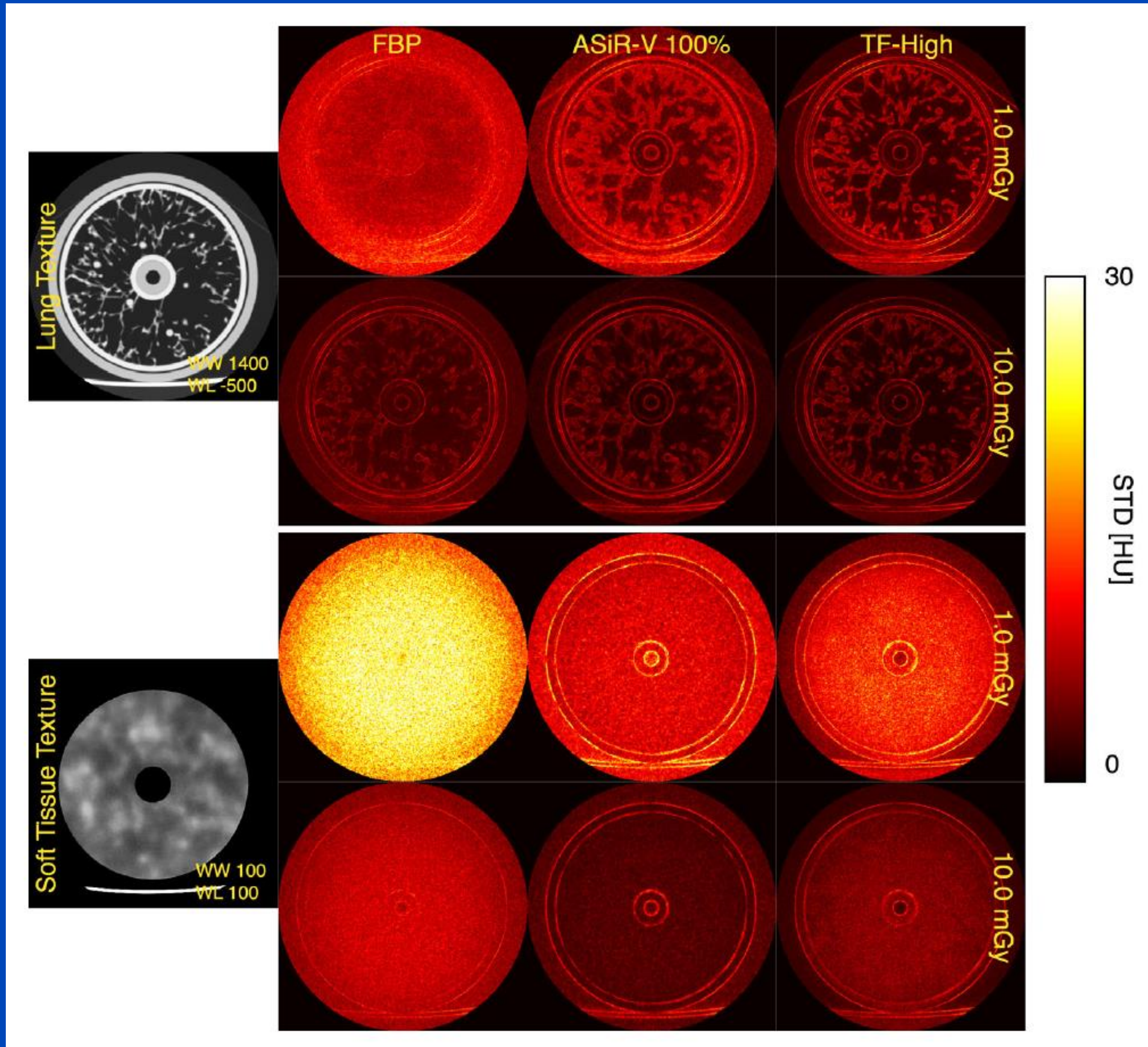

Solomon et al. Noise and spatial resolution properties of a commercially available deep learning-based CT reconstruction algorithm. Med. Phys. 47(9):3961-3971, Sept. 2020

Noise Removal: Philips' Precise Image

- Noise-injected data serve as low dose examples while their original reconstructions are the labels. A CNN learns how to denoise the low dose images.

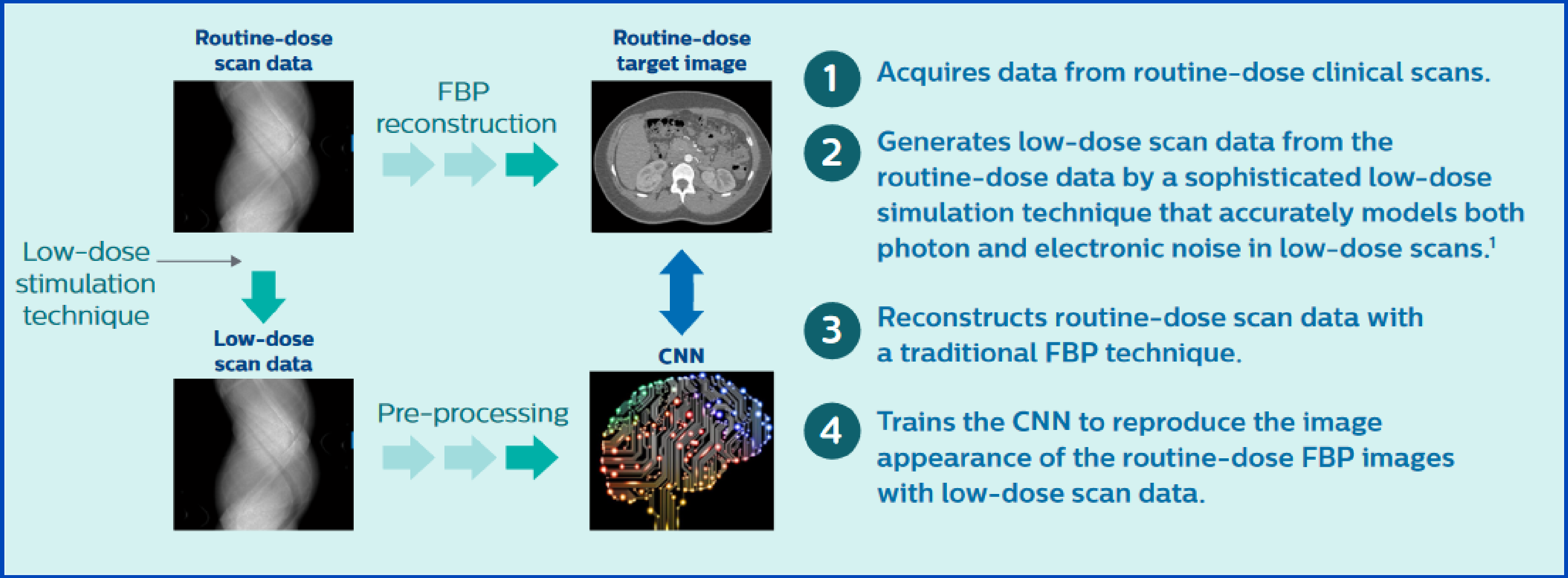

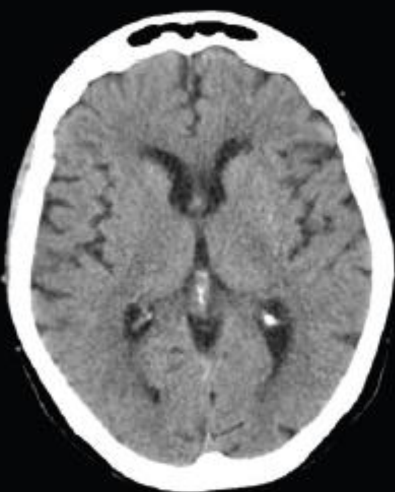

iDose⁴ 1.4 mSv

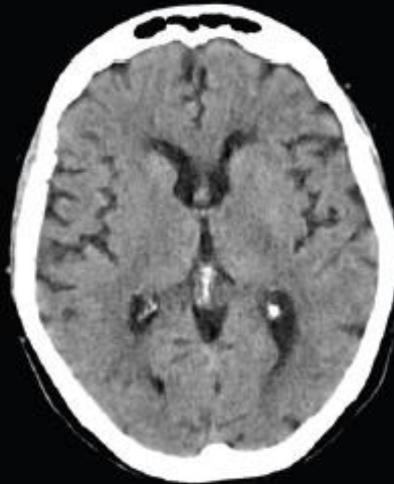

Precise Image 0.7 mSv

iDose⁴ 5.1 mSv

Precise Image 2.6 mSv

iDose⁴ 1.5 mSv

Precise Image 0.75 mSv

iDose⁴ 5.4 mSv

Precise Image 2.6 mSv

Taken from https://www.philips.com/c-dam/b2bhc/master/resource-catalog/landing/precise-suite/incisive_precise_image.pdf

Study	Topic	Dose Reduction	Assessment	Reconstruction
Beregi et al., 2022	low-dose abdomen phantom	79%	objective	AiCE
Hirai et al., 2022a	low-dose multiphase hepatic	52%	objective, subjective	AiCE
Hirai et al., 2022b	low-dose pediatric 80 kV	54%	objective, subjective	AiCE
Jin et al., 2022	low-dose interstitial lung disease	62%	objective, subjective	AiCE
Loffroy et al., 2022	low-dose head & neck	43%	objective, subjective	AiCE
Sun et al., 2022	ultra-low-dose urolithiasis	75%	objective, subjective	AiCE
Yoshioka et al., 2022	low-dose contrast abdomen	40%	objective, subjective	AiCE
Awai et al., 2021	low-dose abdominal UHR	30%	objective, subjective	AiCE
Dillman et al., 2021	pediatric detectability	52%	objective, subjective	AiCE
Loffroy et al., 2021	cardiac CTA stroke	40%	objective, subjective	AiCE
Kalra et al., 2020	low-dose lesion detection	83%	subjective	AiCE
Willemink et al., 2023	principles & prospects	71%	mixed	meta
Strigari et al., 2023	image quality phantom	96%	objective	Precise Image
Deng et al., 2022	ultra-low-dose pulmonary nodules phantom	72%	objective, subjective	TrueFidelity
Lee et al., 2021	pediatric chest & abdomen	63%	objective, subjective	TrueFidelity

True and Fake DECT

Existing true DECT approaches (for more than one decade):

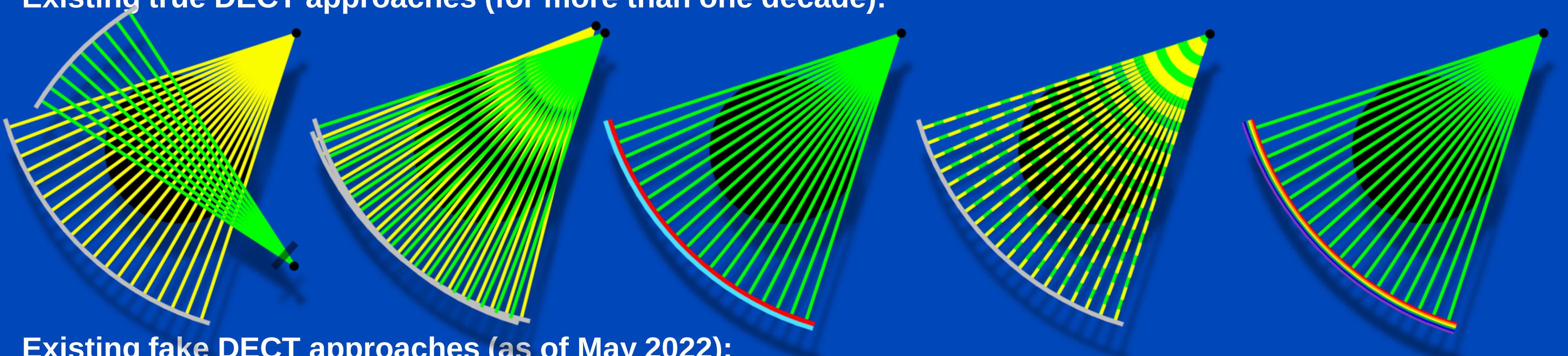

Existing fake DECT approaches (as of May 2022):

[1] J. Ma, Y. Liao, Y. Wang, S. Li, J. He, D. Zeng, Z. Bian, "Pseudo dual energy CT imaging using deep learning-based framework: basic material estimation", *SPIE Medical Imaging 2018*.

[2] W. Zhao, T. Lv, P. Gao, L. Shen, X. Dai, K. Cheng, M. Jia, Y. Chen, L. Xing, "A deep learning approach for dual-energy CT imaging using a single-energy CT data", *Fully3D 2019.*

[3] D. Lee, H. Kim, B. Choi, H. J. Kim, "Development of a deep neural network for generating synthetic dual-energy chest x-ray images with single x-ray exposure", PMB 64(11), 2019.

[4] L. Yao, S. Li, D. Li, M. Zhu, Q. Gao, S. Zhang, Z. Bian, J. Huang, D. Zeng, J. Ma, "Leveraging deep generative model for direct energy-resolving CT imaging via existing energy-integrating CT images", *SPIE Medical Imaging 2020*.

[5] D. P. Clark, F. R. Schwartz, D. Marin, J. C. Ramirez-Giraldo, C. T. Badea, "Deep learning based spectral extrapolation for dual-source, dual-energy x-ray CT", Med. Phys. 47 (9): 4150–4163, 2020.

[6] C. K. Liu, C. C. Liu, C. H. Yang, H. M. Huang, "Generation of brain dual-energy CT from single-energy CT using deep learning", Journal of Digital Imaging 34(1):149–161, 2021.

[7] T. Lyu, W. Zhao, Y. Zhu, Z. Wu, Y. Zhang, Y. Chen, L. Luo, S. Li, L. Xing, "Estimating dual-energy CT imaging from single-energy CT data with material decomposition convolutional neural network", Medical Image Analysis 70:1–10, 2021.

[8] F. R. Schwartz, D. P. Clark, Y. Ding, J. C. Ramirez-Giraldo, C. T. Badea, D. Marin, "Evaluating renal lesions using deep-learning based extension of dual-energy FoV in dual-source CT—A retrospective pilot study", European Journal of Radiology 139:109734, 2021.

[9] Y. Li, X. Tie, K. Li, J. W. Garrett, G.-H. Chen, "Deep-En-Chroma: mining the spectral fingerprints in single-kV CT acquisitions using energy integration detectors", *SPIE Medical Imaging 2022*.

Pseudo Dual-Energy vs. True Dual-Energy

Training:

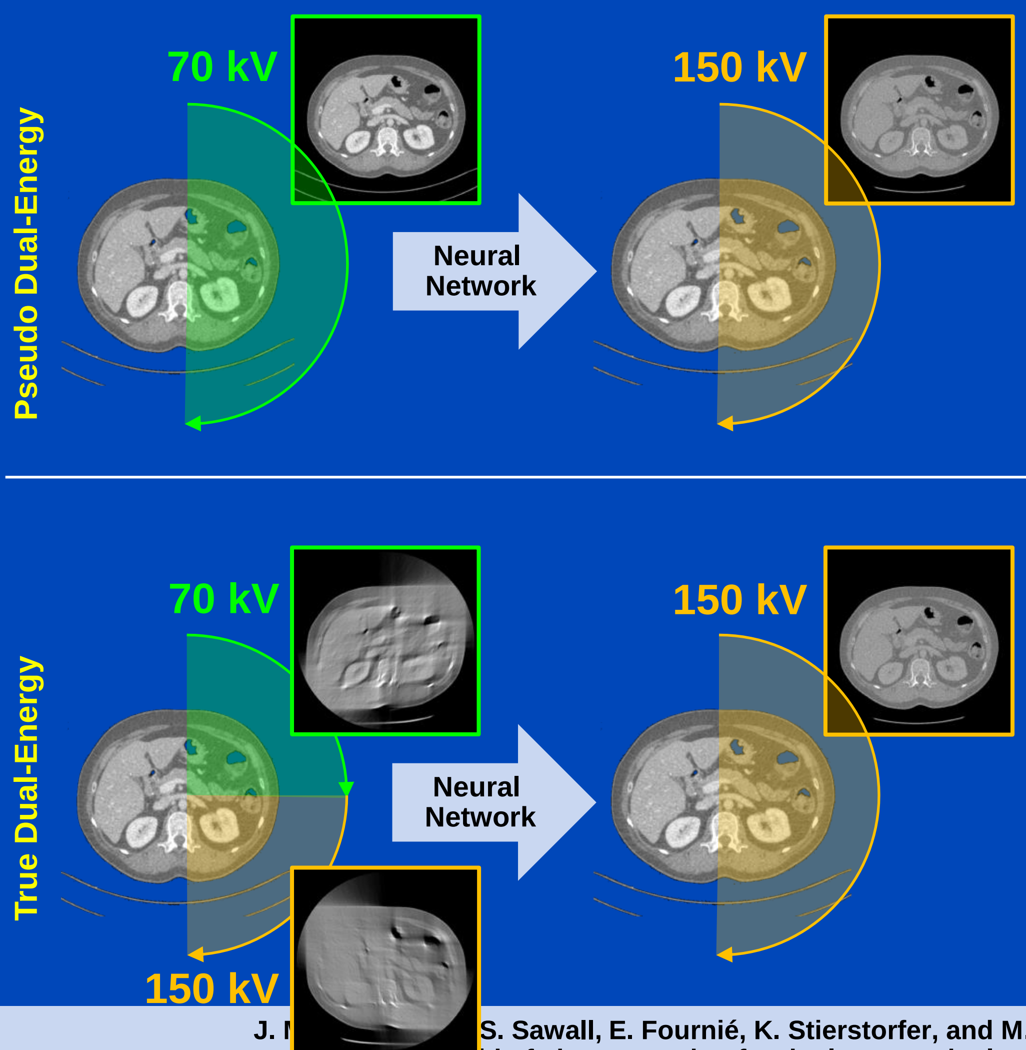

Testing:

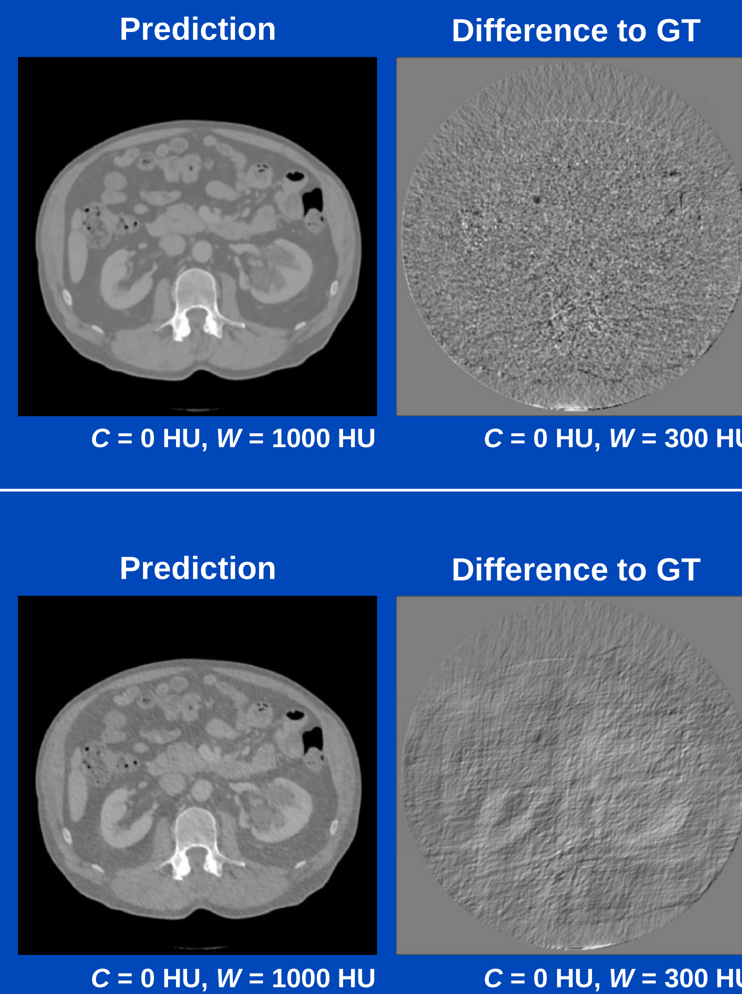

J. M… S. Sawall, E. Fournié, K. Stierstorfer, and M. Kachelrieß. Raw data consisten deep learning-based field of view extension for dual-source dual-energy CT. Med. Phys. 50:in press, 2023.

dkfz.

Pseudo Dual-Energy vs. True Dual-Energy

Training:

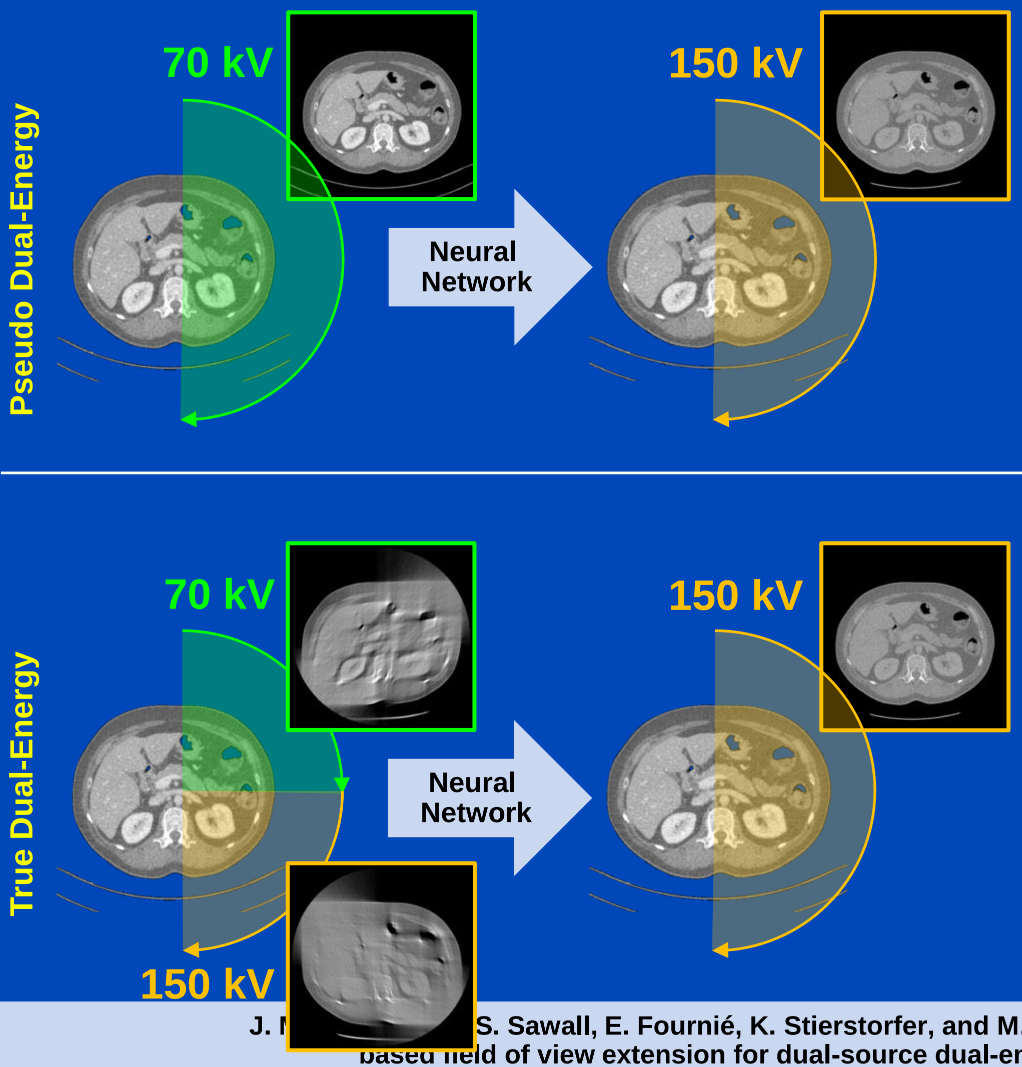

Testing:

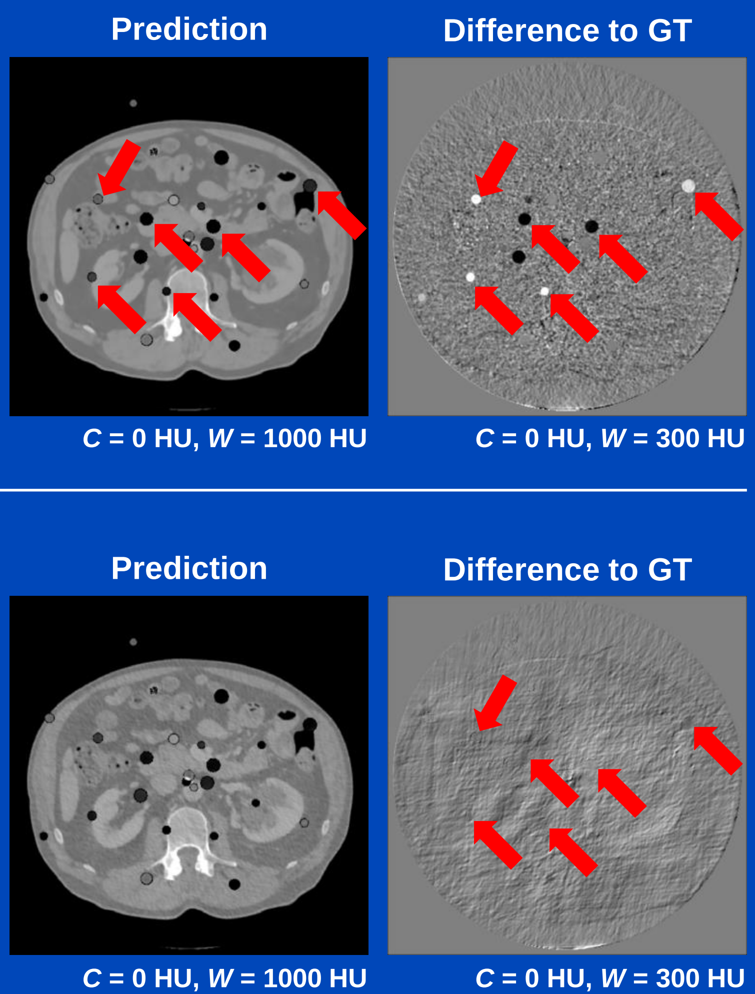

J. M… S. Sawall, E. Fournié, K. Stierstorfer, and M. Kachelrieß. Raw data consisten deep learning-based field of view extension for dual-source dual-energy CT. Med. Phys. 50:in press, 2023.

dkfz.

Algorithm for Partial DECT

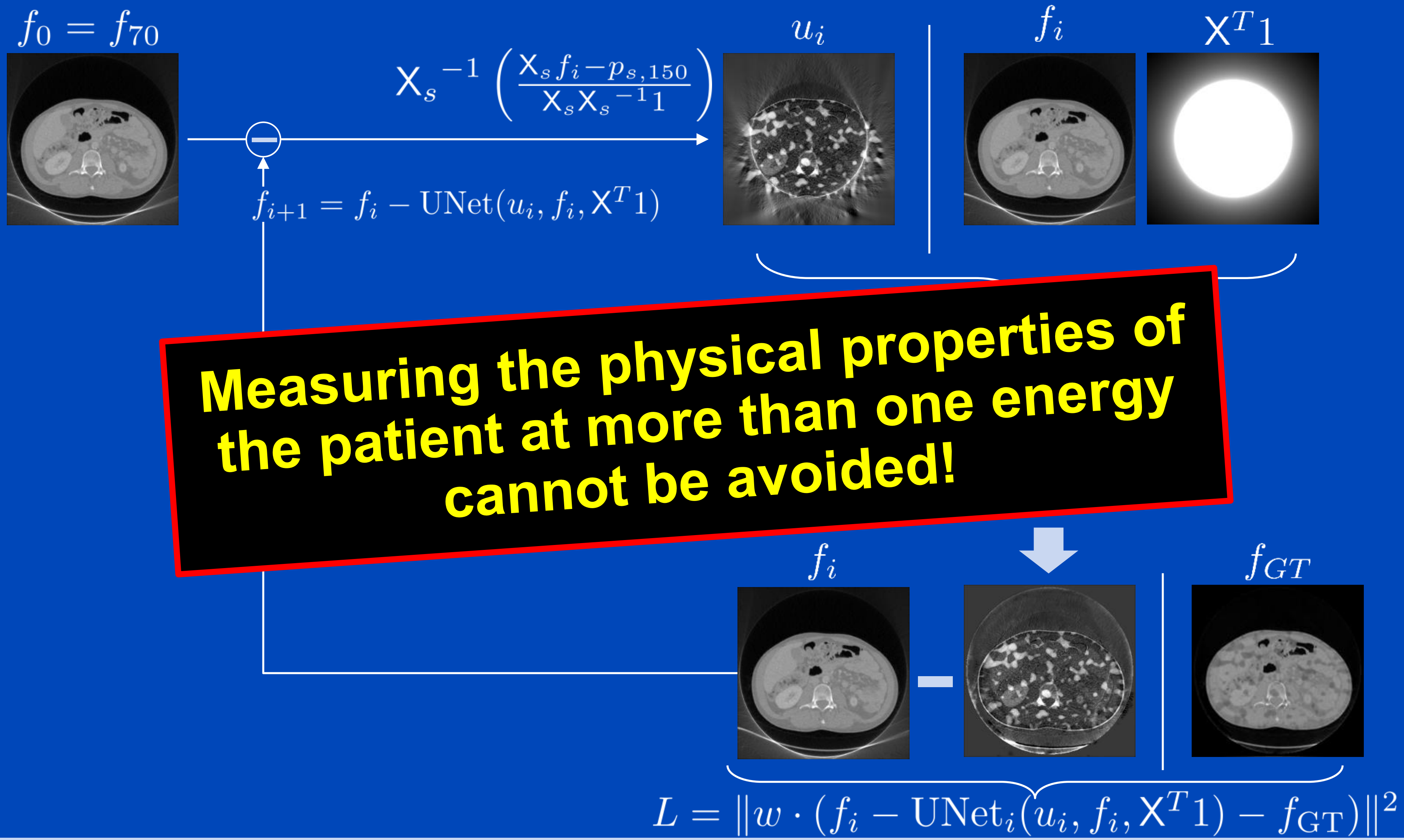

Measuring the physical properties of the patient at more than one energy cannot be avoided!

J. Maier, J. Erath, S. Sawall, E. Fournié, K. Stierstorfer, and M. Kachelrieß. Raw data consisten deep learning-based field of view extension for dual-source dual-energy CT. Med. Phys. 50:in press, 2023.

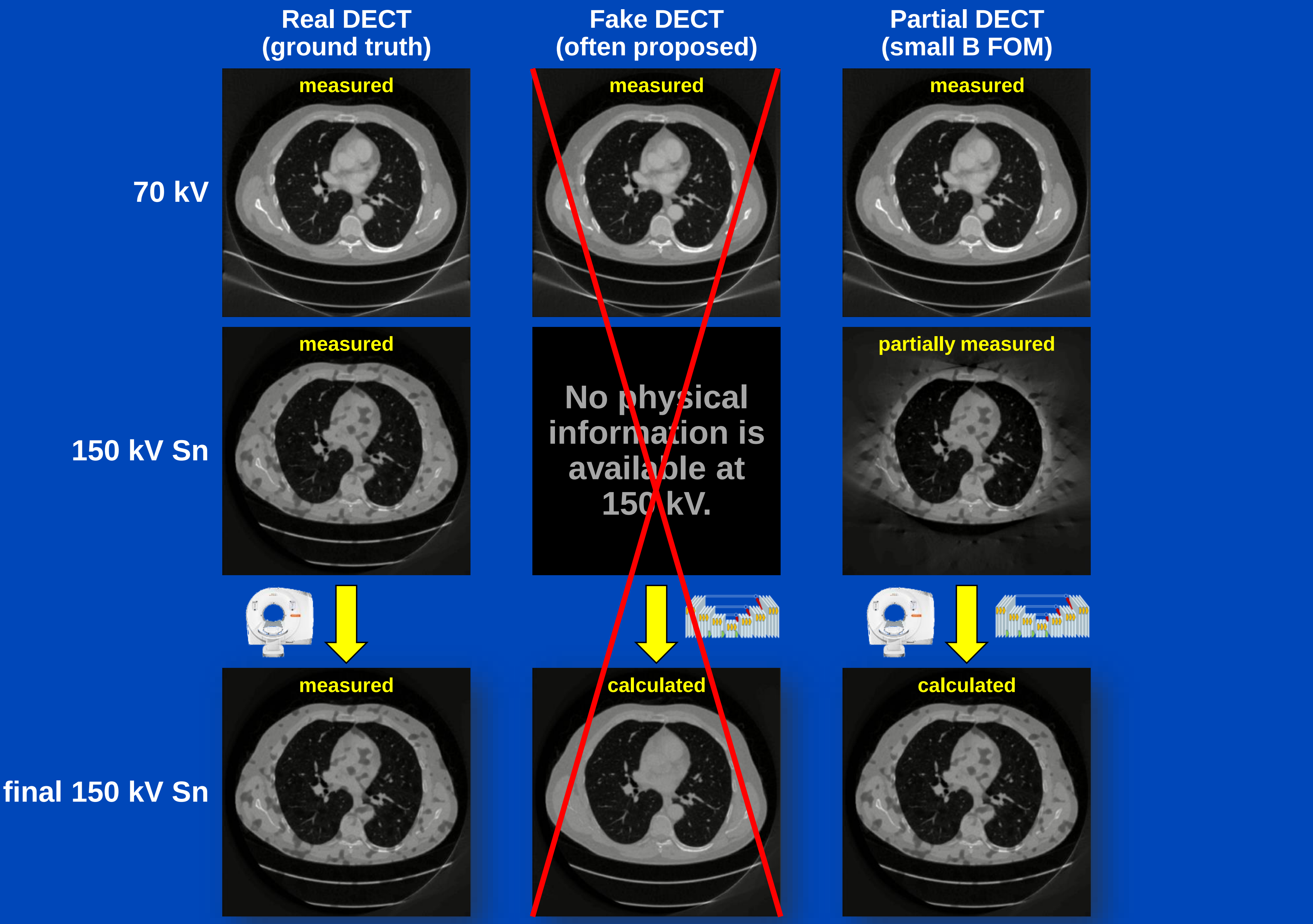

J. Maier, J. Erath, S. Sawall, E. Fournié, K. Stierstorfer, and M. Kachelrieß. Raw data consisten deep learning-based field of view extension for dual-source dual-energy CT. Med. Phys. 50:in press, 2023.

Scatter Estimation

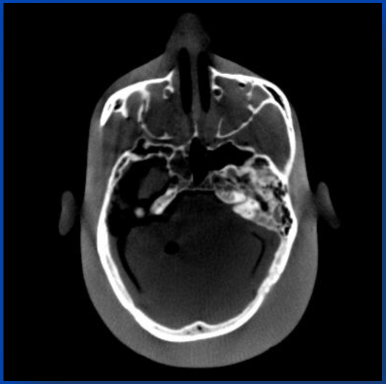

???

In real time?

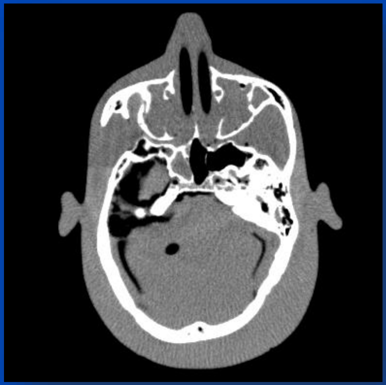

Deep Scatter Estimation (DSE)

TOP DOWNLOADED PAPER 2018-2019

CONGRATULATIONS TO

Marc Kachelriess

whose paper has been r

WILEY

MEDICAL PHYSICS

The International Journal of Medical Physics Research and Practice

Congratulations — your work was one of the top downloaded in recent publication history!

Dear MARC

research, published in *Medical Physics*, is
aded papers!

ion for medical CT using the deep
d and robustness analysis with
nies, dose levels, tube voltages, and

This work received the
Behnken-Berger Award
at the DGMP annual meeting 2021

BEHNKEN-BERGER STIFTUNG

APER 2018-2019

ATIONS TO

Joscha Maier

whose paper has been recognized as
one of the most read in
Medical Physics

Motivation

- X-ray scatter is a major cause of image quality degradation in CT and CBCT.
- Appropriate scatter correction is crucial to maintain the diagnostic value of the CT examination.

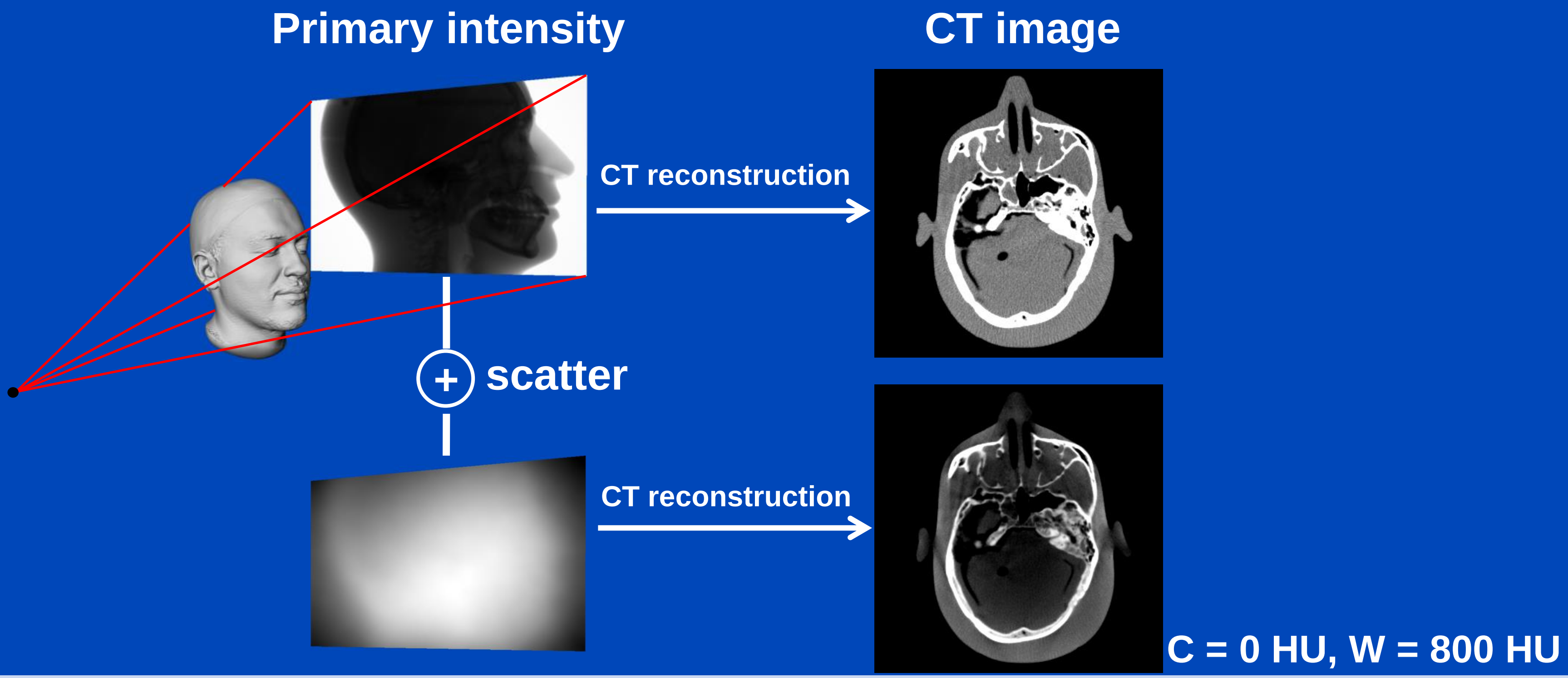

dkfz.

Monte Carlo Scatter Estimation

- Simulation of photon trajectories according to physical interaction probabilities.
- Simulating a large numb… …ries well approximat…

1 to 10 hours per tomographic data set

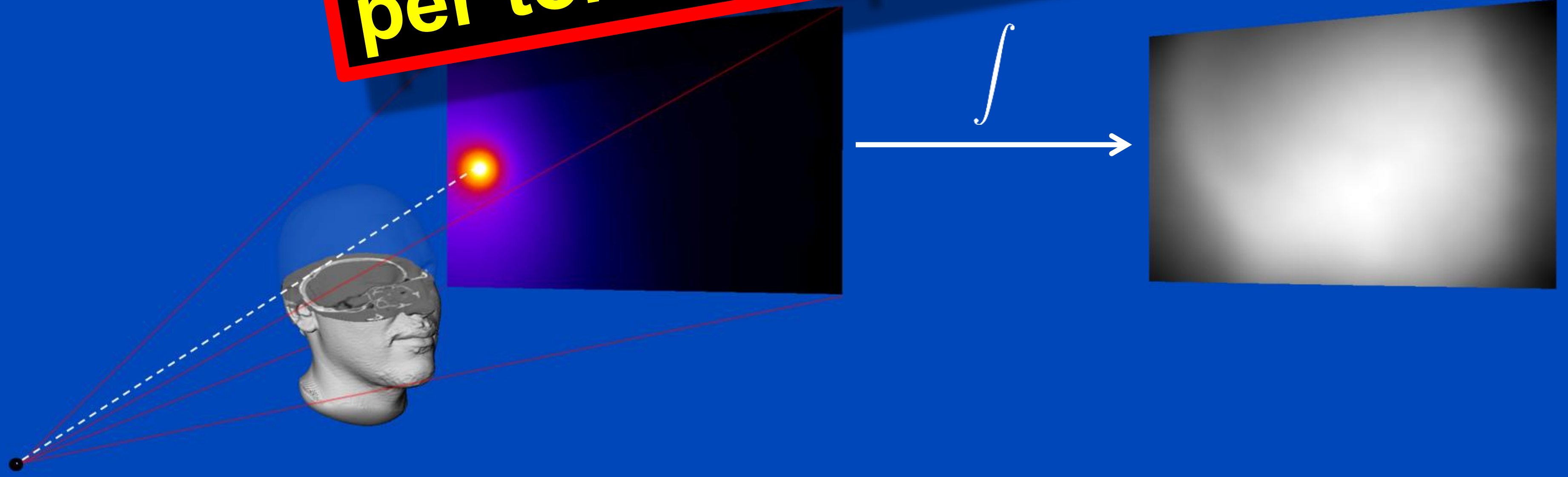

Deep Scatter Estimation

Network architecture & scatter estimation framework

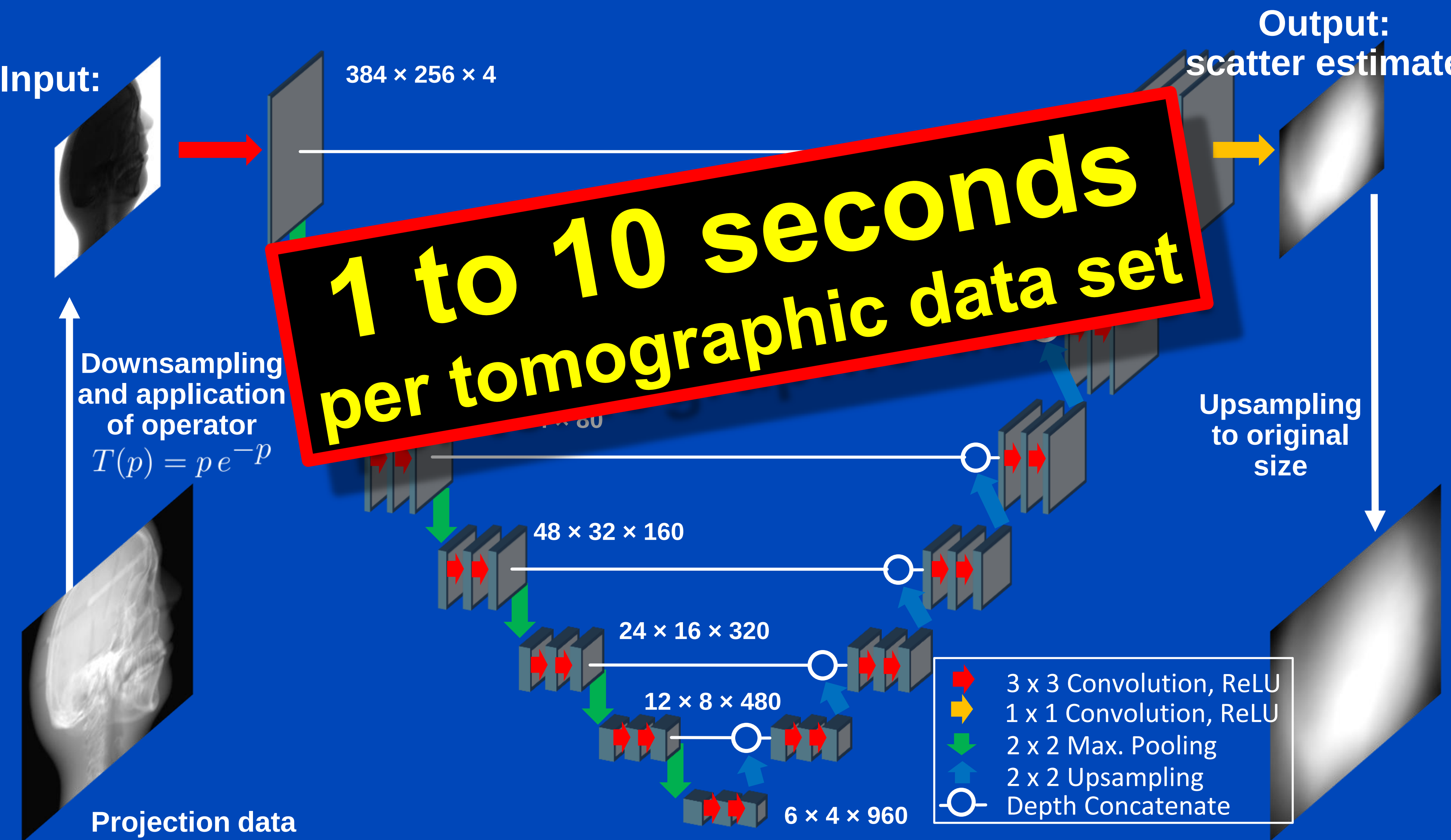

J. Maier, M. Kachelrieß et al. Deep scatter estimation (DSE). SPIE 2017 and Journal of Nondestructive Evaluation 37:57, July 2018.
J. Maier, M. Kachelrieß et al. Robustness of DSE. Med. Phys. 46(1):238-249, January 2019.

PEP

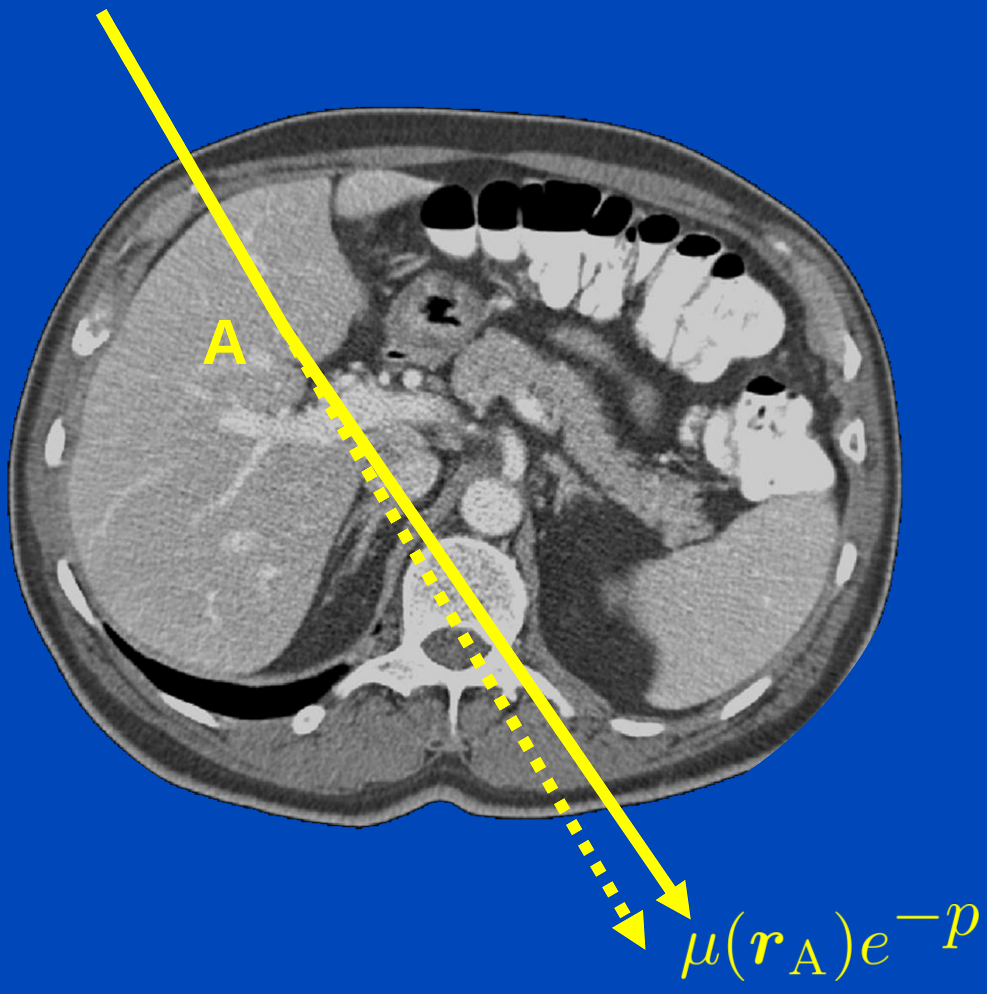

PEP

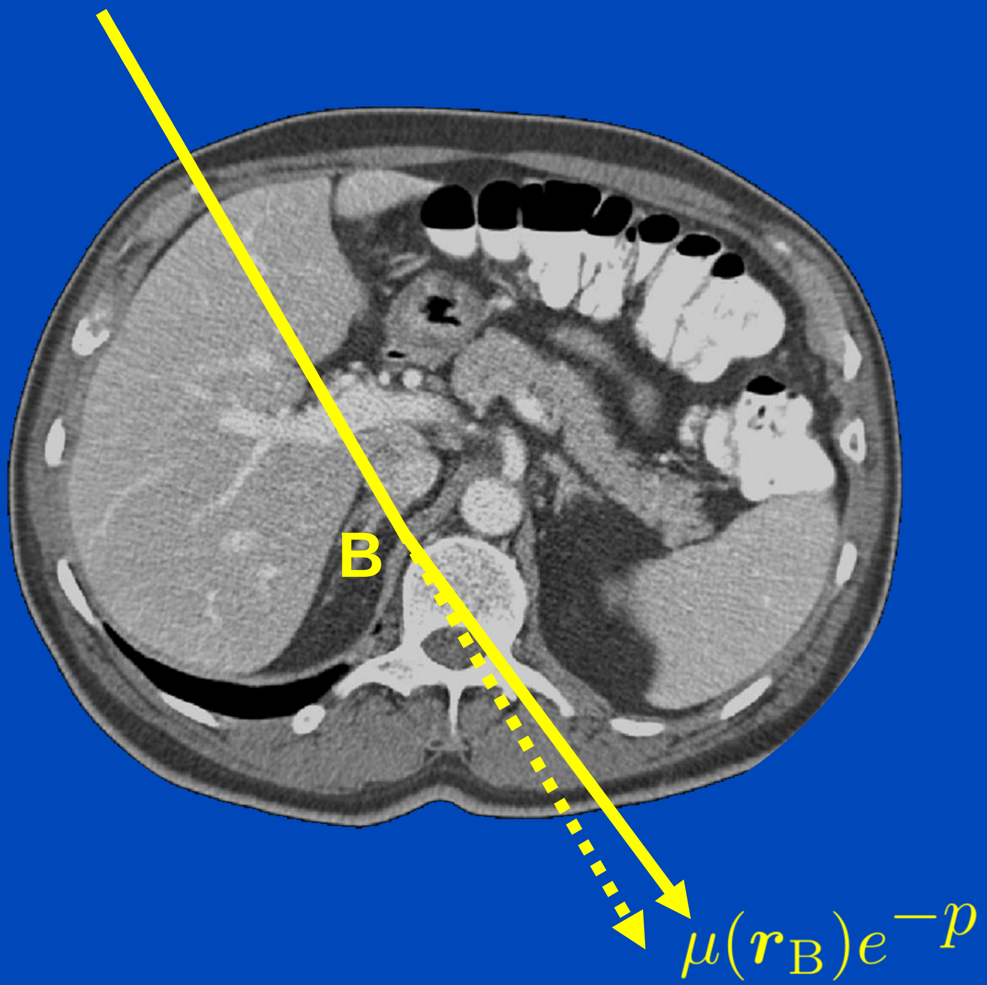

PEP

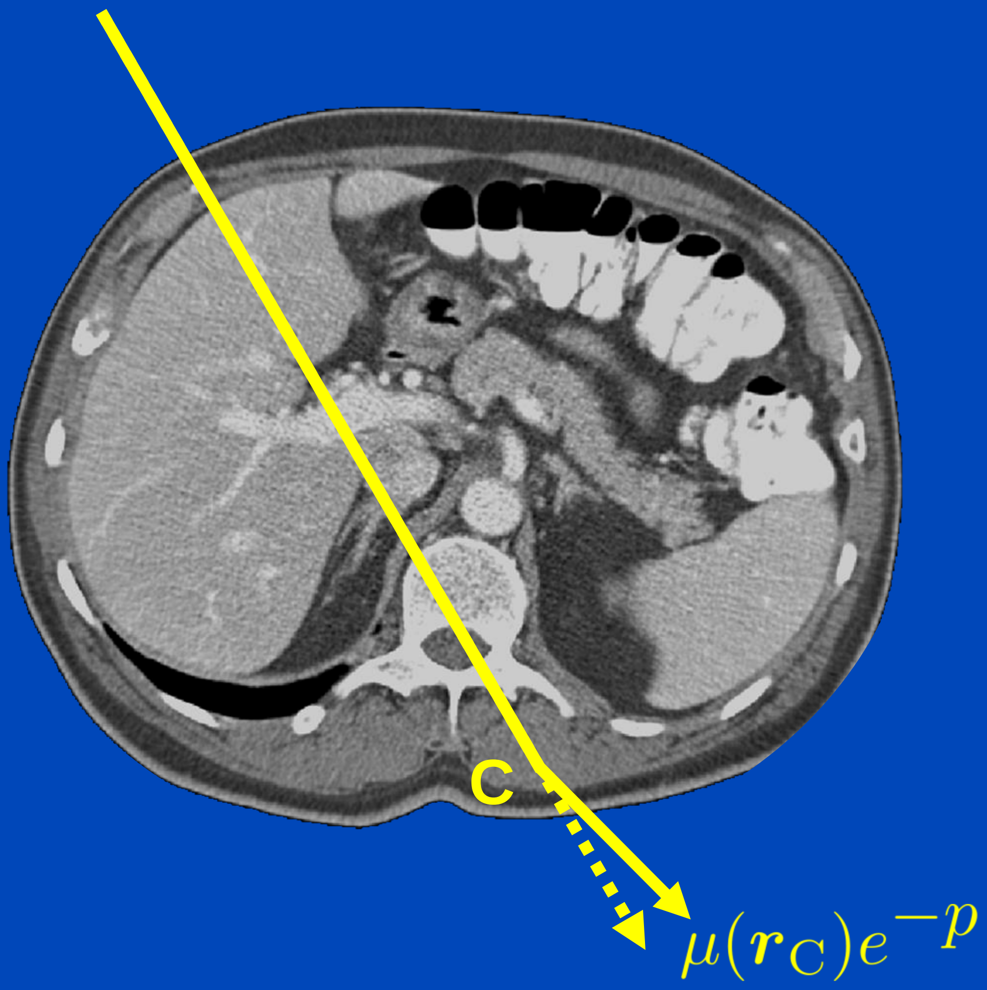

PEP

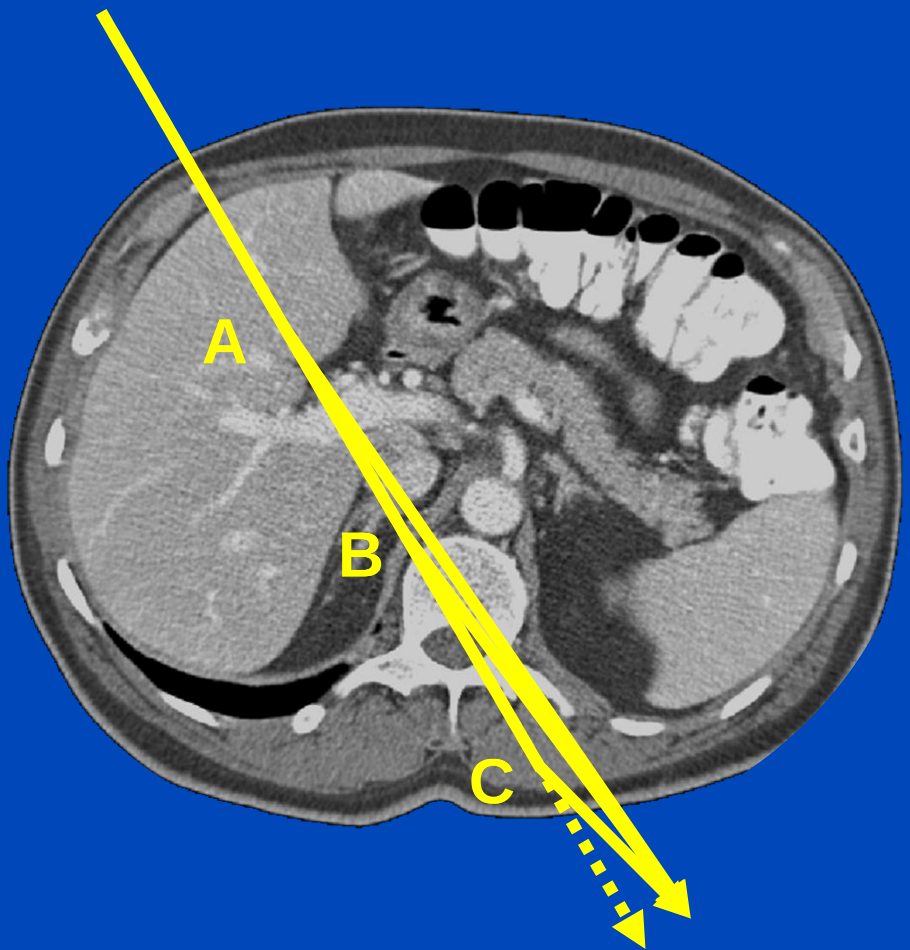

$$\big(\mu(\boldsymbol{r}_{\mathrm{A}}) + \mu(\boldsymbol{r}_{\mathrm{B}}) + \mu(\boldsymbol{r}_{\mathrm{C}})\big)e^{-p} = p\,e^{-p}$$

PEP for CT

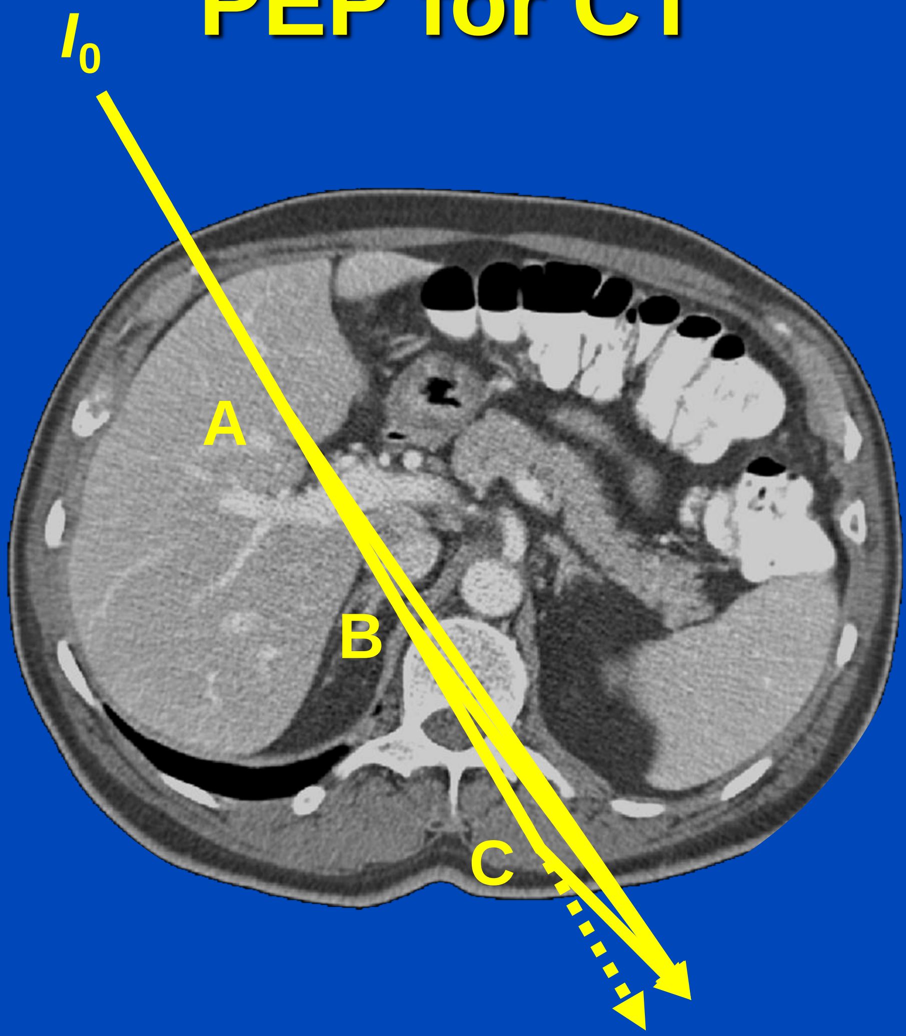

$$I_0\big(\mu(\boldsymbol{r}_\mathrm{A})+\mu(\boldsymbol{r}_\mathrm{B})+\mu(\boldsymbol{r}_\mathrm{C})\big)e^{-p}=I_0\,p\,e^{-p}$$

PEP for PET

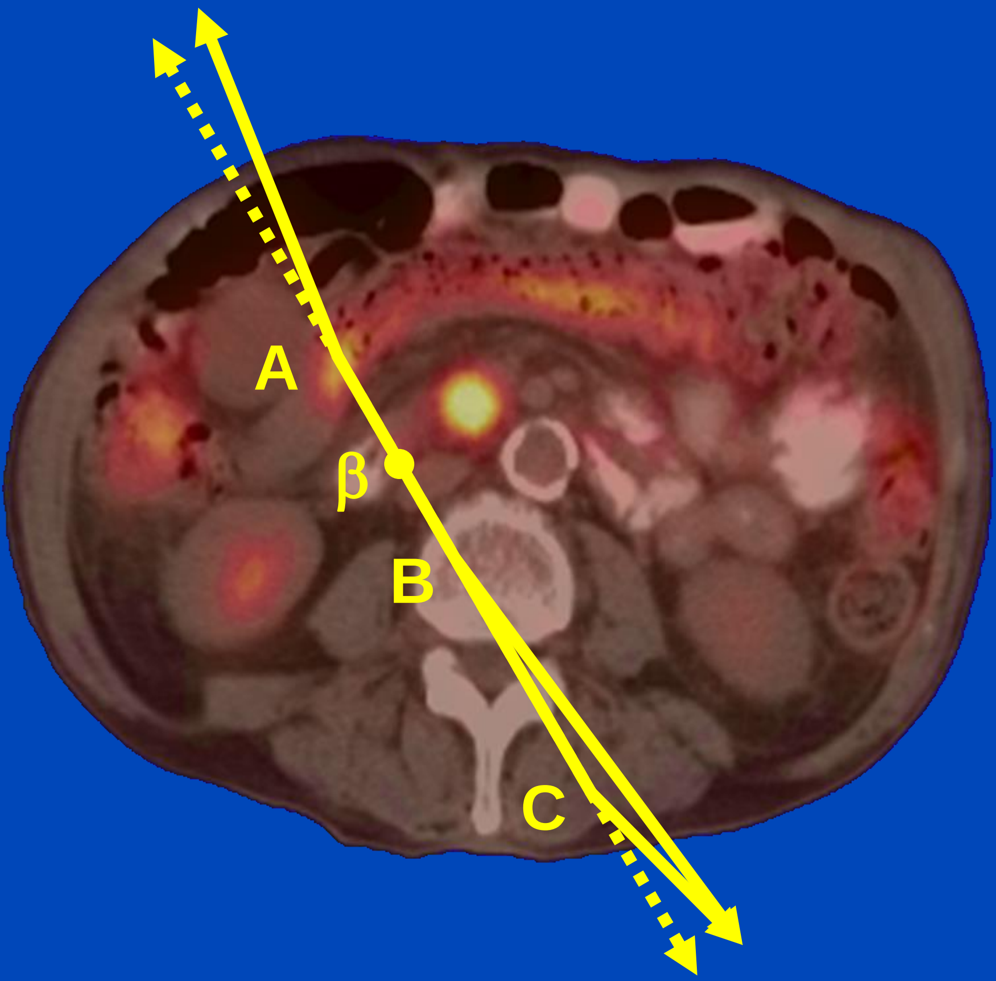

$$a(\boldsymbol{r}_\beta)\big(\mu(\boldsymbol{r}_\mathrm{A})+\mu(\boldsymbol{r}_\mathrm{B})+\mu(\boldsymbol{r}_\mathrm{C})\big)e^{-p}=a(\boldsymbol{r}_\beta)\,p\,e^{-p}$$

PEP for PET

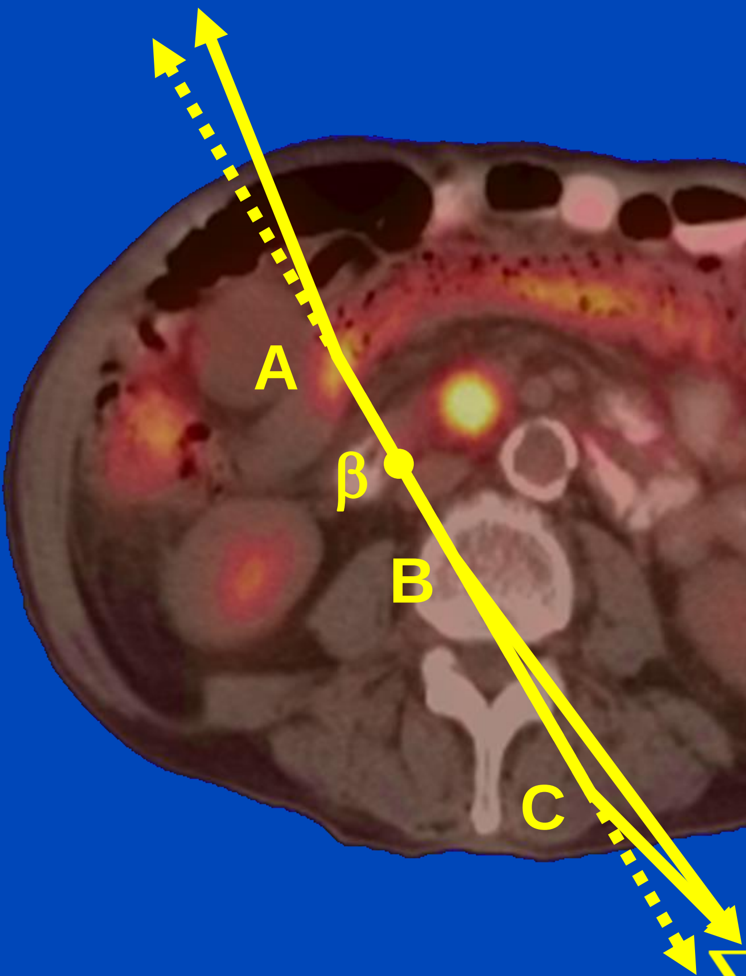

$$\sum_{\mathrm{LOR}} a(\boldsymbol{r})\, p\, e^{-p}$$

Results on Simulated Projection Data

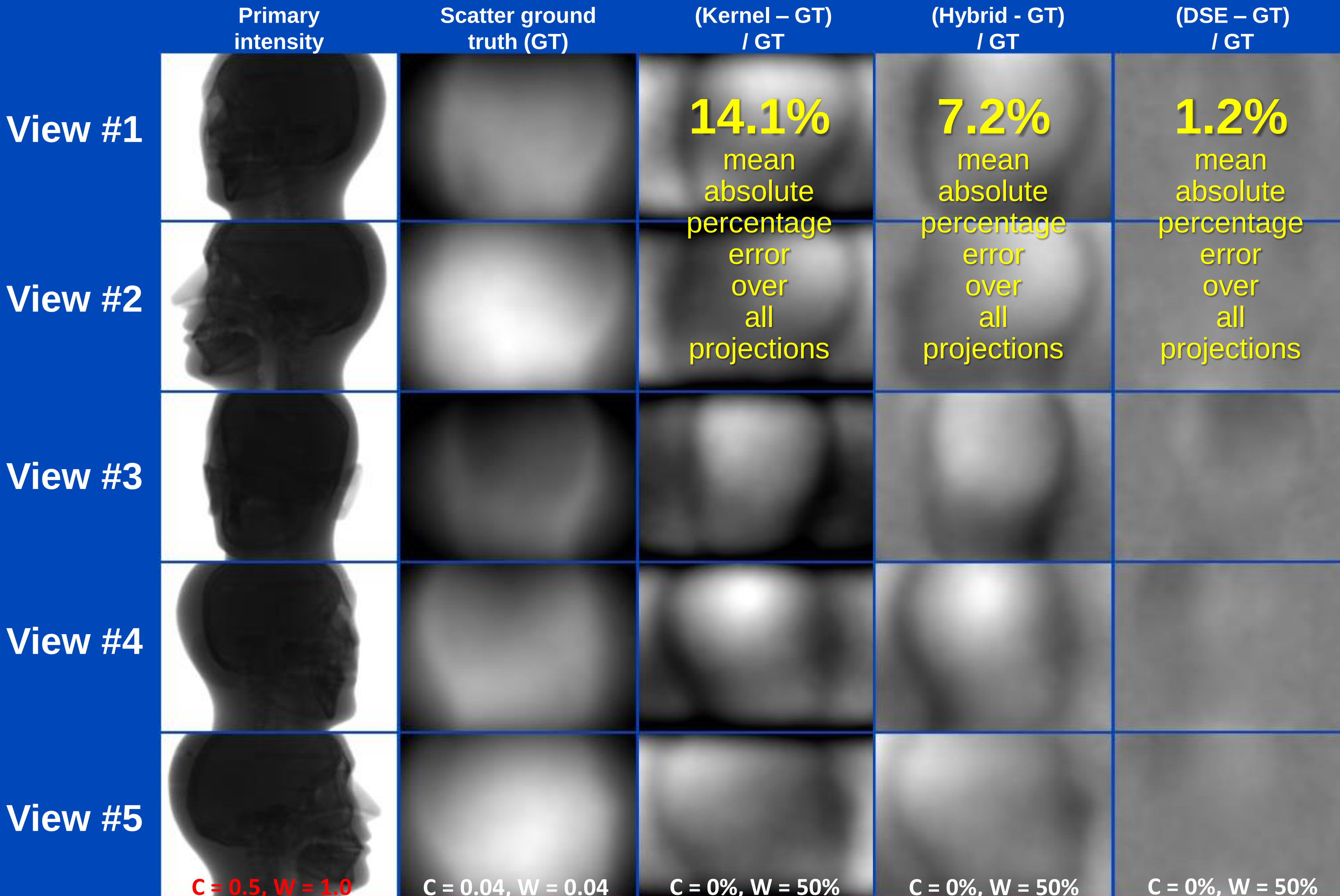

DSE trained to estimate scatter from **primary plus scatter**: High accuracy

dkfz.

Reconstructions of Simulated Data

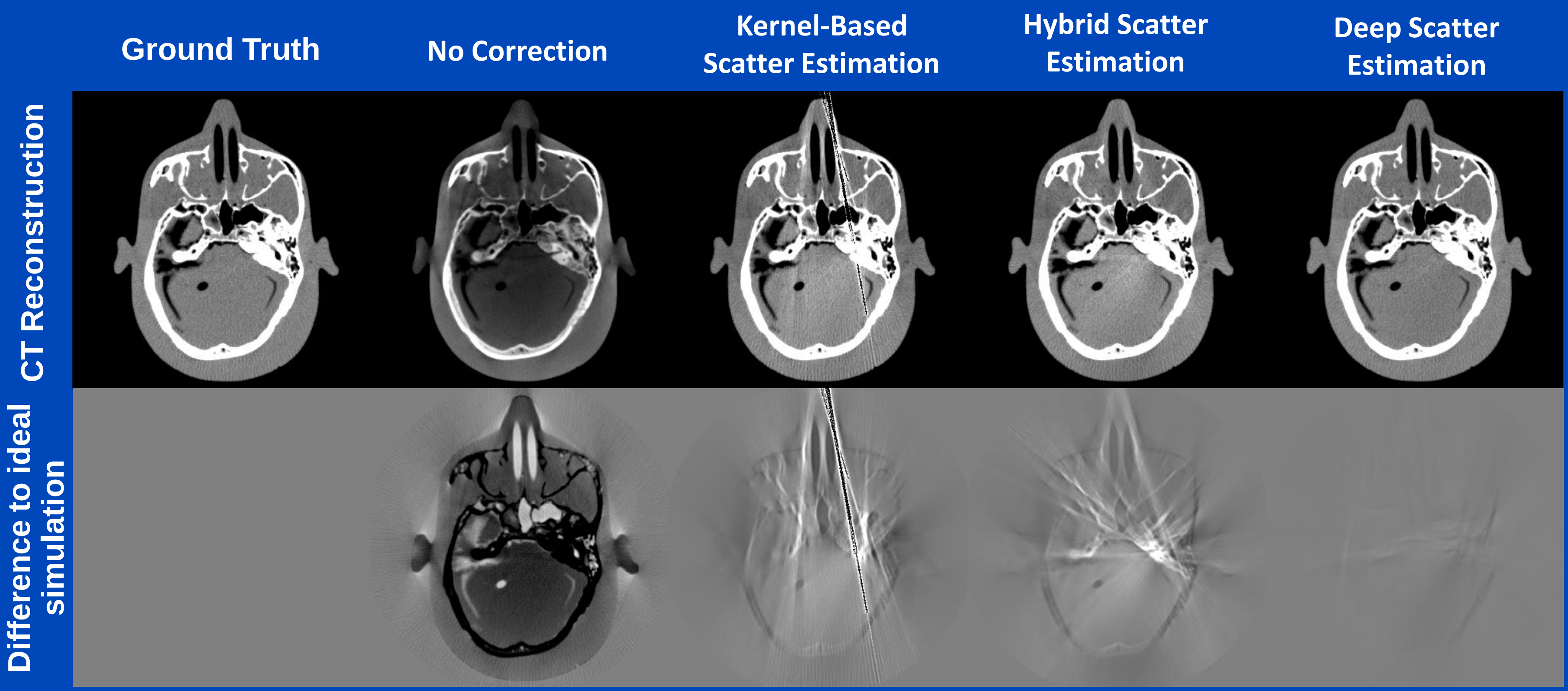

C = 0 HU, *W* = 1000 HU

J. Maier, M. Kachelrieß et al. Deep scatter estimation (DSE). SPIE 2017 and Journal of Nondestructive Evaluation 37:57, July 2018.
J. Maier, M. Kachelrieß et al. Robustness of DSE. Med. Phys. 46(1):238-249, January 2019.

Testing of the DSE Network for Measured Data (120 kV)

DKFZ table-top CT

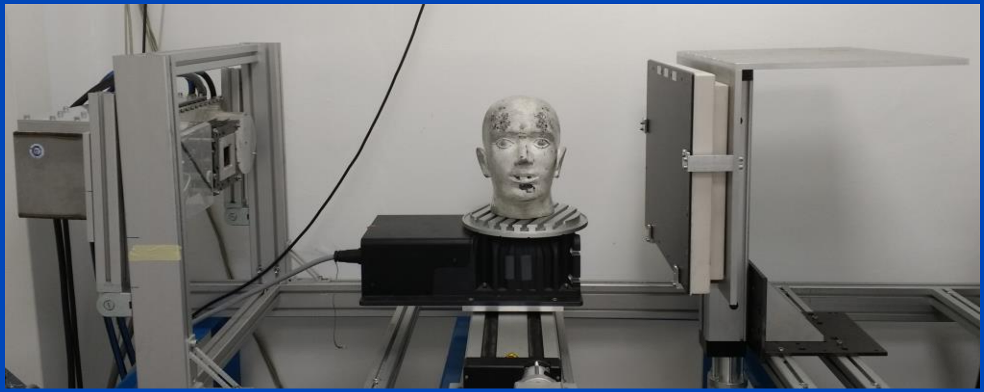

- Measurement of a head phantom at our in-house table-top CT.
- Slit scan measurement serves as ground truth.

Measurement to be corrected

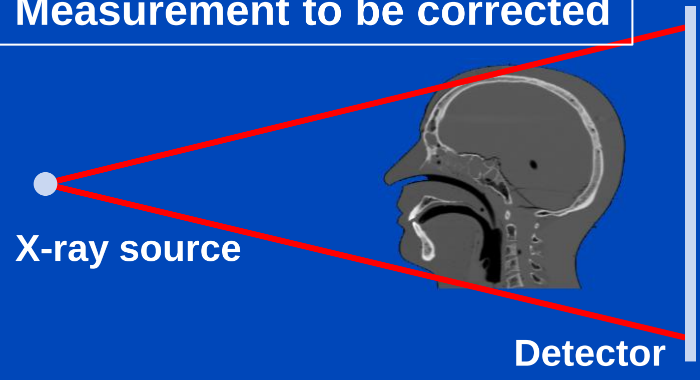

Ground truth: slit scan

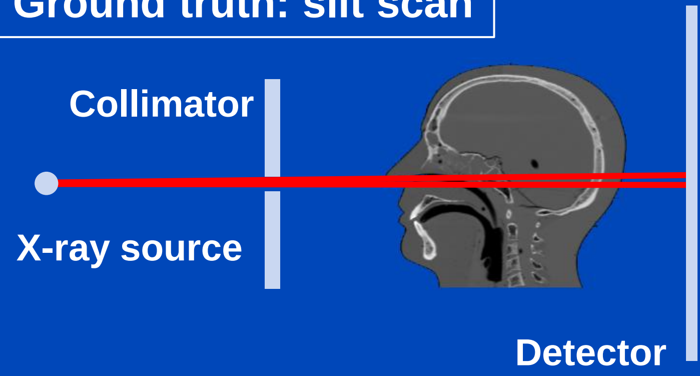

J. Maier, M. Kachelrieß et al. Deep scatter estimation (DSE). SPIE 2017 and Journal of Nondestructive Evaluation 37:57, July 2018.
J. Maier, M. Kachelrieß et al. Robustness of DSE. Med. Phys. 46(1):238-249, January 2019.

dkfz.

Reconstructions of Measured Data

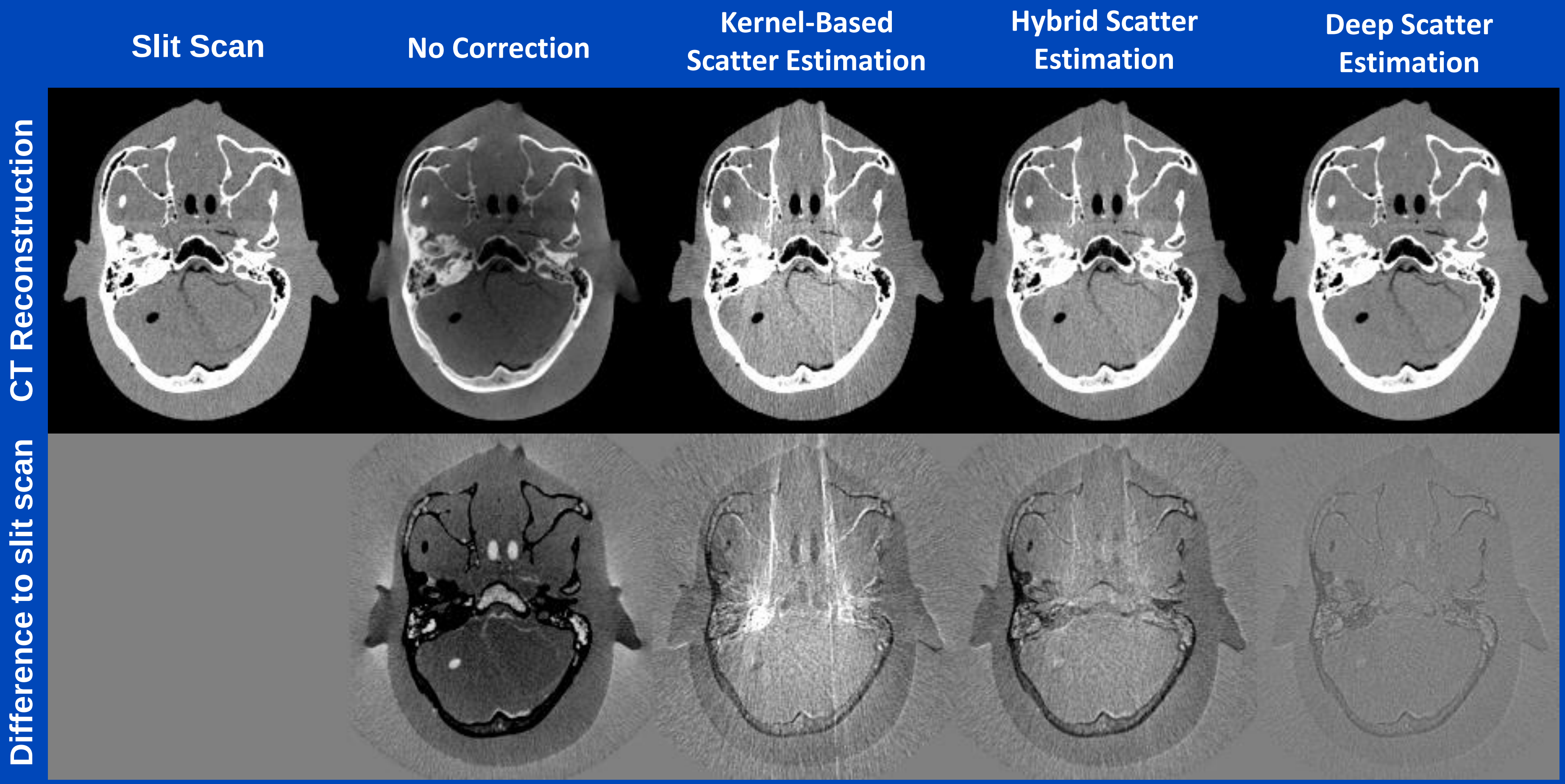

C = 0 HU, W = 1000 HU

J. Maier, M. Kachelrieß et al. Deep scatter estimation (DSE). SPIE 2017 and Journal of Nondestructive Evaluation 37:57, July 2018.
J. Maier, M. Kachelrieß et al. Robustness of DSE. Med. Phys. 46(1):238-249, January 2019.

A simple detruncation was applied to the rawdata before reconstruction. Images were clipped to the FOM before display. C = -200 HU, W = 1000 HU.

Truncated DSE

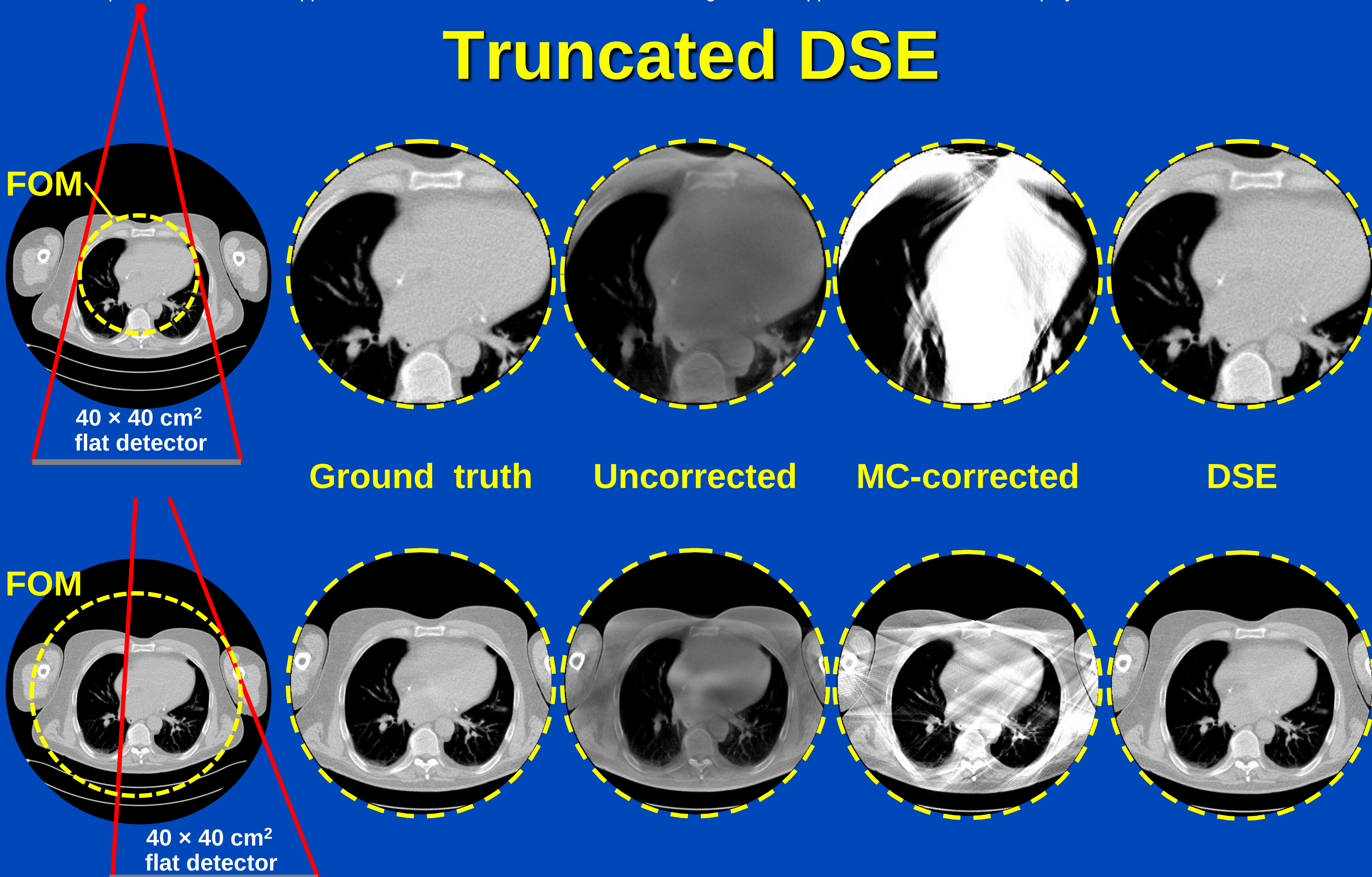

To learn why MC fails at truncated data and what significant efforts are necessary to cope with that situation see [Kachelrieß et al. Effect of detruncation on the accuracy of MC-based scatter estimation in truncated CBCT. Med. Phys. 45(8):3574-3590, August 2018].

J. Maier, M. Kachelrieß et al. Deep scatter estimation (DSE). SPIE 2017 and Journal of Nondestructive Evaluation 37:57, July 2018.
J. Maier, M. Kachelrieß et al. Robustness of DSE. Med. Phys. 46(1):238-249, January 2019.

Does DSE Generalize to Different Anatomical Regions?

- **Simulation parameters:**
  - 7 head and 14 thorax/abdomen clinical CT data sets
  - Apply affine transforms to obtain 28 volumes for each region
  - Regions: head, thorax and abdomen
  - Tube Voltage: 120 kV, 140 kV.
  - Prior volumes: 28 head phantoms
  - Simulate 45 projections over 360° for each volume and voltage
  - Number of z-Positions: 1 for head, 4 for thorax and abdomen
  - Data augmentation for head: vertical & horizontal flipping
  - Total number of projections: 2 × 28 × 45 × 2 × 2 = 10080

Results

KSE	Head	Thorax	Abdomen
Head	14.5	26.8	32.5
Thorax	16.2	18.5	19.4
Abdomen	16.8	22.1	17.8
All data	14.9	20.5	19.3

DSE	Head	Thorax	Abdomen
Head	1.2	21.1	32.7
Thorax	8.8	1.5	9.1
Abdomen	11.9	10.9	1.3
All data	1.8	1.4	1.4

Values shown are the mean absolute percentage errors (MAPEs) of the testing data.
Note that thorax and head suffer from truncation due to the small size of the 40×30 cm flat detector.

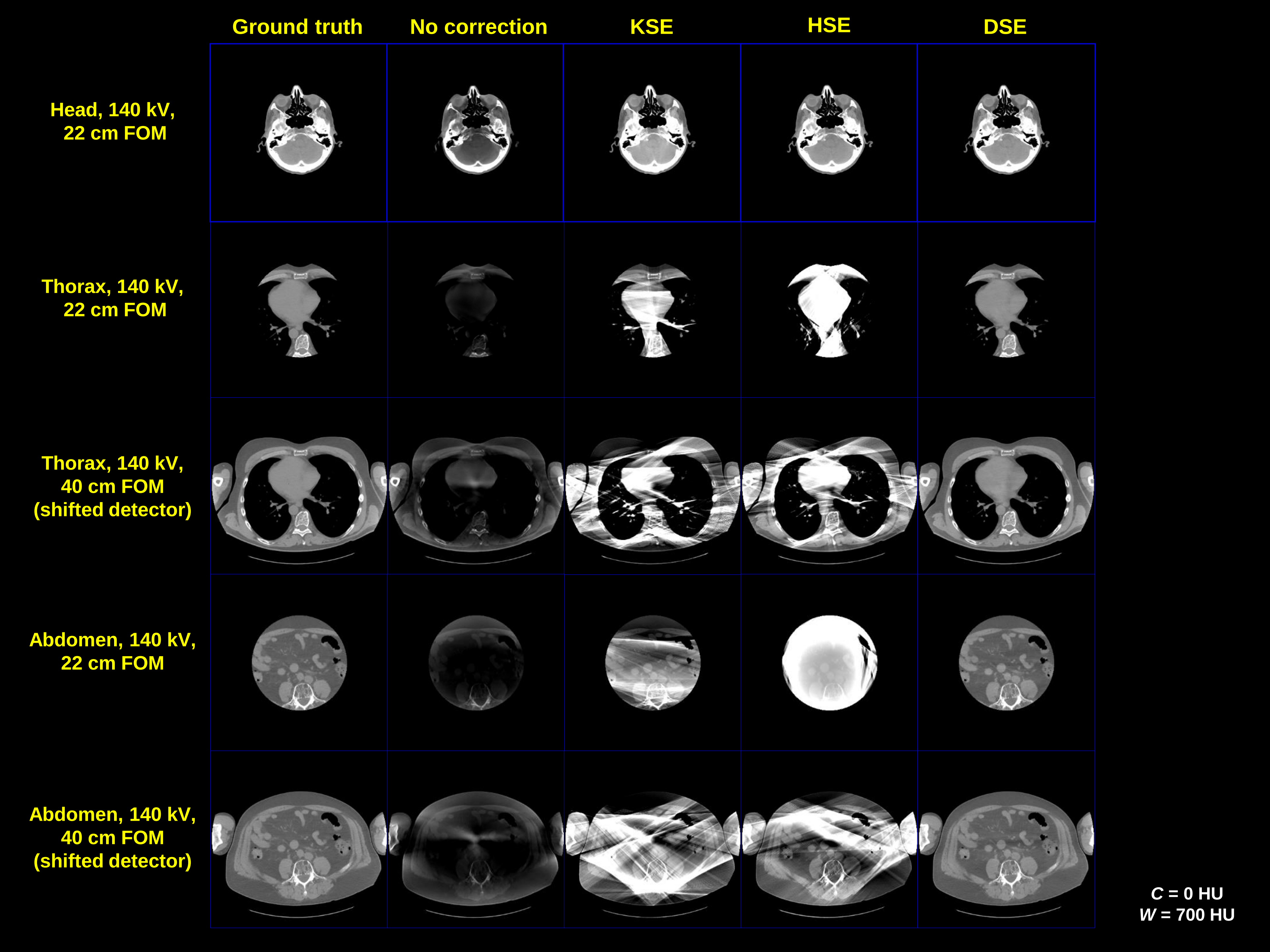
Ground truth
No correction
KSE
HSE
DSE
Head, 140 kV, 22 cm FOM
Thorax, 140 kV, 22 cm FOM
Thorax, 140 kV, 40 cm FOM (shifted detector)
Abdomen, 140 kV, 22 cm FOM
Abdomen, 140 kV, 40 cm FOM (shifted detector)
C = 0 HU
W = 700 HU

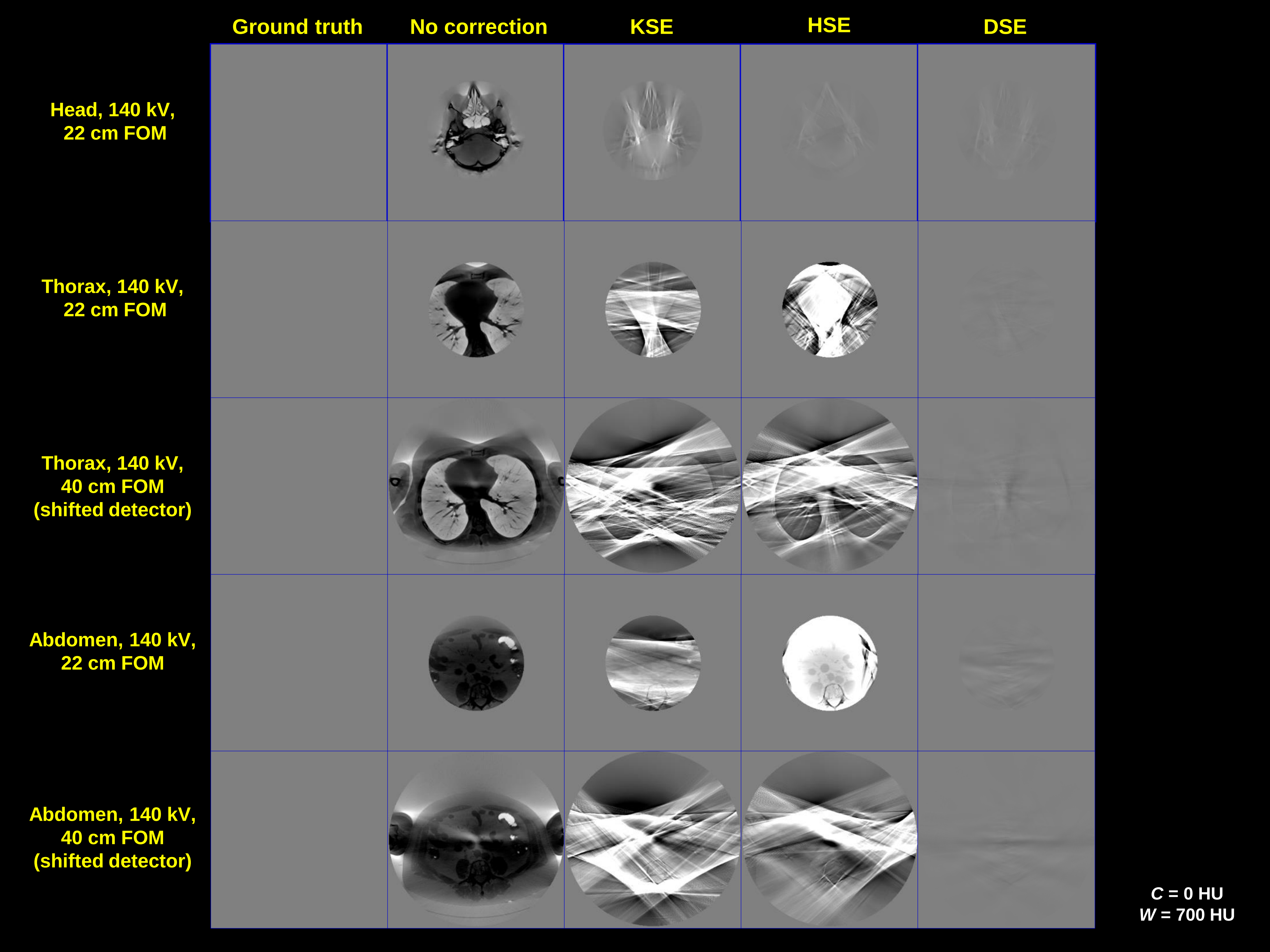

Ground truth
No correction
KSE
HSE
DSE
Head, 140 kV, 22 cm FOM
Thorax, 140 kV, 22 cm FOM
Thorax, 140 kV, 40 cm FOM (shifted detector)
Abdomen, 140 kV, 22 cm FOM
Abdomen, 140 kV, 40 cm FOM (shifted detector)
C = 0 HU
W = 700 HU

Scatter in Dual Source CT (DSCT)

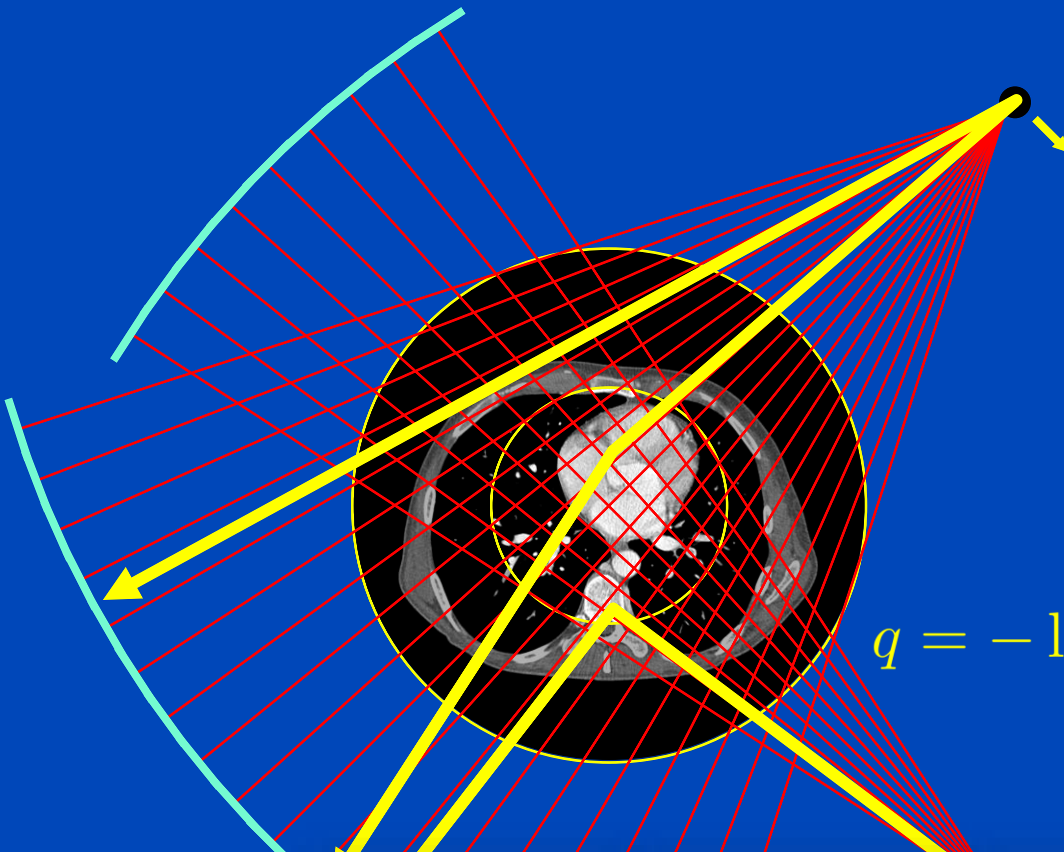

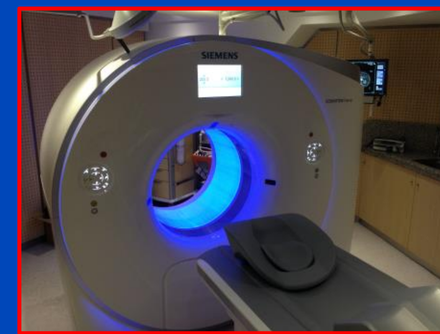

Siemens SOMATOM Force
dual source cone-beam spiral CT

$$q = -\ln \frac{I_{\text{primary}} + S_{\text{forward}} + \rho\, S_{\text{cross}}}{I_0}$$

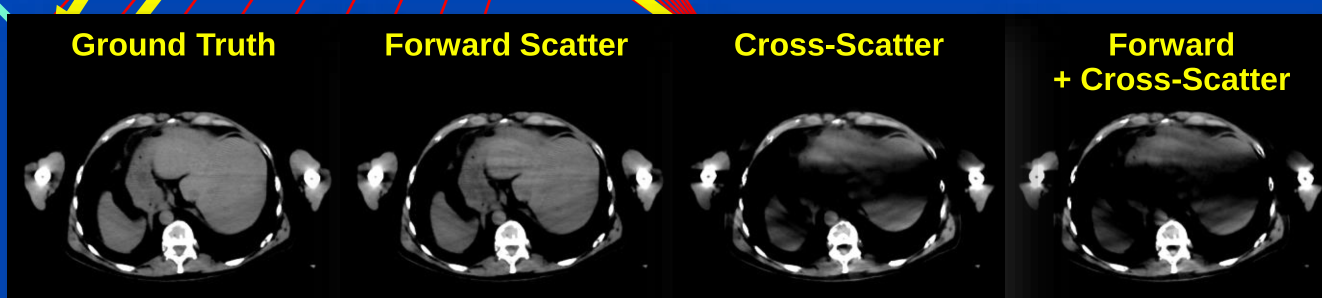

C = 40 HU, *W* = 300 HU, with 2D anti-scatter grid

J. Erath, T. Vöth, J. Maier, E. Fournié, M. Petersilka, K. Stierstorfer, and M. Kachelrieß. Deep learning-based forward and cross-scatter correction in dual source CT. Med. Phys. 48:4824–4842, July 2021.

Measurement-Based Scatter Estimation

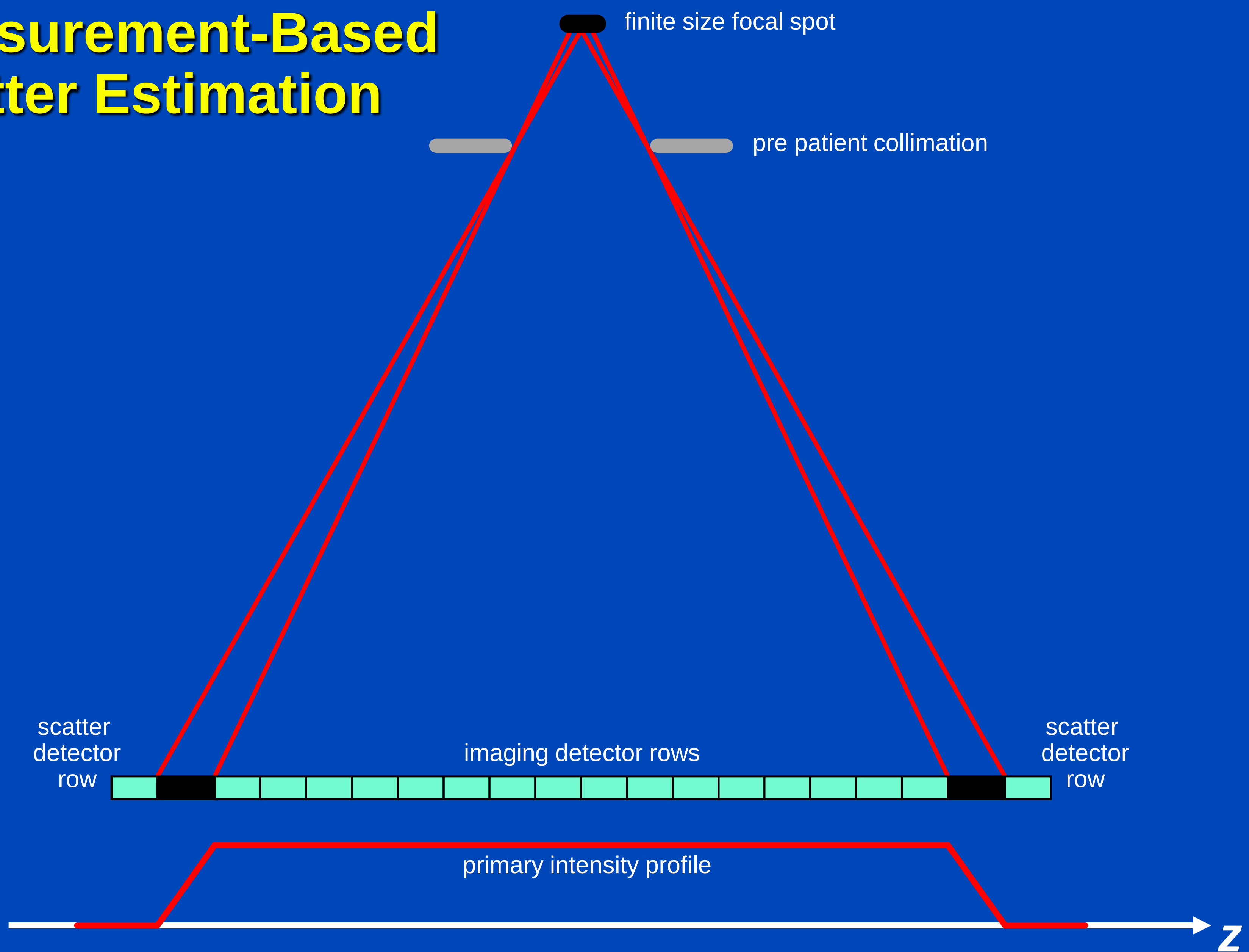

J. Erath, T. Vöth, J. Maier, E. Fournié, M. Petersilka, K. Stierstorfer, and M. Kachelrieß. Deep learning-based forward and cross-scatter correction in dual source CT. Med. Phys. 48:4824–4842, July 2021.

Cross-DSE

Ground Truth | **Uncorrected** | **xDSE (2D, xSSE)** | **Measurement-based**

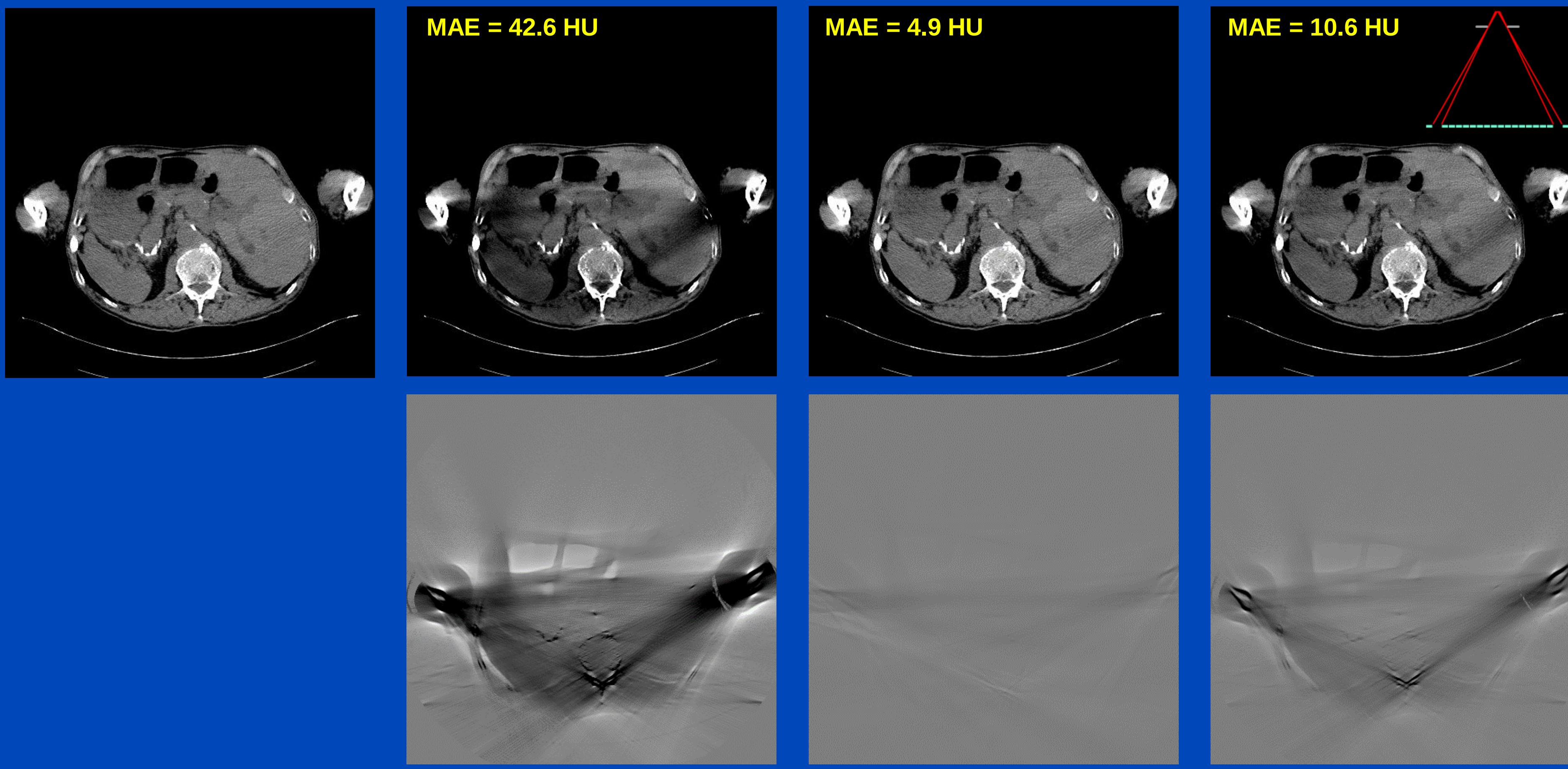

xDSE (2D, xSSE) maps

primary + forward scatter + cross-scatter + cross-scatter approximation → cross-scatter

Images *C* = 40 HU, *W* = 300 HU, difference images *C* = 0 HU, *W* = 300 HU

J. Erath, T. Vöth, J. Maier, E. Fournié, M. Petersilka, K. Stierstorfer, and M. Kachelrieß. Deep learning-based forward and cross-scatter correction in dual source CT. Med. Phys. 48:4824–4842, July 2021.

Conclusions on DSE

- DSE needs about 3 ms per CT and 10 ms per CBCT projection (as of 2020).
- DSE is a fast and accurate alternative to MC simulations.
- DSE outperforms kernel-based approaches in terms of accuracy and speed.
- Facts:
  – DSE can estimate scatter from a single (!) x-ray image.
  – DSE can accurately estimate scatter from a primary+scatter image.
  – DSE generalizes to all anatomical regions.
  – DSE works for geometries and beam qualities differing from training.
  – DSE may outperform MC even though DSE is trained with MC.
- DSE is not restricted to reproducing MC scatter estimates.
- DSE can rather be trained with any other scatter estimate, including those based on measurements.

Scatter Artifacts of Coarse ASG

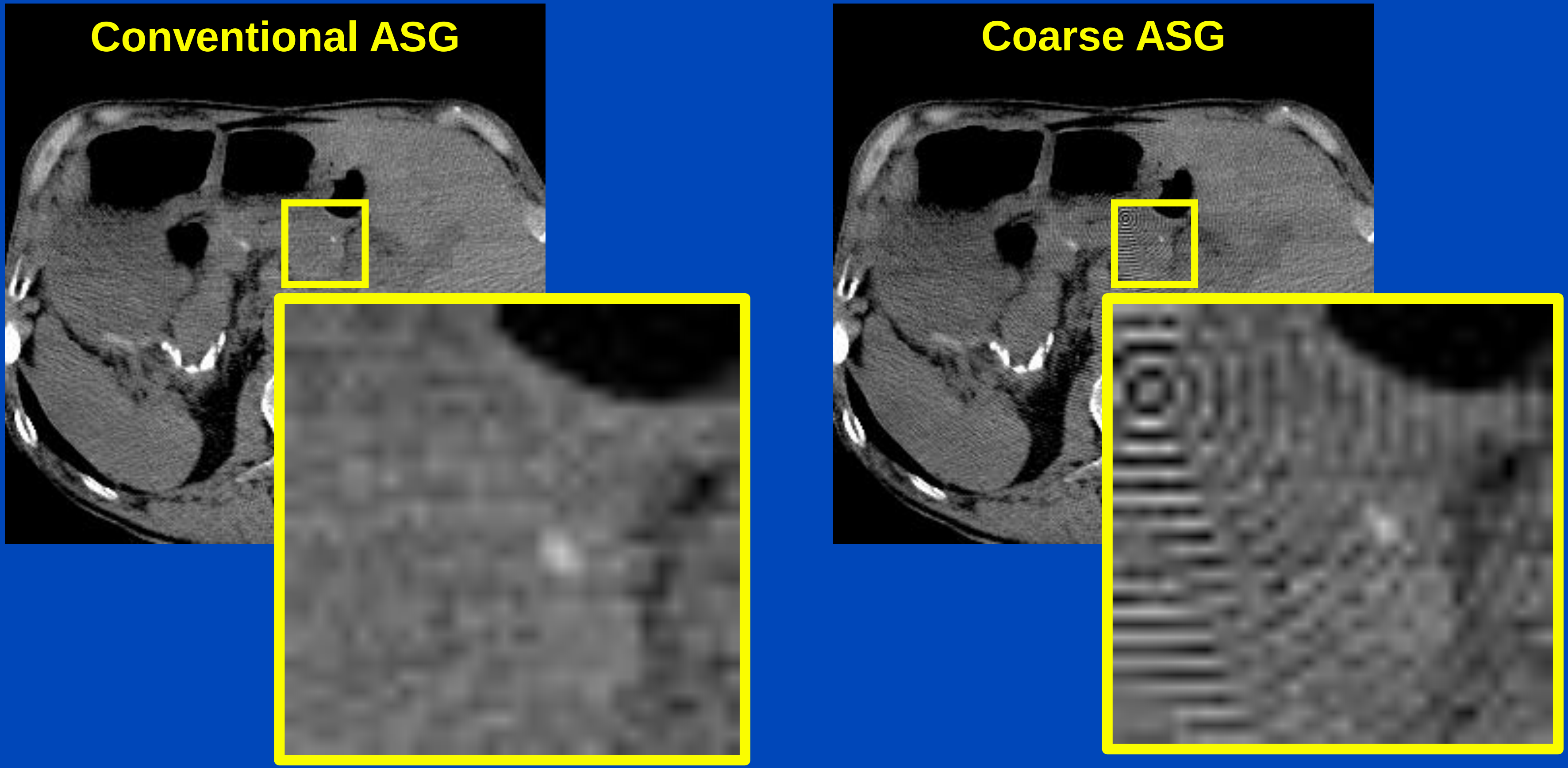

Coarse ASG can lead to scatter-induced moiré artifacts.

Scatter of Coarse ASG

Conventional ASG
Somatom Force
920 × 96 detector pixels
pixel size 0.52 × 0.56 mm at iso

Coarse ASG
Naeotom Alpha
1376 × 144 macro pixels
pixel size 0.3 × 0.352 mm at iso

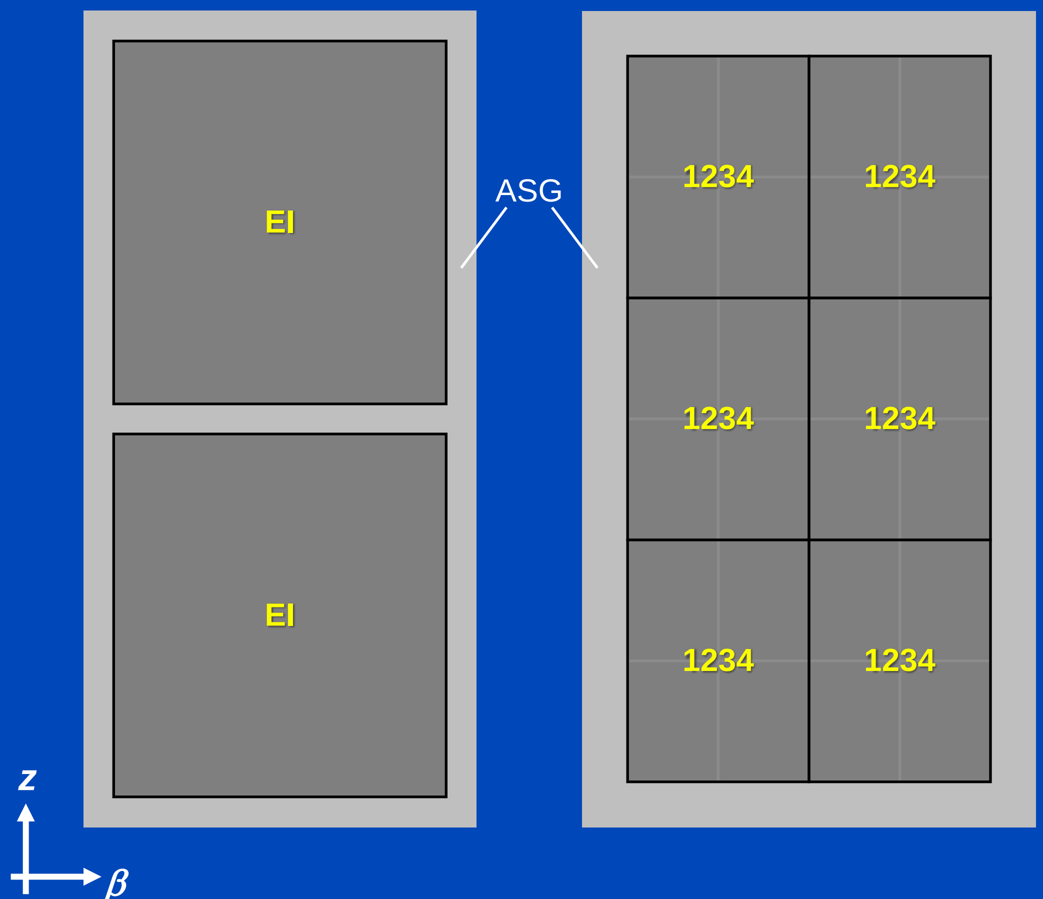

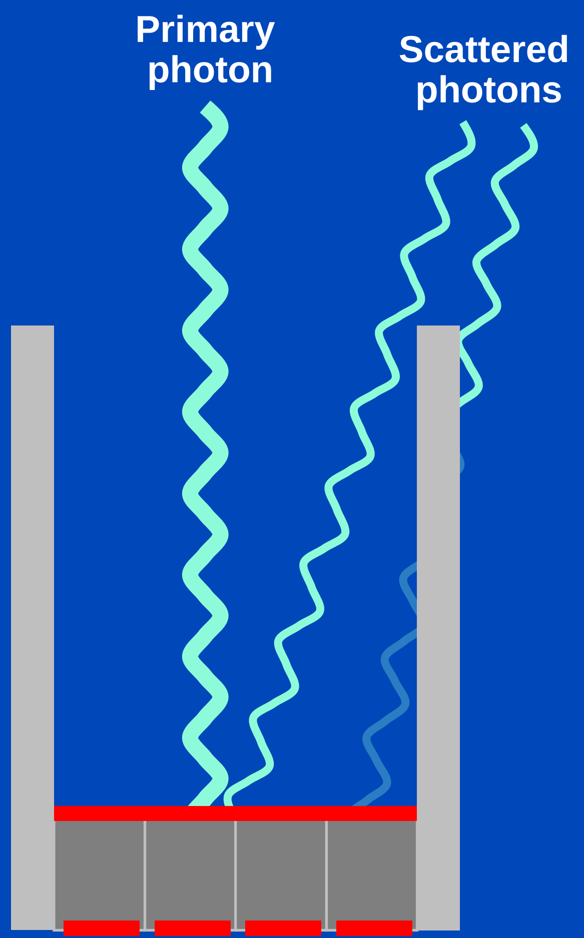

Coarse ASGs lead to changing scatter intensity between neighboring pixels.

This paper received the "Highest Impact Paper Award" for the highest impact score at the 7th International Conference on Image Formation in X-Ray Computed Tomography in June 2022

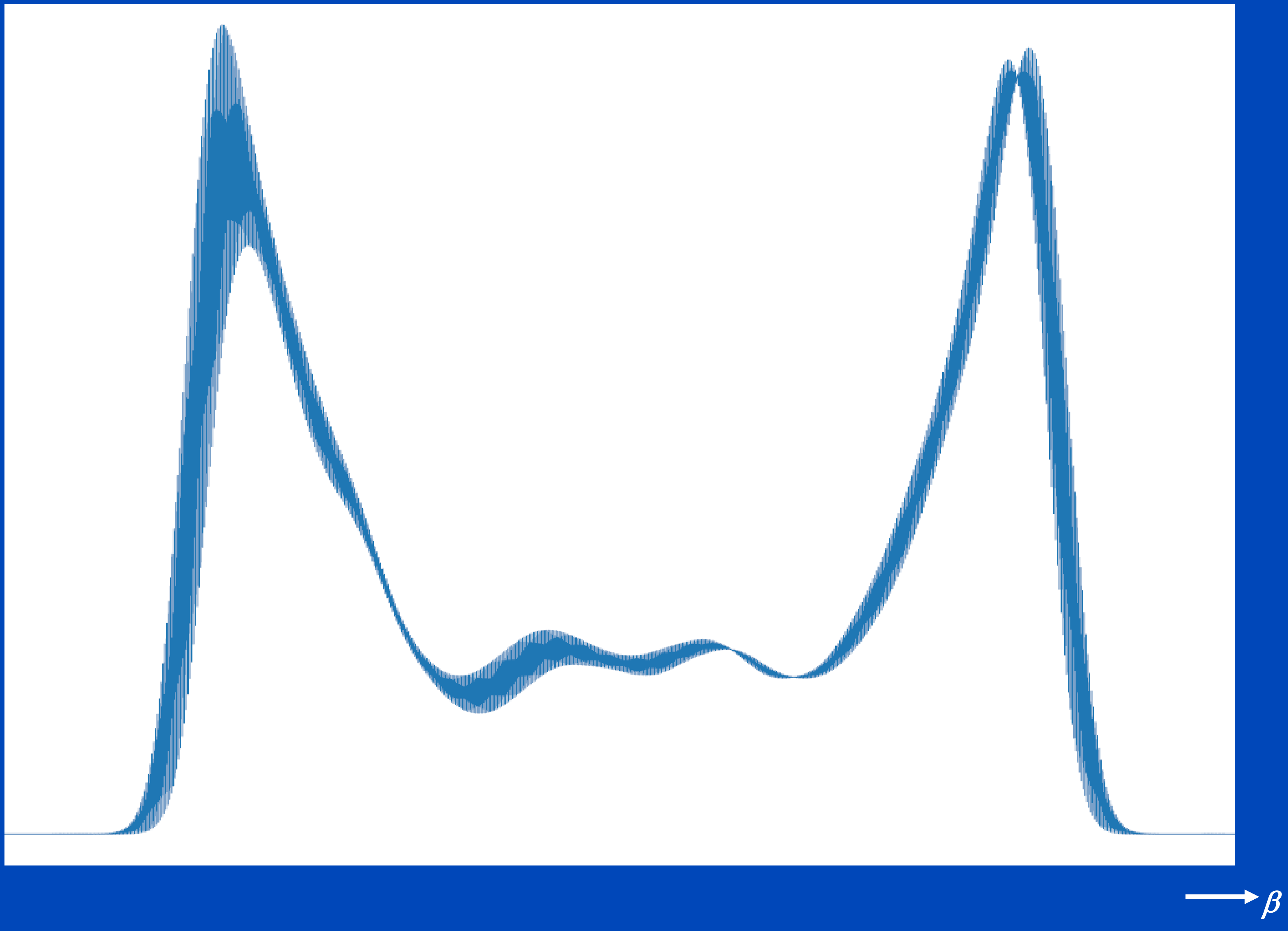

Scatter distribution averaged over all detector rows

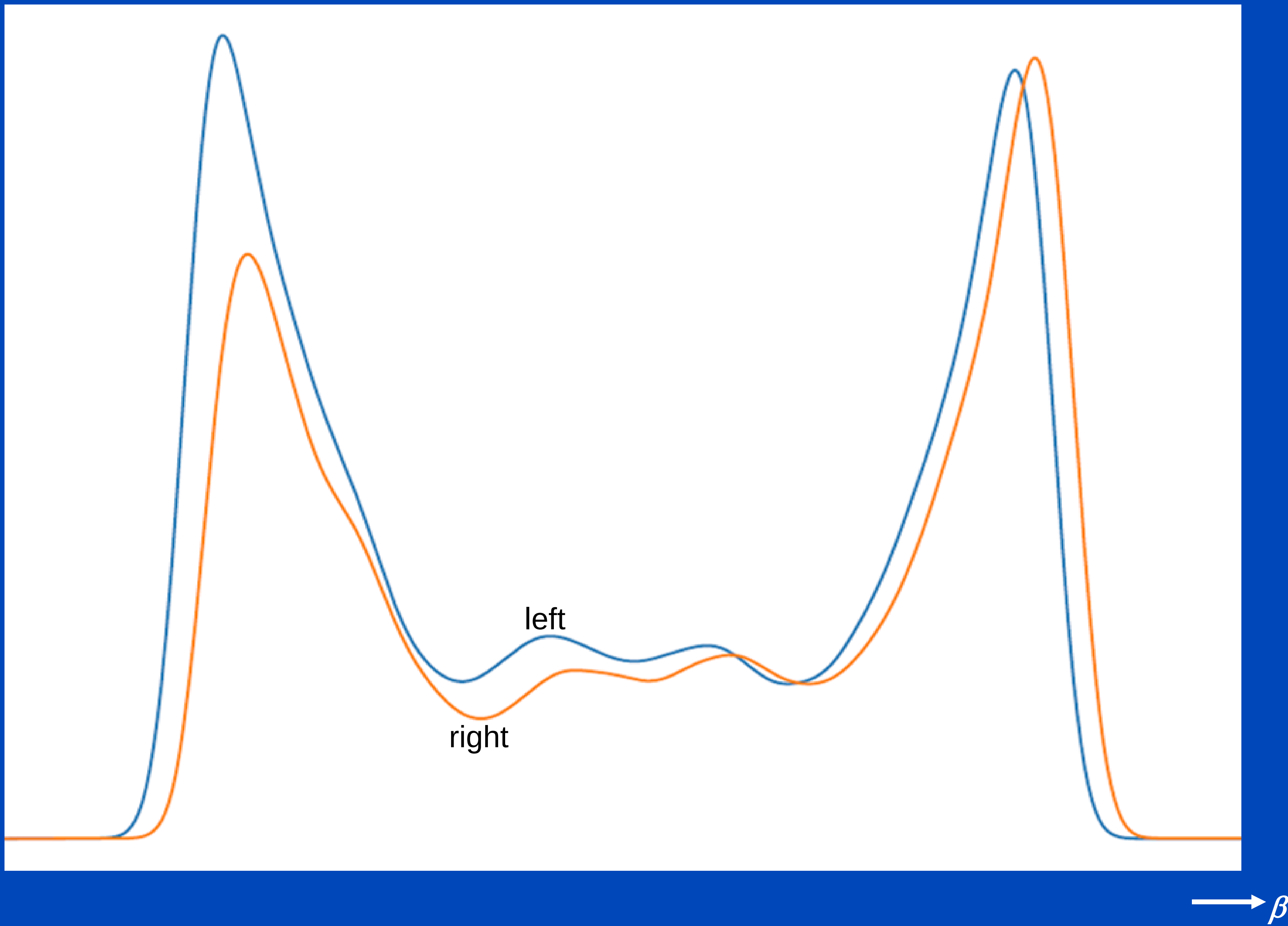

Scatter distribution averaged over all detector rows

Training and Validation Data

- **Monte Carlo simulation** with the geometry of the photon counting CT scanner NAEOTOM Alpha (Siemens Healthineers)
- 12 patients for training and 4 for validation
- 14 z-positions with 36 projections each simulated for each patient
- **8064 paired** scatter and primary **data pairs**
- Simulation of coarse ASG with macro pixel with detector dimension of **1376 × 144 pixels**
- 6 different macro pixels locations
- Smooth only across same macro-pixel locations

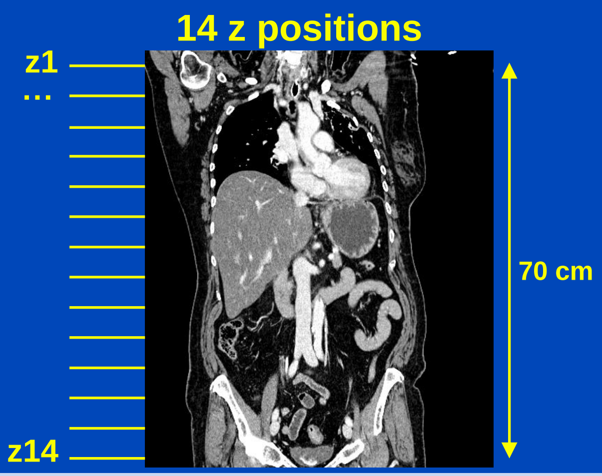

Training and validation patients with high variety and different clinical situations, important to consider **scatter-to-primary ratio**

Example of validation data set:

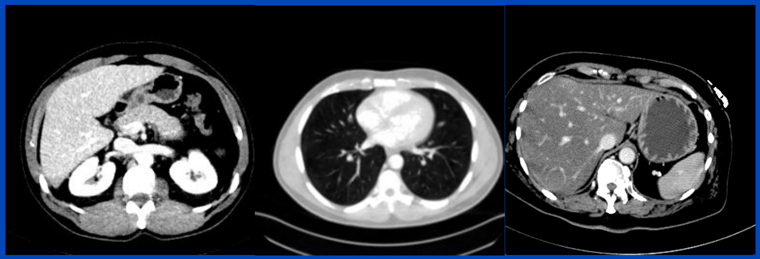

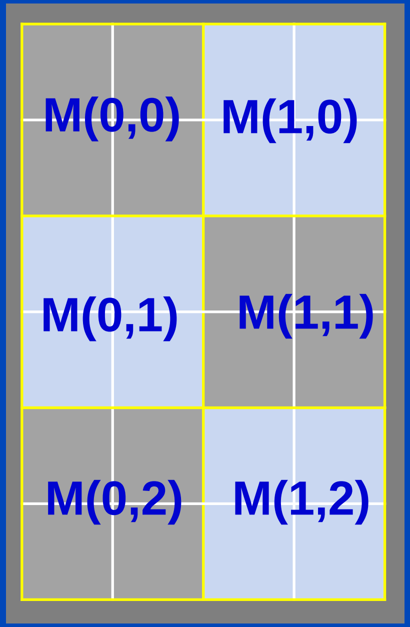

DSE for coarse ASG

Detector dimension
1376×144
Input mapping

$$p = -\ln\left(\frac{I_{\text{primary}}}{I_0} + \frac{I_{\text{scatter}}}{I_0}\right)$$

Each channel corresponds to a different pixel position between the lamallea of the ASG

Merging 6 different channels to obtain total scatter correction term

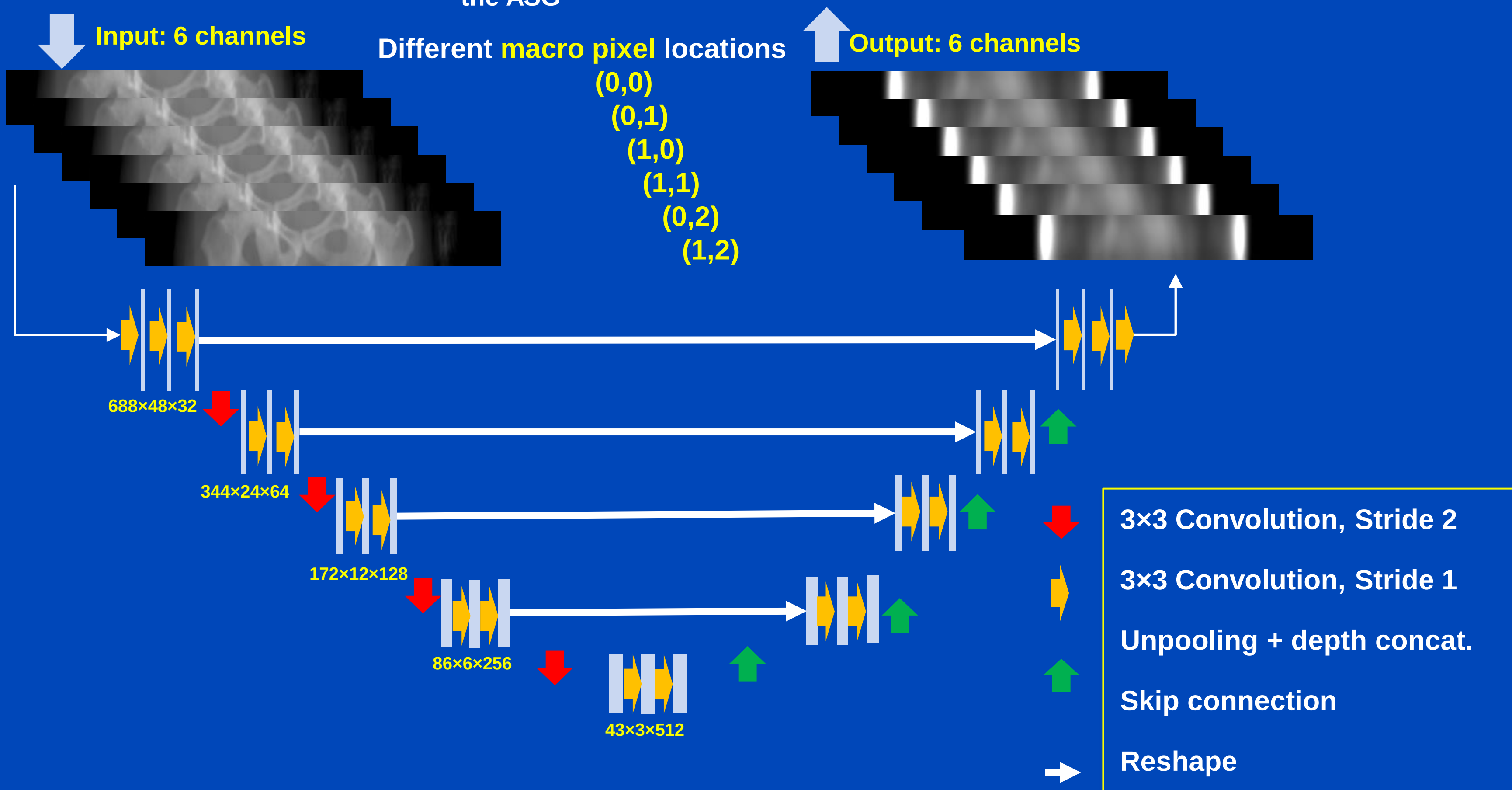

This paper received the "Highest Impact Paper Award" for the highest impact score at the 7th International Conference on Image Formation in X-Ray Computed Tomography in June 2022

Results in Reconstructed Images

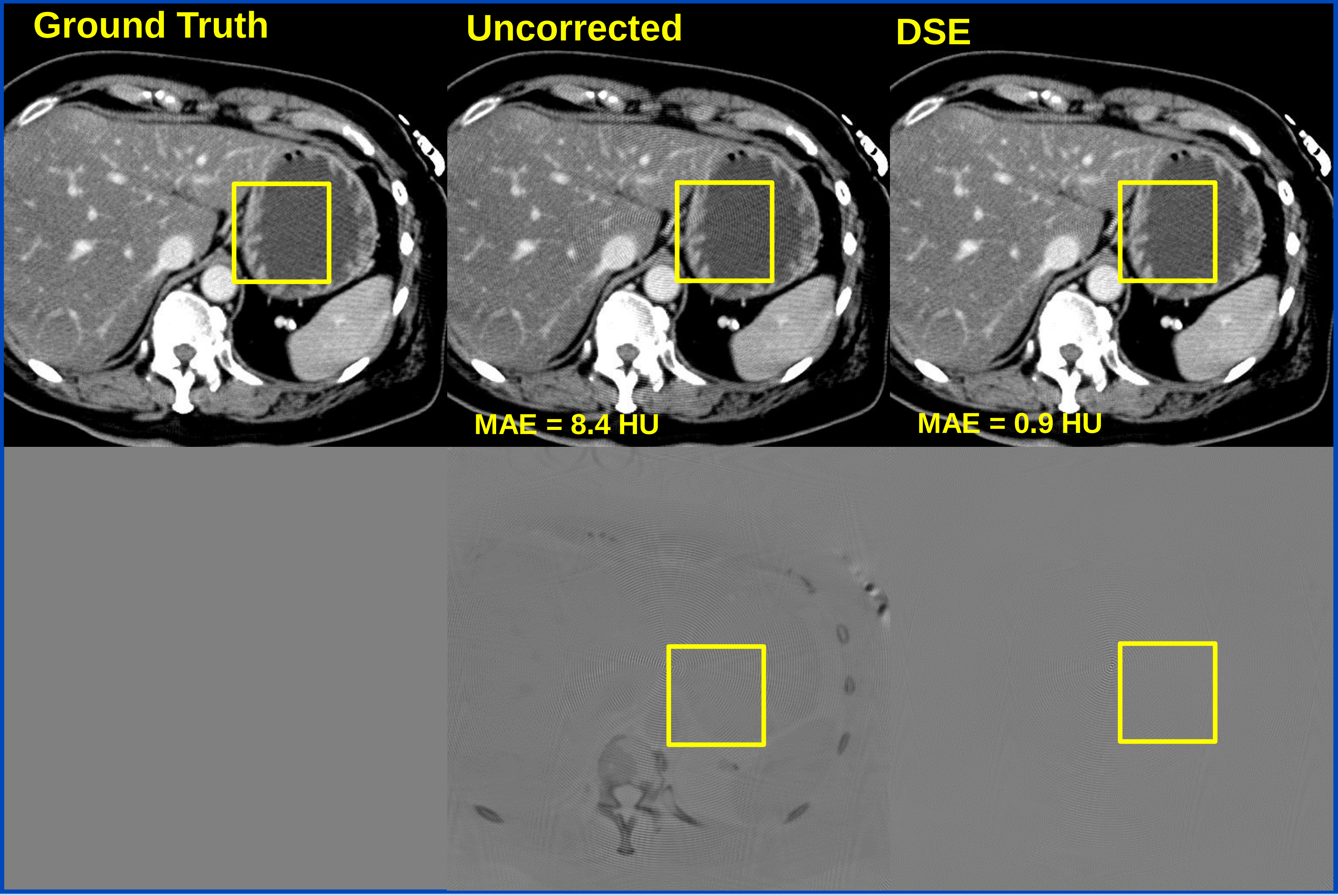

Simulated Reconstruction C = 0 HU, W = 400 HU,
Difference to GT C = 0 HU, W = 50 HU

Results in Reconstructed Images

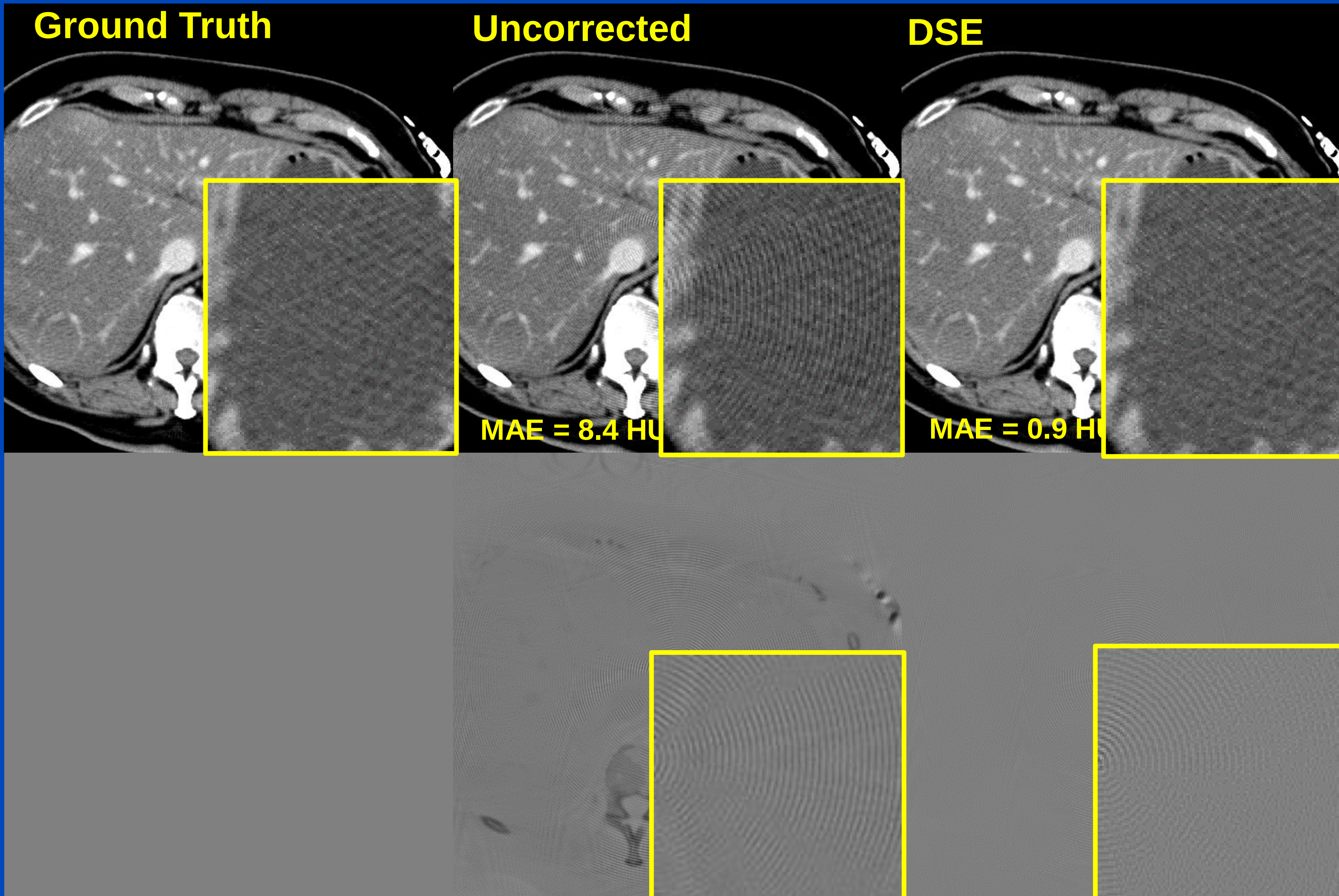

Simulated Reconstruction C = 0 HU, W = 400 HU,
Difference to GT C = 0 HU, W = 50 HU

Results in Reconstructed Images

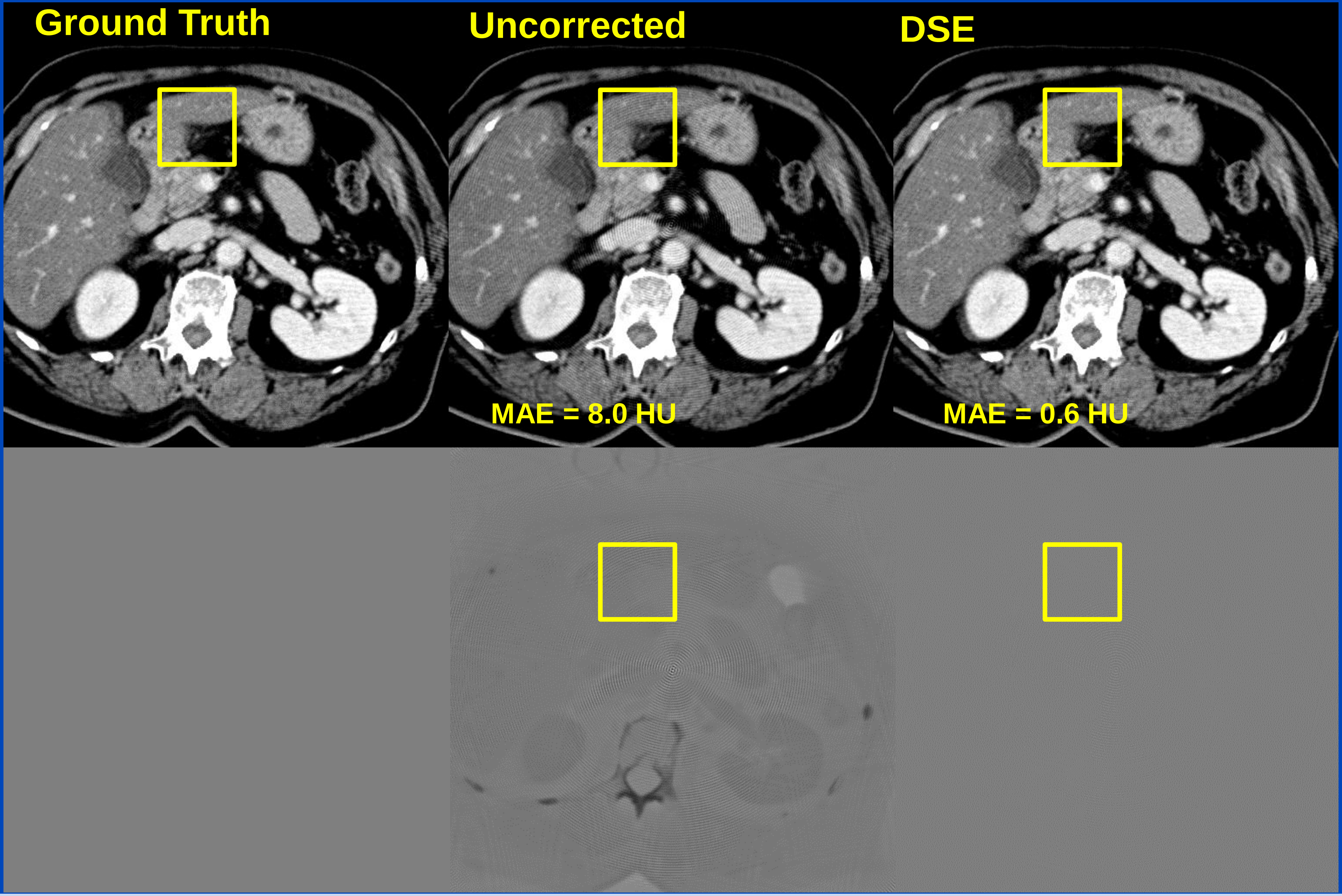

Simulated Reconstruction C = 0 HU, W = 400 HU,
Difference to GT C = 0 HU, W = 50 HU

Results in Reconstructed Images

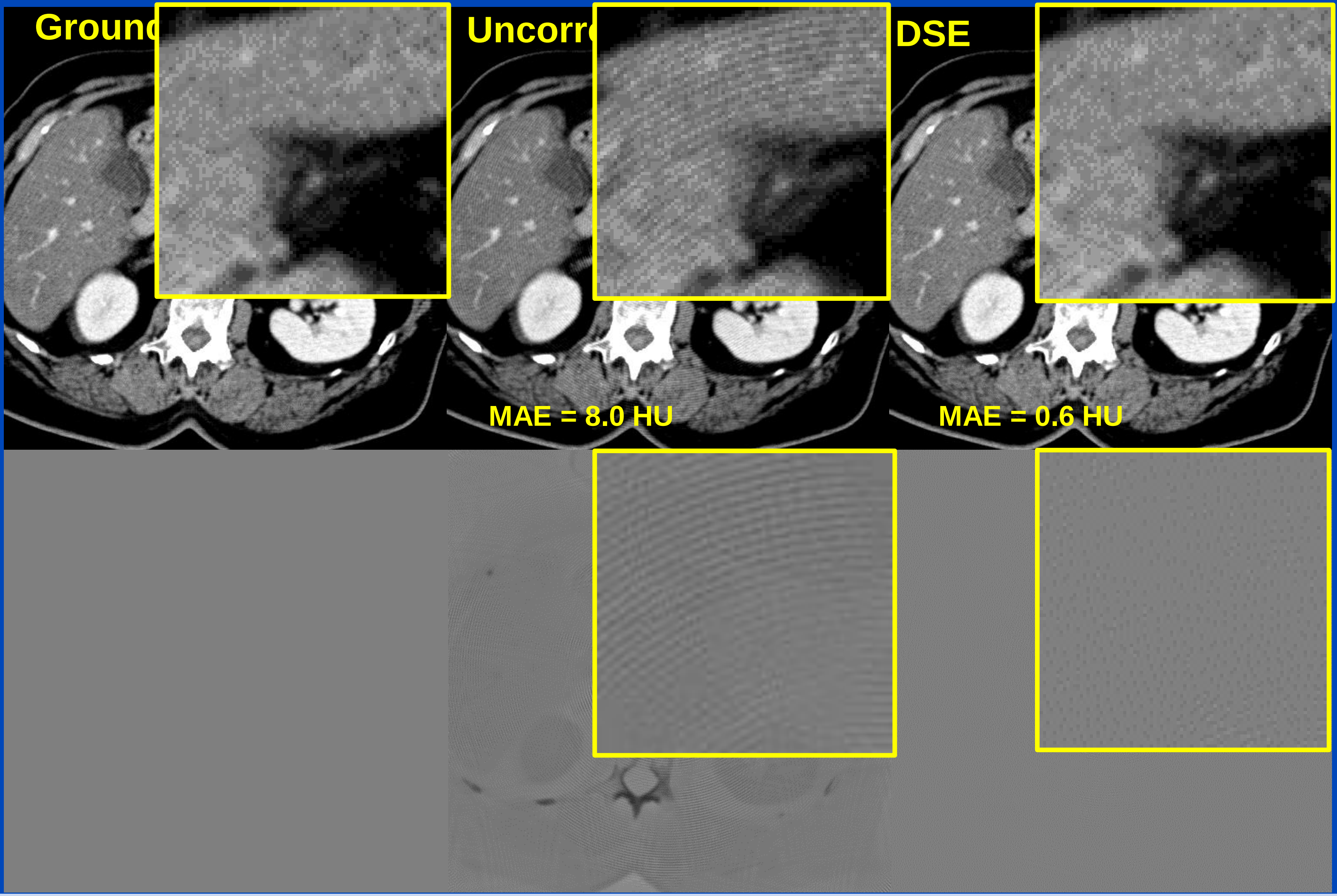

Simulated Reconstruction C = 0 HU, W = 400 HU,
Difference to GT C = 0 HU, W = 50 HU

Conclusions

- Coarse anti-scatter grid can lead to moiré artifacts due to scattered radiation.
- DSE reduces the mean absolute error (MAE) from about 9 HU to under 1 HU.
- The moiré pattern‘s amplitude can be reduced from 30 HU to less than 5 HU.

Deep Dose Estimation

???

In real time?

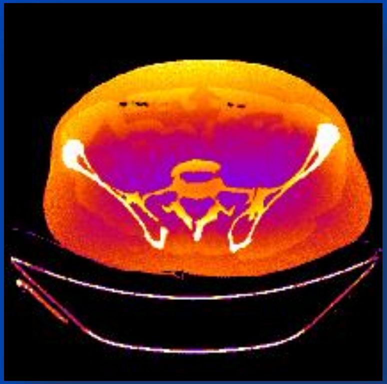

Estimation of Dose Distributions

- **Useful to study dose reduction techniques**
  - Tube current modulation
  - Prefiltration and shaped filtration
  - Tube voltage settings
  - …
- **Useful to estimate patient dose**
  - Risk assessment requires segmentation of the organs (difficult)
  - Often semiantropomorphic patient models take over
  - The infamous k-factors that convert DLP into D_{eff} are derived this way, e.g. k_{chest} = 0.014 mSv/mGy/cm
  - …
- **Could be useful for patient-specific CT scan protocol optimization**
- **However: Dose estimation does not work in real time!**

J. Maier, L. Klein, E. Eulig, S. Sawall, and M. Kachelrieß. Real-time estimation of patient-specific dose distributions for medical CT using the deep dose estimation. Med. Phys. 49(4):2259-2269, April 2022. *Best Paper within Machine Learning at ECR 2019!*

Motivation

- The potential risk of ionizing radiation makes dose assessment an important issue in CT imaging.
- Limitation of common metrics (e.g. $CTDI_w$, $CTDI_{vol}$, DLP, k-factor, SSDE, …) to provide information on organ or patient dose.

CTDI phantom | Small patient | Medium patient | Large patient

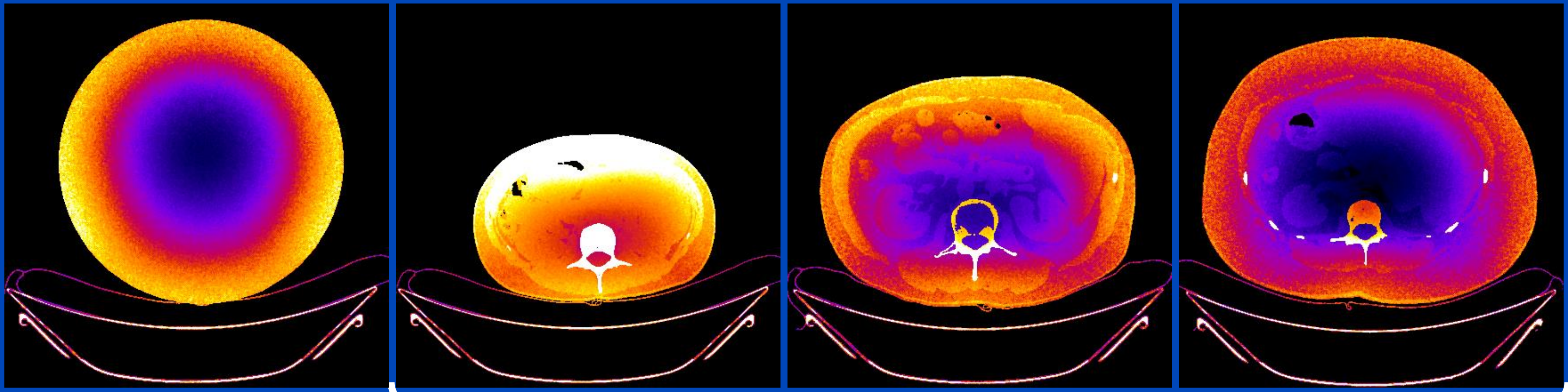

Same CTDI, but different dose distribution

Dose values in air voxels are set to zero (black) in this presentation.

MC Dose Simulation for a 360° Scan

1 to 10 hours
per tomographic data set

J. Maier, L. Klein, E. Eulig, S. Sawall, and M. Kachelrieß. Real-time estimation of patient-specific dose distributions for medical CT using the deep dose estimation. Med. Phys. 49(4):2259-2269, April 2022. *Best Paper within Machine Learning at ECR 2019!*

Influence of Bowtie Filter

- Commercial CT-scanners are usually equipped with a bowtie filter in order to optimize the patient dose distribution.
- Monte-Carlo dose calculations or statistical reconstruction algorithms require exact knowledge of the bowtie filter.
- The shape as well as the composition of the bowtie filter is usually not disclosed by the CT vendors.

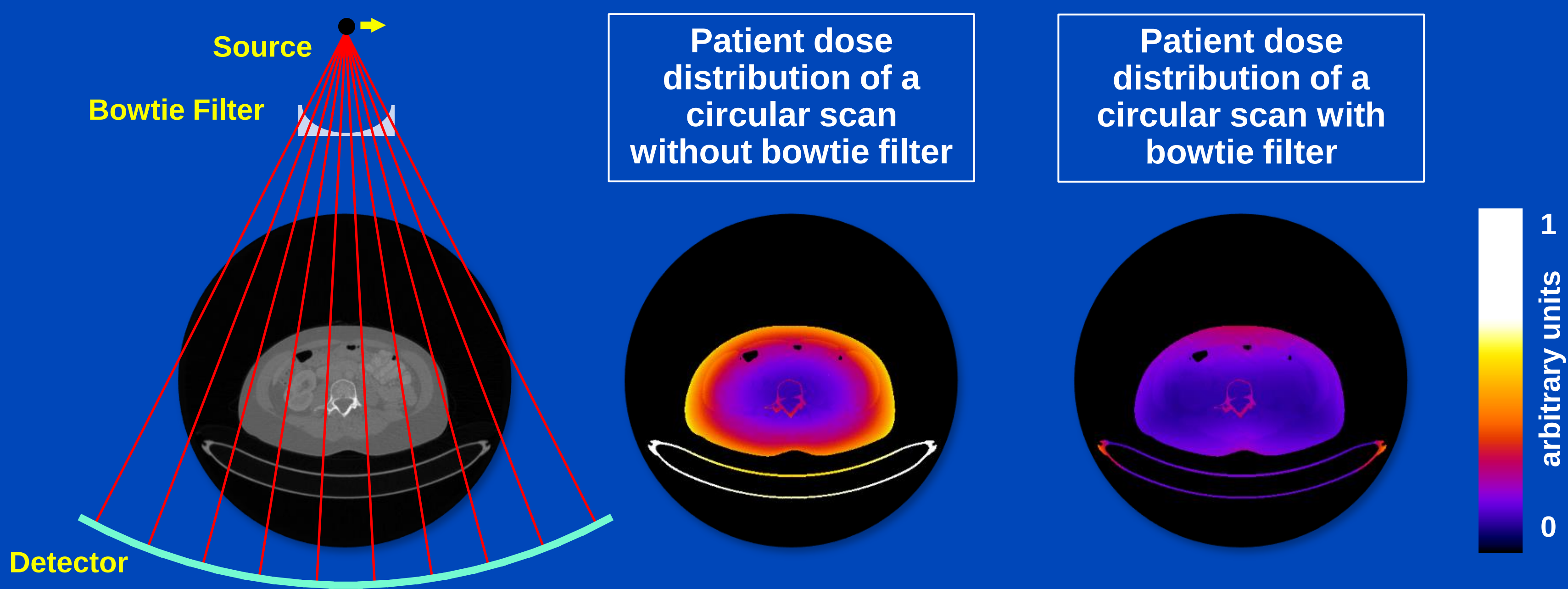

J. Maier, L. Klein, E. Eulig, S. Sawall, and M. Kachelrieß. Real-time estimation of patient-specific dose distributions for medical CT using the deep dose estimation. Med. Phys. 49(4):2259-2269, April 2022. *Best Paper within Machine Learning at ECR 2019!*

Patient-Specific Dose Estimation

- **Accurate solutions:**
  - Monte Carlo (MC) simulation[1], gold standard, stochastic LBTE solver
  - Analytic linear Boltzmann transport equation (LBTE) solver[2]

  → **Accurate but computationally expensive**

- **Fast alternatives:**
  - Application of patient-specific conversion factors to the DLP[3].
  - Application of look-up tables using MC simulations of phantoms[4].
  - Analytic approximation of CT dose deposition[5].

  → **Fast but less accurate**

[1]G. Jarry et al., "A Monte Carlo-based method to estimate radiation dose from spiral CT", Phys. Med. Biol. 48, 2003.
[2]A. Wang et al., "A fast, linear Boltzmann transport equation solver for computed tomography dose calculation (Acuros CTD)". Med. Phys. 46(2), 2019.
[3]B. Moore et al., "Size-specific dose estimate (SSDE) provides a simple method to calculate organ dose for pediatric CT examinations", Med. Phys. 41, 2014.
[4]A. Ding et al., "VirtualDose: a software for reporting organ doses from CT for adult and pediatric patients", Phys. Med. Biol. 60, 2015.
[5]B. De Man, "Dose reconstruction for real-time patient-specific dose estimation in CT", Med. Phys. 42, 2015.

Deep Dose Estimation (DDE)

- Train a UNet to predict patient dose given a CT image and a photo effect dose image
- Training data
  - 15 CT patient data sets segmented into air, fat, soft tissue, and bone
  - Simulate projection data by forward projection (120 kV, 720 projections, circle scans at 20 different z-positions to equally cover pelvis, abdomen, thorax and head).
  - Simulate scans without bowtie, with botwie, with bowtie and TCM
  - In total 15×20×3 = 900 data sets are reconstructed
  - Use Monte Carlo software RayConStruct-MC to calculate the patient dose distribution, thereby accounting for Rayleigh, Compton and photo effect.
  - Calculate photo effect dose distribution by direct backprojection and energy deposition in each voxel
- Training
  - U-Net sees the CT volumes and the corresponding first order (photoeffect) dose volumes and is trained to predict the patient dose distribution.
  - Since bone is underrepresented in all of the data sets, bone voxels received a twenty-fold weight in our MSE-based pixel-wise loss function

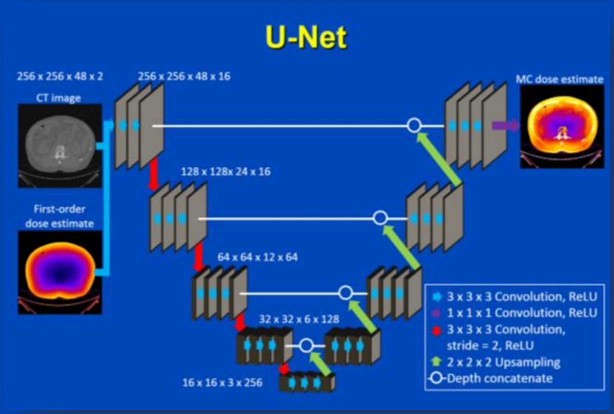

J. Maier, L. Klein, E. Eulig, S. Sawall, and M. Kachelrieß. Real-time estimation of patient-specific dose distributions for medical CT using the deep dose estimation. Med. Phys. 49(4):2259-2269, April 2022. *Best Paper within Machine Learning at ECR 2019!*

Deep Dose Estimation (DDE)

- Combine fast and accurate CT dose estimation using a deep convolutional neural network.
- Train the network to re… …mates given the CT … …mate.

1 to 10 seconds per tomographic data set

2-channel …

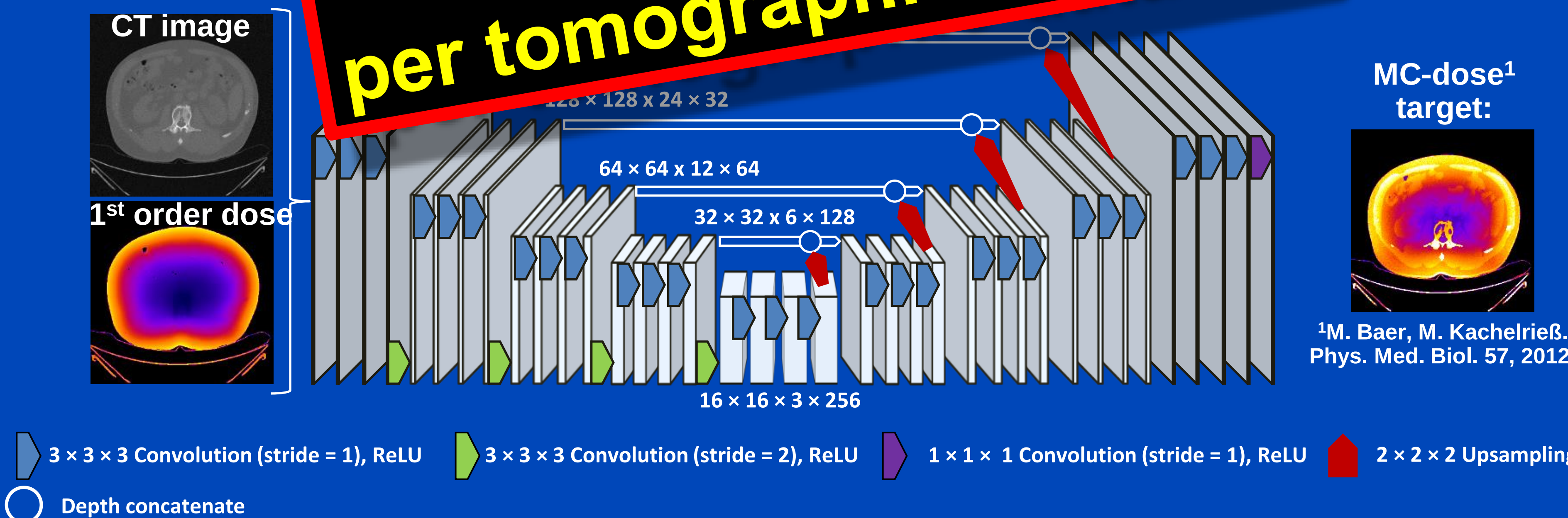

J. Maier, L. Klein, E. Eulig, S. Sawall, and M. Kachelrieß. Real-time estimation of patient-specific dose distributions for medical CT using the deep dose estimation. Med. Phys. 49(4):2259-2269, April 2022. *Best Paper within Machine Learning at ECR 2019!*

Results

Thorax, tube A, 120 kV, no bowtie

CT image

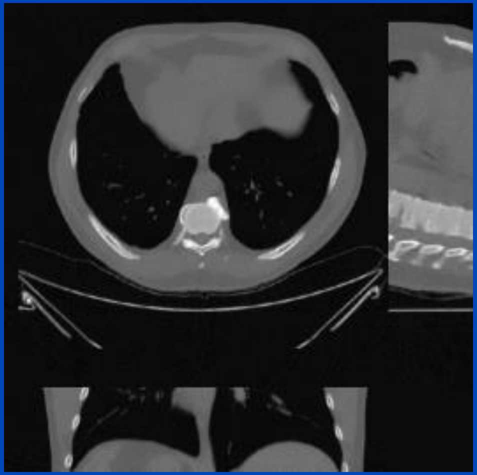

First order dose

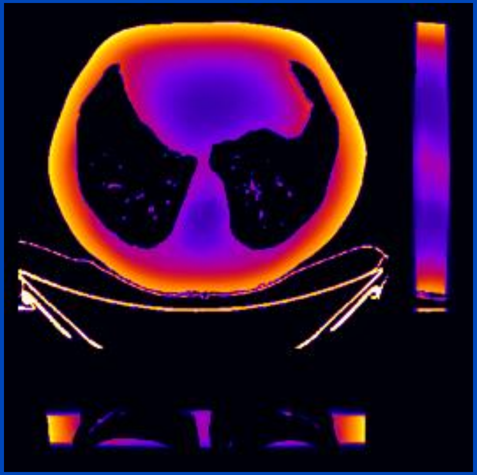

	MC	DDE
48 slices	1 h	0.25 s
whole body	20 h	5 s

MC uses 16 CPU kernels
DDE uses one Nvidia Quadro P600 GPU

DDE training took 74 h for 300 epochs, 1440 samples, 48 slices per sample

MC ground truth

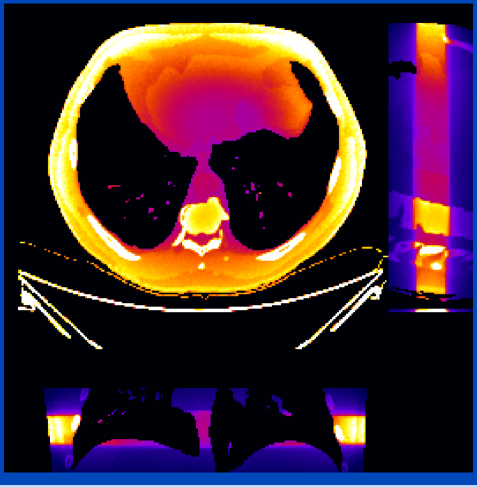

DDE

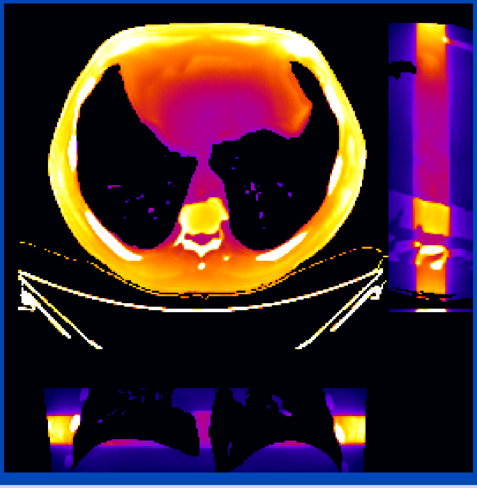

Relative error

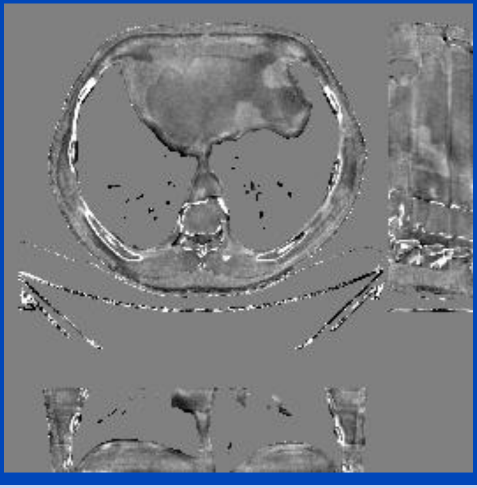

C = 0%
W = 40%

J. Maier, L. Klein, E. Eulig, S. Sawall, and M. Kachelrieß. Real-time estimation of patient-specific dose distributions for medical CT using the deep dose estimation. Med. Phys. 49(4):2259-2269, April 2022. *Best Paper within Machine Learning at ECR 2019!*

Results

Abdomen, tube A, 120 kV, no bowtie

CT image

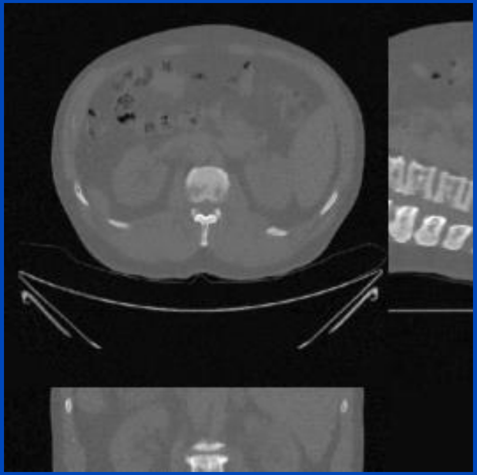

First order dose

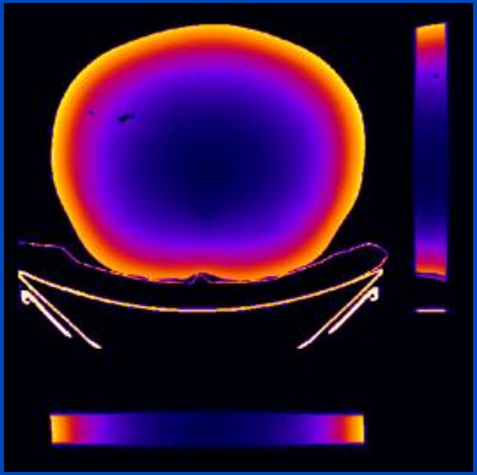

	MC	DDE
48 slices	1 h	0.25 s
whole body	20 h	5 s

MC uses 16 CPU kernels
DDE uses one Nvidia Quadro P600 GPU

DDE training took 74 h for 300 epochs, 1440 samples, 48 slices per sample

MC ground truth

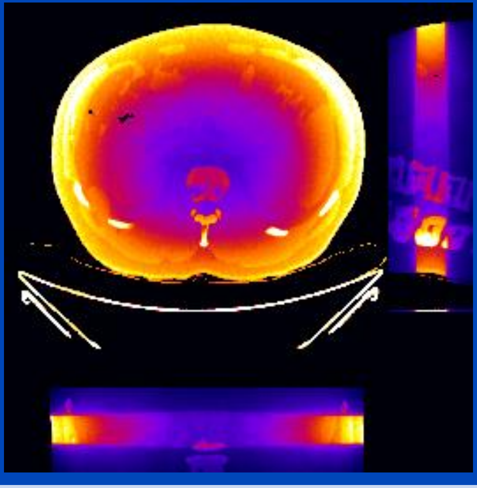

DDE

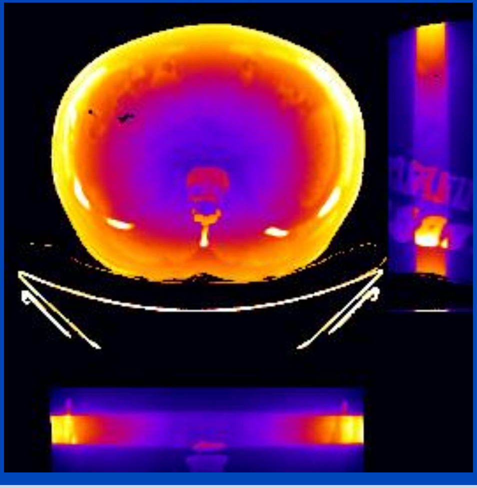

Relative error

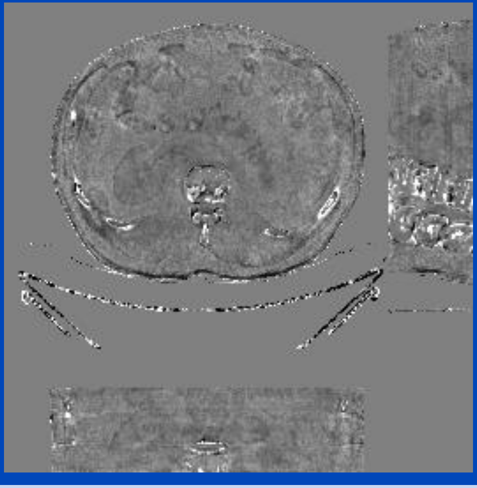

C = 0%
W = 40%

J. Maier, L. Klein, E. Eulig, S. Sawall, and M. Kachelrieß. Real-time estimation of patient-specific dose distributions for medical CT using the deep dose estimation. Med. Phys. 49(4):2259-2269, April 2022. *Best Paper within Machine Learning at ECR 2019!*

DDE's Organ Dose and D_{eff} MAPEs

Organ and ICRP weight		80 kV	100 kV	120 kV
Bone marrow	0.12	5.2%	6.7%	7.1%
Bone surface	0.01	5.7%	7.0%	7.2%
Brain	0.01	5.1%	4.9%	5.3%
Breast	0.12	1.0%	1.4%	2.1%
Colon	0.12	0.9%	1.7%	1.9%
Esophagus	0.04	1.3%	2.4%	2.3%
Gonads	0.08	3.2%	2.7%	2.2%
Liver	0.04	2.9%	1.1%	0.8%
Lung	0.12	1.7%	3.5%	4.0%
Remainder	0.12	0.9%	1.9%	2.3%
Salivary glands	0.01	4.9%	5.1%	5.3%
Skin	0.01	2.8%	3.3%	4.2%
Stomach	0.12	2.3%	1.1%	0.8%
Thyroid gland	0.04	3.1%	3.0%	2.3%
Urinary bladder	0.04	1.7%	1.7%	1.3%
Effective dose		**1.2%**	**2.5%**	**2.7%**

Weighting factors and mean absolute percentage error of the DDE organ dose values with respect to the ground truth Monte Carlo organ dose values.

Conclusions on DDE

- DDE provides accurate dose predictions
  - for circle scans
  - for sequence scans
  - for partial scans (less than 360°)
  - for limited angle scans (less than 180°)
  - for spiral scans
  - for different tube voltages
  - for scans with and without bowtie filtration
  - for scans with tube current modulation
  - for DSCT scanners, i.e. with large (A) and small (B) detector
- In practice it may therefore be not necessary to perform separate training runs for these cases.
- Thus, accurate real-time patient dose estimation may become feasible with DDE.

J. Maier, L. Klein, E. Eulig, S. Sawall, and M. Kachelrieß. Real-time estimation of patient-specific dose distributions for medical CT using the deep dose estimation. Med. Phys. 49(4):2259-2269, April 2022. *Best Paper within Machine Learning at ECR 2019!*

Patient Risk-Minimizing Tube Current Modulation

1. **Coarse reconstruction from two scout views**
   – E.g. X. Ying, et al. X2CT-GAN: Reconstructing CT from biplanar x-rays with generative adversarial networks. CVPR 2019.
2. **Segmentation of radiation-sensitive organs**
   – E.g. S. Chen, M. Kachelrieß et al., Automatic multi-organ segmentation in dual-energy CT (DECT) with dedicated 3D fully convolutional DECT networks. Med. Phys. 2019.
3. **Calculation of the effective dose per view using the deep dose estimation (DDE)**
   – J. Maier, E. Eulig, S. Dorn, S. Sawall and M. Kachelrieß. Real-time patient-specific CT dose estimation using a deep convolutional neural network. IEEE Medical Imaging Conference Record, M-03-178: 3 pages, Nov. 2018.
4. **Determination of the tube current modulation curve that minimizes the radiation risk**
   – L. Klein, C. Liu, J. Steidel, L. Enzmann, M. Knaup, S. Sawall, A. Maier, M. Lell, J. Maier, and M. Kachelrieß. Patient-specific radiation risk-based tube current modulation for diagnostic CT. Med. Phys. 49(7):4391-4403, July 2022.

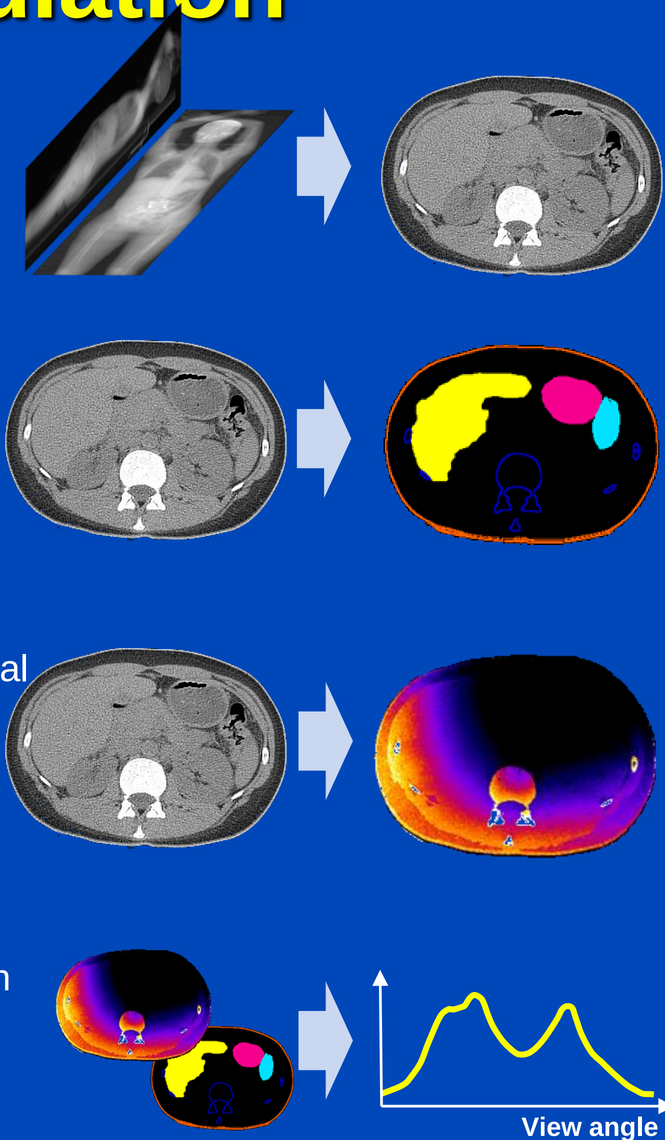

[1]L. Klein, C. Liu, J. Steidel, L. Enzmann, M. Knaup, S. Sawall, A. Maier, M. Lell, J. Maier, and M. Kachelrieß.
Patient-specific radiation risk-based tube current modulation for diagnostic CT. Med. Phys. 49(7):4391-4403, July 2022.

riskTCM Recognition

- Editor's Choice in Medical Physics 2022
- Best Research Presentation Award within the topic Physics in Medical Imaging at the European Congress of Radiology (ECR) 2022
- Moses&Sylvia Greenfield Award 2023 for the best scientific paper on imaging in Medical Physics in 2022 (AAPM)

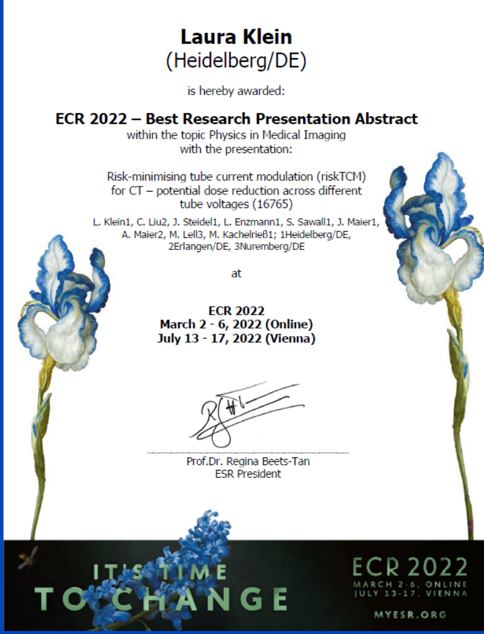

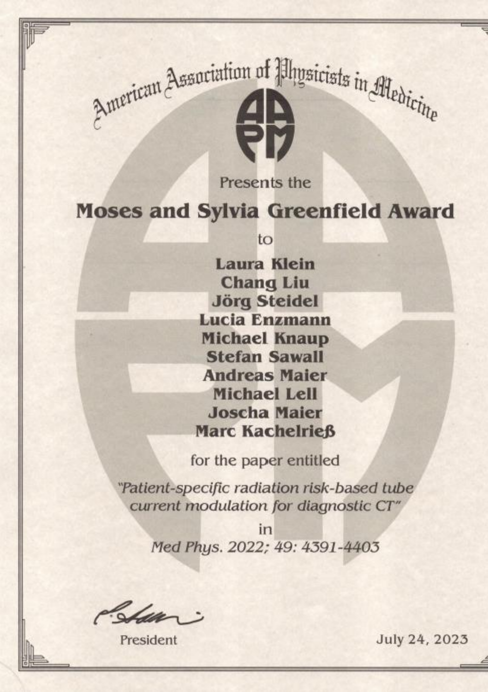

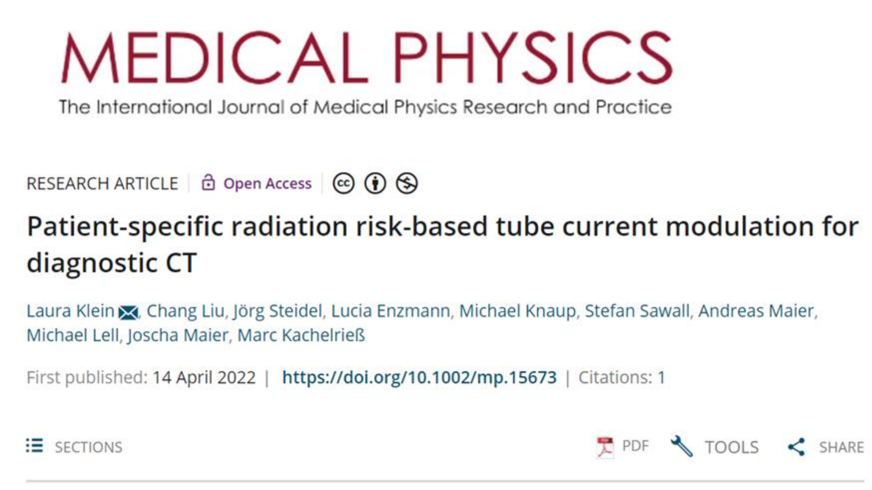

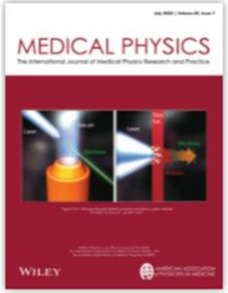

dkfz.

Patient 03 - Neck

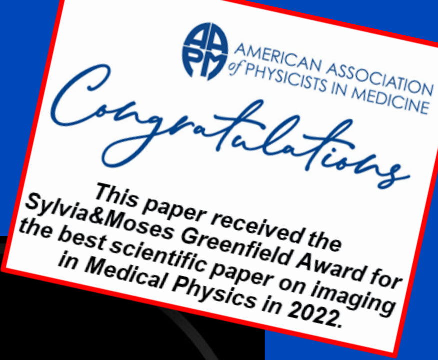

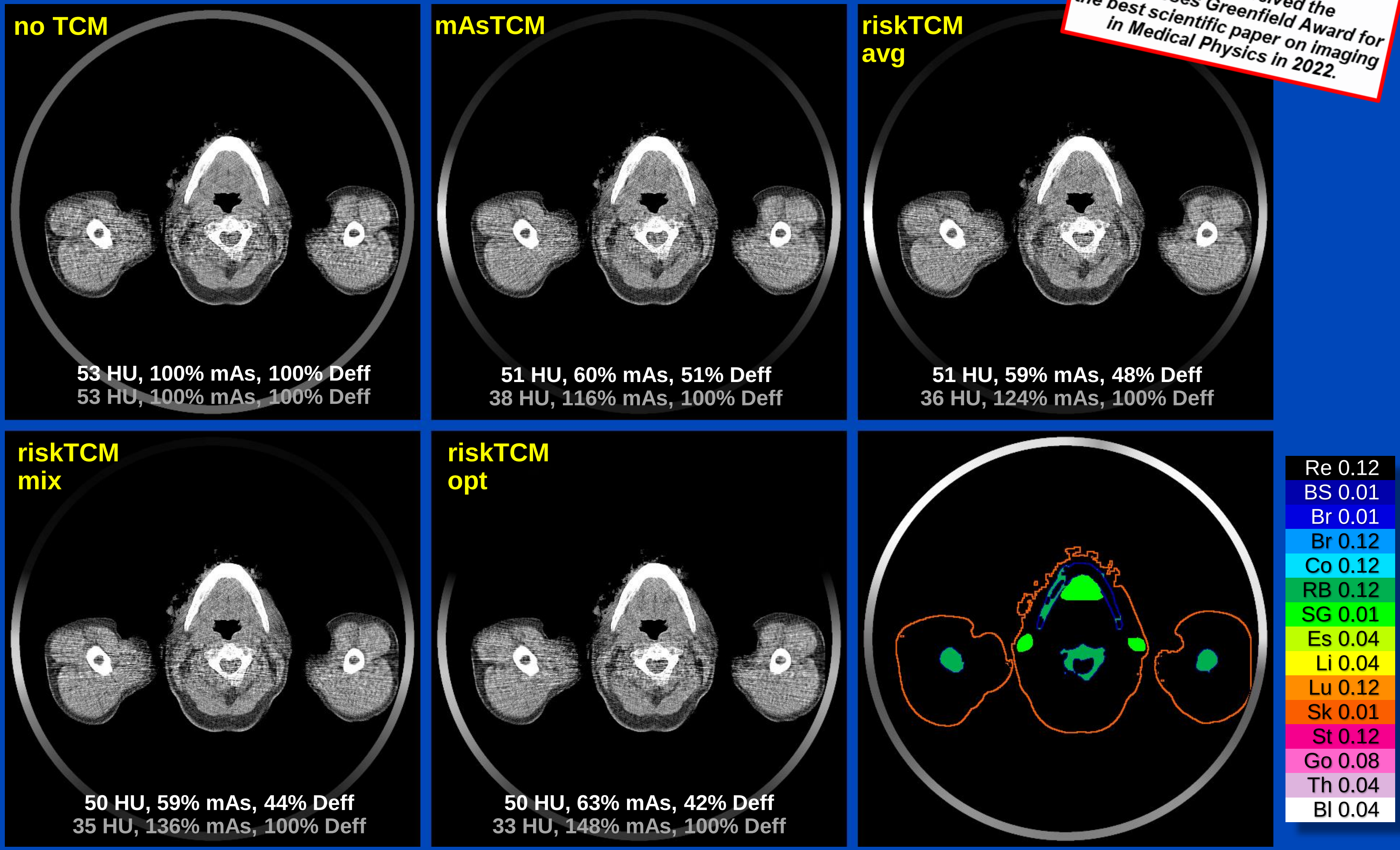

C = 25 HU, *W* = 400 HU

[1]L. Klein, C. Liu, J. Steidel, L. Enzmann, M. Knaup, S. Sawall, A. Maier, M. Lell, J. Maier, and M. Kachelrieß.
Patient-specific radiation risk-based tube current modulation for diagnostic CT. Med. Phys. 49(7):4391-4403, July 2022.
This paper received the Sylvia&Moses Greenfield Award for the best scientific paper on imaging in Medical Physics in 2022.

Patient 04 - Abdomen

AMERICAN ASSOCIATION of PHYSICISTS IN MEDICINE

Congratulations

This paper received the Sylvia&Moses Greenfield Award for the best scientific paper on imaging in Medical Physics in 2022.

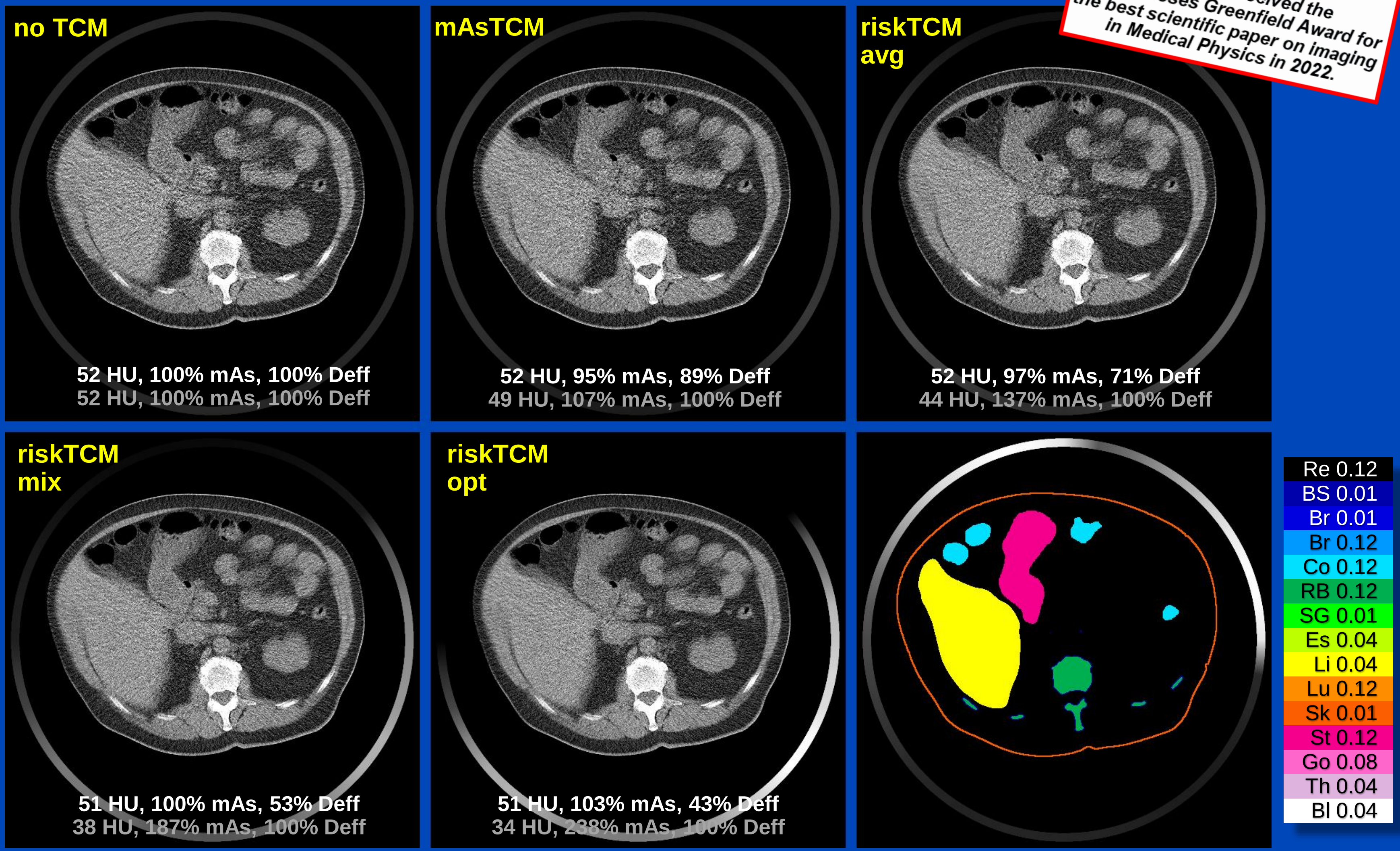

C = 25 HU, *W* = 400 HU

[1]L. Klein, C. Liu, J. Steidel, L. Enzmann, M. Knaup, S. Sawall, A. Maier, M. Lell, J. Maier, and M. Kachelrieß. Patient-specific radiation risk-based tube current modulation for diagnostic CT. Med. Phys. 49(7):4391-4403, July 2022.
This paper received the Sylvia&Moses Greenfield Award for the best scientific paper on imaging in Medical Physics in 2022.

dkfz.

Effective Dose at Same Image Noise Relative to mAsTCM

Average over all patients

Head

Tube Voltage	noTCM	mAsTCM	riskTCM
70 kV	**110%** from 100% to 121%	100%	**91%** from 80% to 96%
100 kV	**110%** from 100% to 122%	100%	**92%** from 83% to 96%
120 kV	**111%** from 101% to 123%	100%	**92%** from 84% to 96%
150 kV	**110%** from 101% to 122%	100%	**92%** from 86% to 96%

Head+Arms

Tube Voltage	noTCM	mAsTCM	riskTCM
70 kV	**163%** from 145% to 178%	100%	**87%** from 84% to 91%
100 kV	**158%** from 139% to 186%	100%	**87%** from 83% to 91%
120 kV	**160%** from 142% to 183%	100%	**88%** from 84% to 94%
150 kV	**161%** from 144% to 183%	100%	**88%** from 82% to 95%

[1]L. Klein, C. Liu, J. Steidel, L. Enzmann, M. Knaup, S. Sawall, A. Maier, M. Lell, J. Maier, and M. Kachelrieß.
Patient-specific radiation risk-based tube current modulation for diagnostic CT. Med. Phys. 49(7):4391-4403, July 2022.
This paper received the Sylvia&Moses Greenfield Award for the best scientific paper on imaging in Medical Physics in 2022.

Effective Dose at Same Image Noise Relative to mAsTCM

Average over all patients

Neck

Tube Voltage	noTCM	mAsTCM	riskTCM
70 kV	**230%** from 175% to 303%	100%	**73%** from 57% to 78%
100 kV	**225%** from 178% to 300%	100%	**76%** from 61% to 80%
120 kV	**221%** from 179% to 299%	100%	**77%** from 62% to 81%
150 kV	**214%** from 175% to 274%	100%	**77%** from 64% to 82%

Thorax

Tube Voltage	noTCM	mAsTCM	riskTCM
70 kV	**113%** from 108% to 118%	100%	**77%** from 67% to 82%
100 kV	**113%** from 107% to 117%	100%	**81%** from 74% to 85%
120 kV	**113%** from 107% to 118%	100%	**82%** from 75% to 86%
150 kV	**113%** from 108% to 118%	100%	**83%** from 76% to 87%

[1]L. Klein, C. Liu, J. Steidel, L. Enzmann, M. Knaup, S. Sawall, A. Maier, M. Lell, J. Maier, and M. Kachelrieß.
Patient-specific radiation risk-based tube current modulation for diagnostic CT. Med. Phys. 49(7):4391-4403, July 2022.
This paper received the Sylvia&Moses Greenfield Award for the best scientific paper on imaging in Medical Physics in 2022.

Effective Dose at Same Image Noise Relative to mAsTCM

Average over all patients

Abdomen

Tube Voltage	noTCM	mAsTCM	riskTCM
70 kV	**113%** from 105% to 135%	100%	**69%** from 57% to 76%
100 kV	**113%** from 103% to 137%	100%	**71%** from 62% to 79%
120 kV	**114%** from 106% to 135%	100%	**72%** from 64% to 79%
150 kV	**115%** from 106% to 136%	100%	**73%** from 66% to 80%

Pelvis

Tube Voltage	noTCM	mAsTCM	riskTCM
70 kV	**153%** from 134% to 189%	100%	**76%** from 65% to 91%
100 kV	**152%** from 134% to 186%	100%	**78%** from 68% to 91%
120 kV	**151%** from 134% to 184%	100%	**80%** from 72% to 92%
150 kV	**151%** from 136% to 184%	100%	**81%** from 72% to 93%

[1]L. Klein, C. Liu, J. Steidel, L. Enzmann, M. Knaup, S. Sawall, A. Maier, M. Lell, J. Maier, and M. Kachelrieß.
Patient-specific radiation risk-based tube current modulation for diagnostic CT. Med. Phys. 49(7):4391-4403, July 2022.
This paper received the Sylvia&Moses Greenfield Award for the best scientific paper on imaging in Medical Physics in 2022.

Conclusions on RiskTCM

- Risk-specific TCM minimizes the patient risk.
- With D_{eff} as a risk model riskTCM can reduce risk by up to 30%, compared with the gold standard mAsTCM.
- Other risk models, in particular age-, weight- and sex-specific models, can be used with riskTCM as well.
- Note:
  -
  - good for the patient
  - detector flux equalizing TCM = good for the detector

It is up to the vendors to take action!

ECR 2022 – Best Research Presentation Abstract
within the topic Physics in Medical Imaging
with the presentation:

Risk-minimising tube current modulation (riskTCM) for CT – potential dose reduction across different tube voltages (16765)

L. Klein1, C. Liu2, J. Steidel1, L. Enzmann1, S. Sawall1, J. Maier1, A. Maier2, M. Lell3, M. Kachelrieß1; 1Heidelberg/DE, 2Erlangen/DE, 3Nuremberg/DE

AMERICAN ASSOCIATION of PHYSICISTS IN MEDICINE

Congratulations

This paper received the Sylvia&Moses Greenfield Award for the best scientific paper on imaging in Medical Physics in 2022.

[1]L. Klein, C. Liu, J. Steidel, L. Enzmann, M. Knaup, S. Sawall, A. Maier, M. Lell, J. Maier, and M. Kachelrieß. Patient-specific radiation risk-based tube current modulation for diagnostic CT. Med. Phys. 49(7):4391-4403, July 2022.
This paper received the Sylvia&Moses Greenfield Award for the best scientific paper on imaging in Medical Physics in 2022.

dkfz.

Deep Cardiac CT MoCo

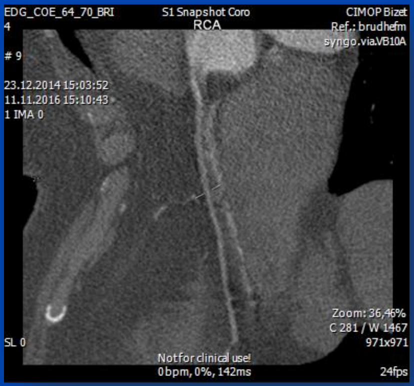

???

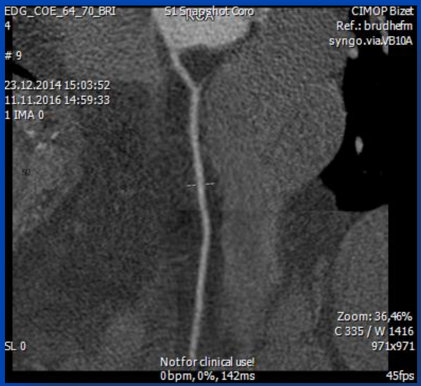

Motivation

C = 0 HU, W = 1200 HU

Motion artifacts

High noise levels

Table 3: Reason for FFR_{CT} Rejection in the ADVANCE Registry and Clinical Cohort *

Reason for Rejection	FFR_{CT} Rejected* ADVANCE Registry (n = 80)	FFR_{CT} Rejected* Clinical Cohort (n = 892)
Inadequate image quality†		
Blooming	4 (5.0)	29 (3.0)
Clipped structure	4 (5.0)	39 (4.3)
Motion artifacts	63 (78.0)	729 (81.4)
Image noise	2 (2.5)	198 (22.1)
Inappropriate submission		
Stent or previous coronary artery bypass graft present	5 (6.2)	116 (13.0)
Cardiac hardware present	2 (2.5)	29 (3.2)

The rejection rate was 892 of 10 416 cases submitted

* G. Pontone et al., "Determinants of Rejection Rate for Coronary CT Angiography Fractional Flow Reserve Analysis", *Radiology*, *292*(3), 597–605 (2019)

Motivation

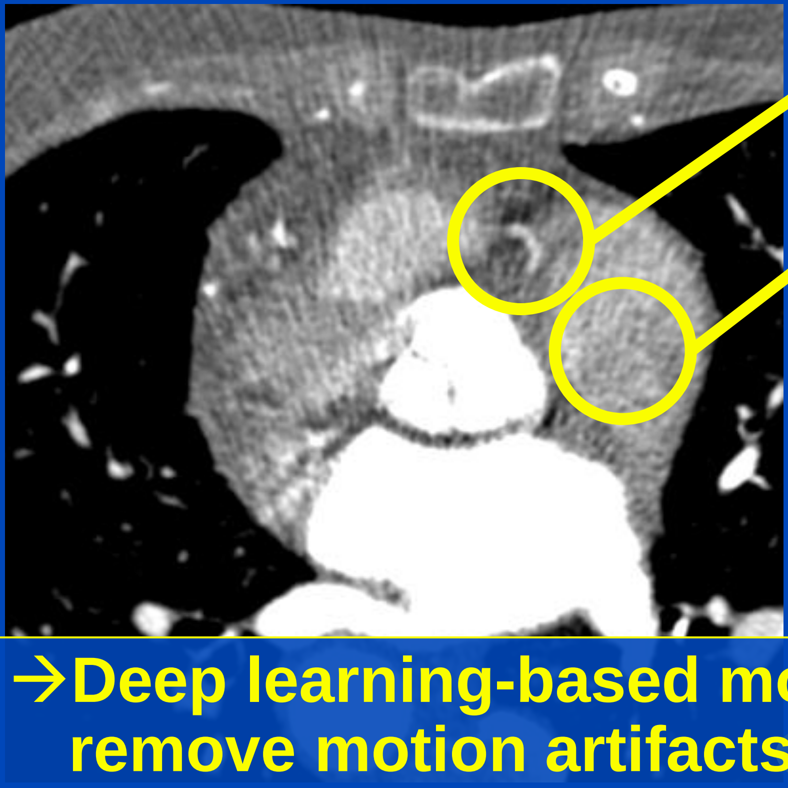

Motion artifacts

High noise levels

Table 3: Reason for FFR_{CT} Rejection in the ADVANCE Registry and Clinical Cohort *

Reason for Rejection	FFR_{CT} Rejected* ADVANCE Registry (n = 80)	Clinical Cohort (n = 892)
Inadequate image quality†		
Blooming	4 (5.0)	29 (3.0)
Clipped structure	4 (5.0)	39 (4.3)
Motion artifact	[illegible]	[illegible]29 (81.4)
Image noise	2 (2.5)	198 (22.1)
Inappropriate submission		
[illegible] previous coronary artery bypass graft present	[illegible]	116 (13.0)
Cardiac hardware present	2 (2.5)	29 (3.2)

The rejection rate was 892 of 10 416 cases submitted

→Deep learning-based motion compensation to remove motion artifacts.

→Iterative reconstruction (Siemens ADMIRE) to reduce noise.

* G. Pontone et al., "Determinants of Rejection Rate for Coronary CT Angiography Fractional Flow Reserve Analysis", *Radiology*, *292*(3), 597–605 (2019)

dkfz.

Partial Angle-Based Motion Compensation (PAMoCo)

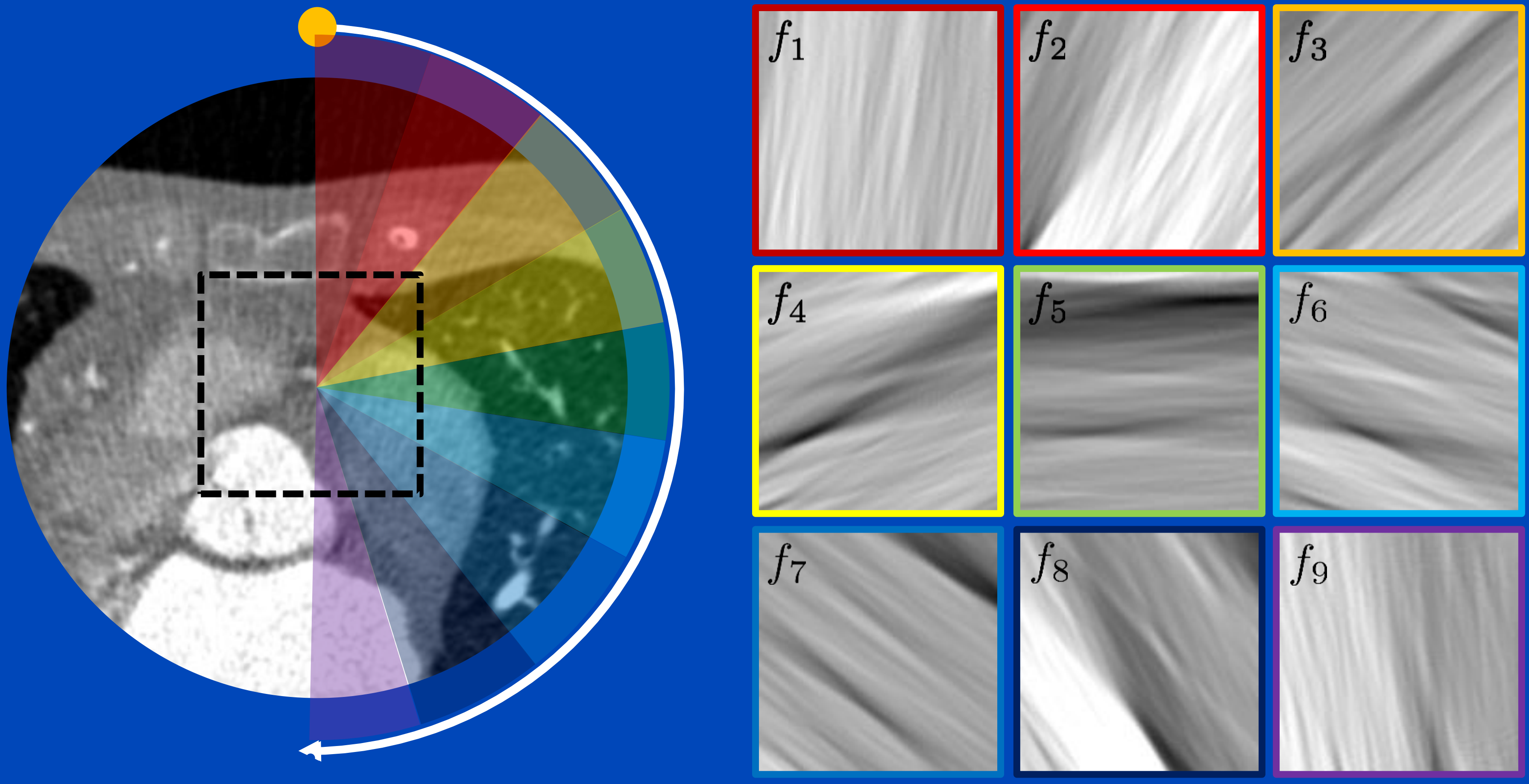

Partial Angle-Based Motion Compensation (PAMoCo)

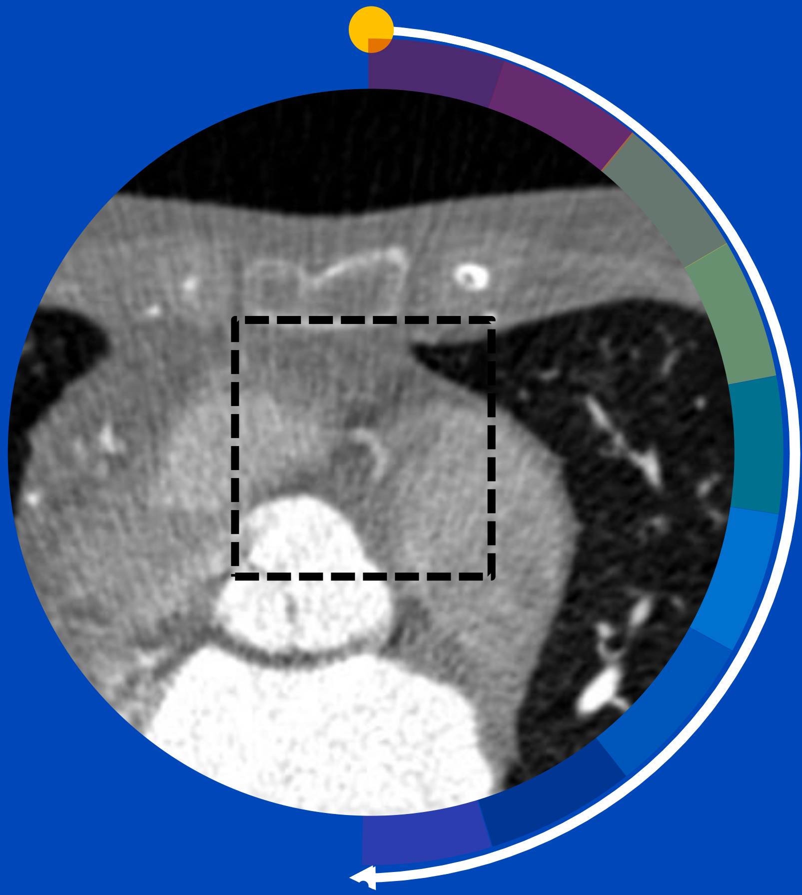

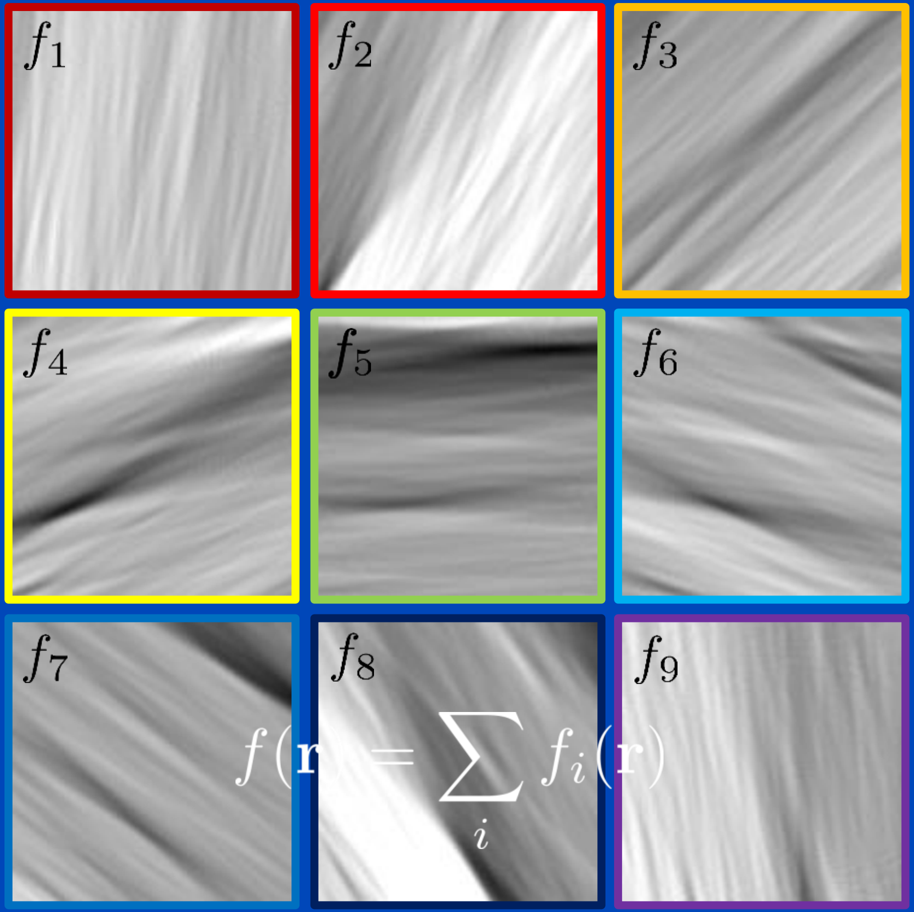

Partial Angle-Based Motion Compensation (PAMoCo)

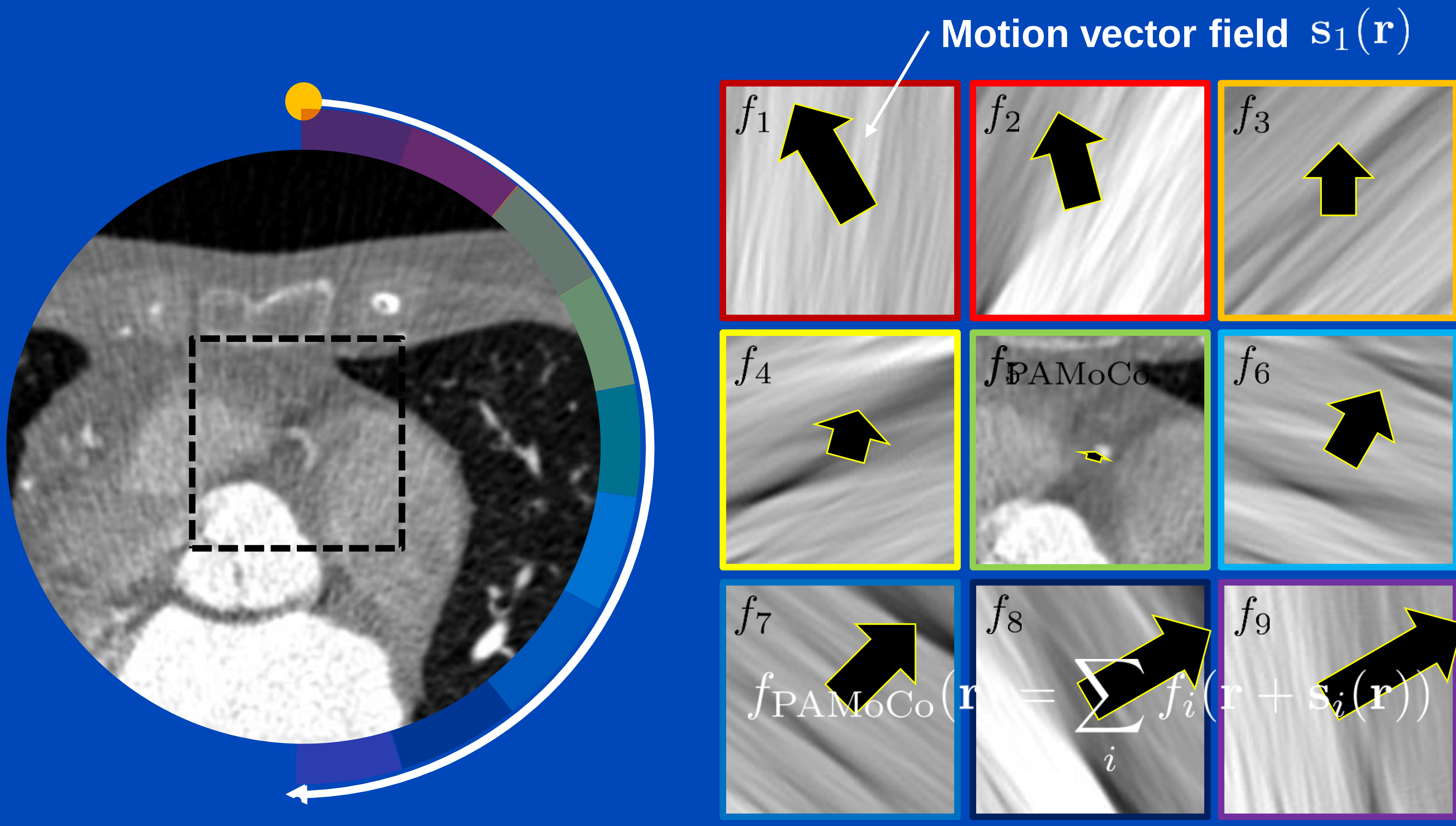

Apply motion vector fields (MVFs) to partial angle reconstructions

Deep Partial Angle-Based Motion Compensation (Deep PAMoCo)

PARs centered around coronary artery

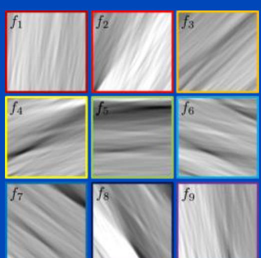

Neural network to predict parameters of a motion model

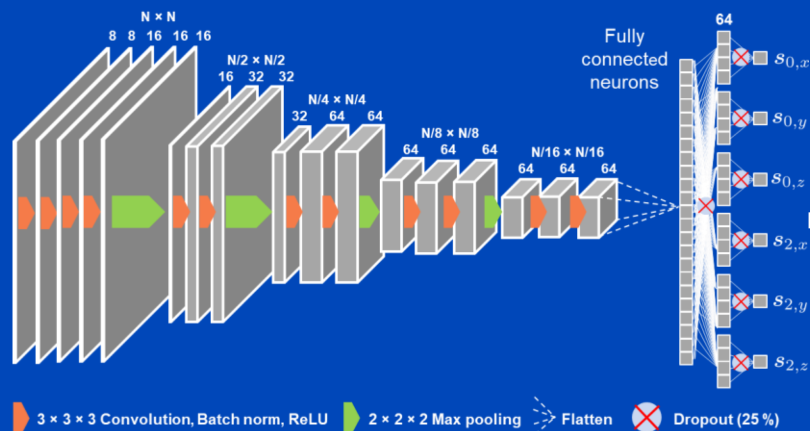

Reinsertion of patch into initial reconstruction

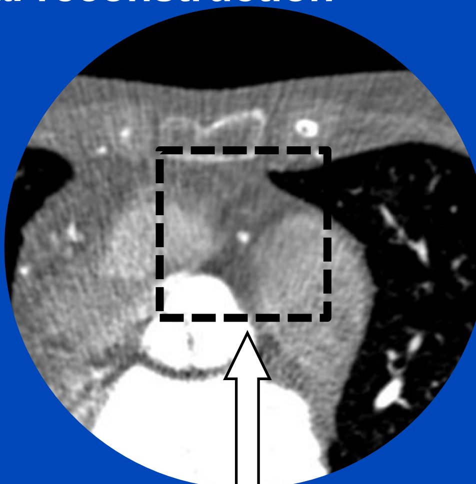

Spatial transformer

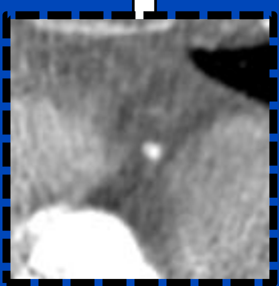

Application of the motion model to the PARs via a spatial transformer

J. Maier, S. Lebedev, J. Erath, E. Eulig, S. Sawall, E. Fournié, K. Stierstorfer, M. Lell, and M. Kachelrieß. Deep learning-based coronary artery motion estimation and compensation for short-scan cardiac CT. Med. Phys. 48(7):3559-3571, July 2021.

Training Data Generation

- Removal of coronary arteries from real CT reconstructions.
- Insertion of artificial coronary arteries with different shape, size, and contrast.
- Simulation of CT scans with coronary artery motion.

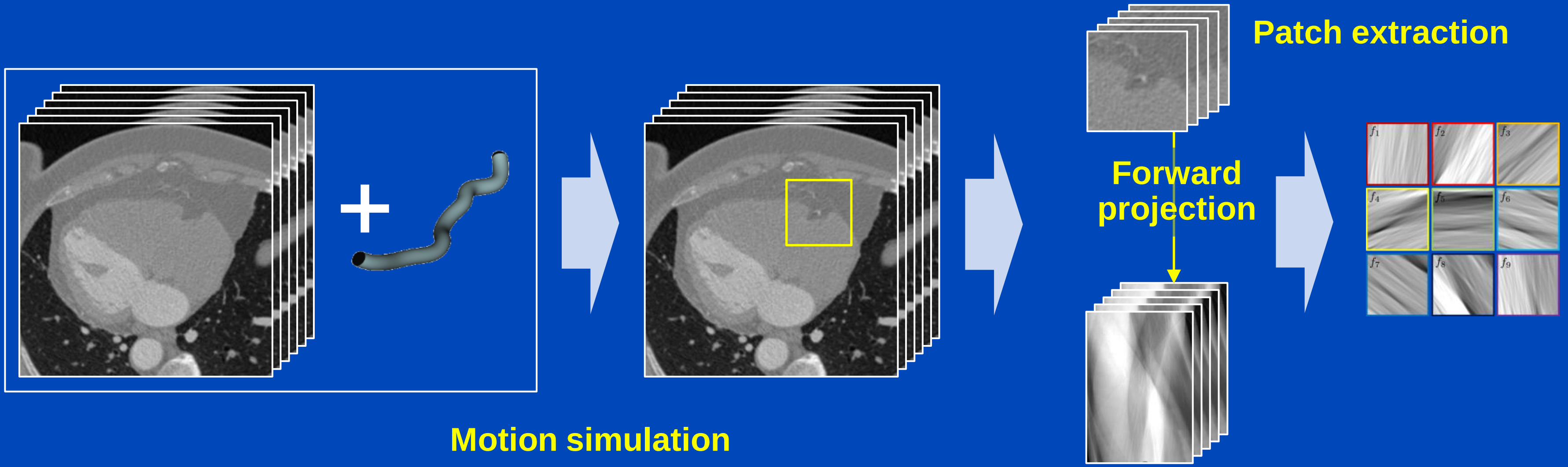

J. Maier, S. Lebedev, J. Erath, E. Eulig, S. Sawall, E. Fournié, K. Stierstorfer, M. Lell, and M. Kachelrieß. Deep learning-based coronary artery motion estimation and compensation for short-scan cardiac CT. Med. Phys. 48(7):3559-3571, July 2021.

Results

Measurements at a Siemens Somatom AS, patient 1

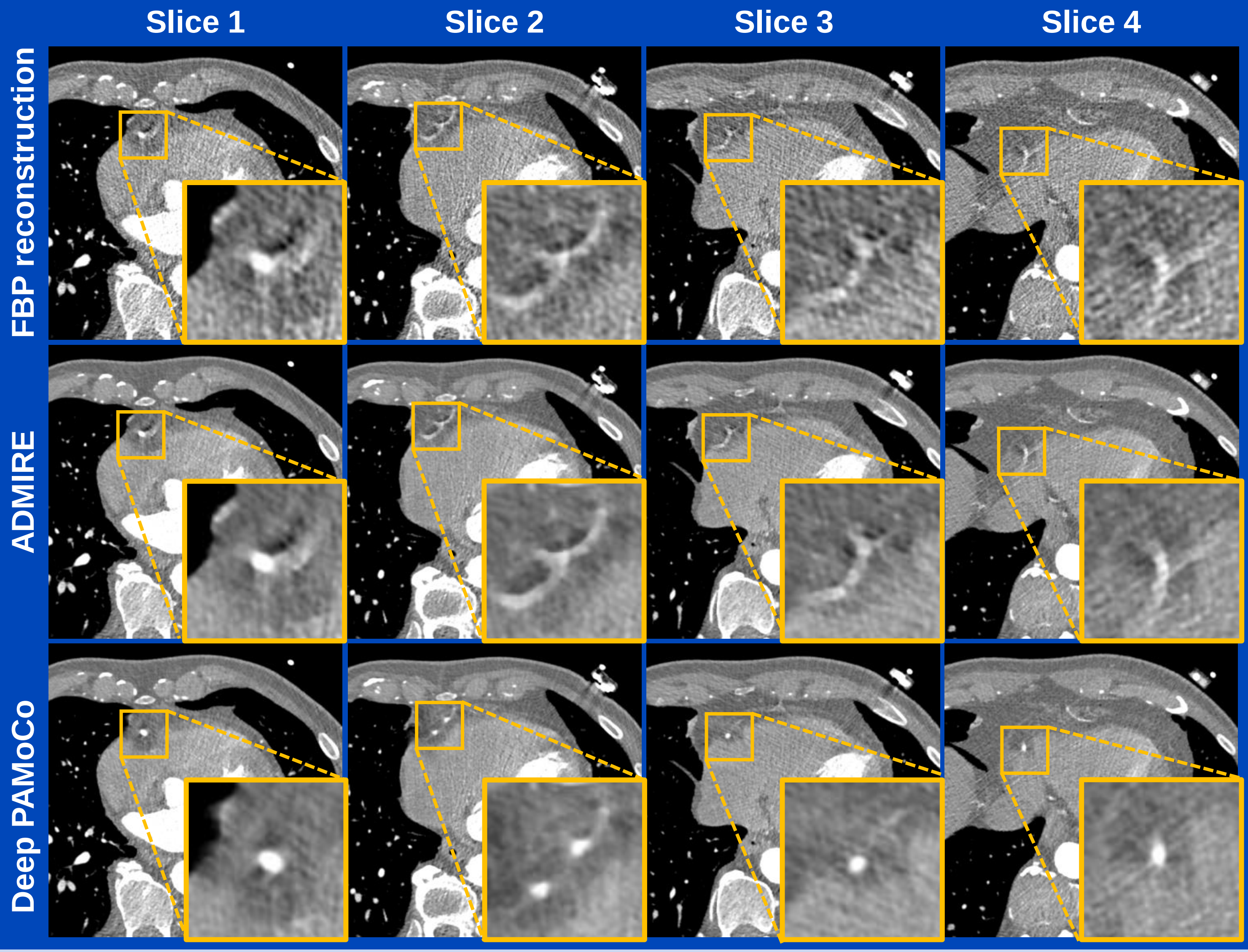

C = 0 HU, W = 1200 HU

Results

Measurements at a Siemens Somatom AS, patient 2

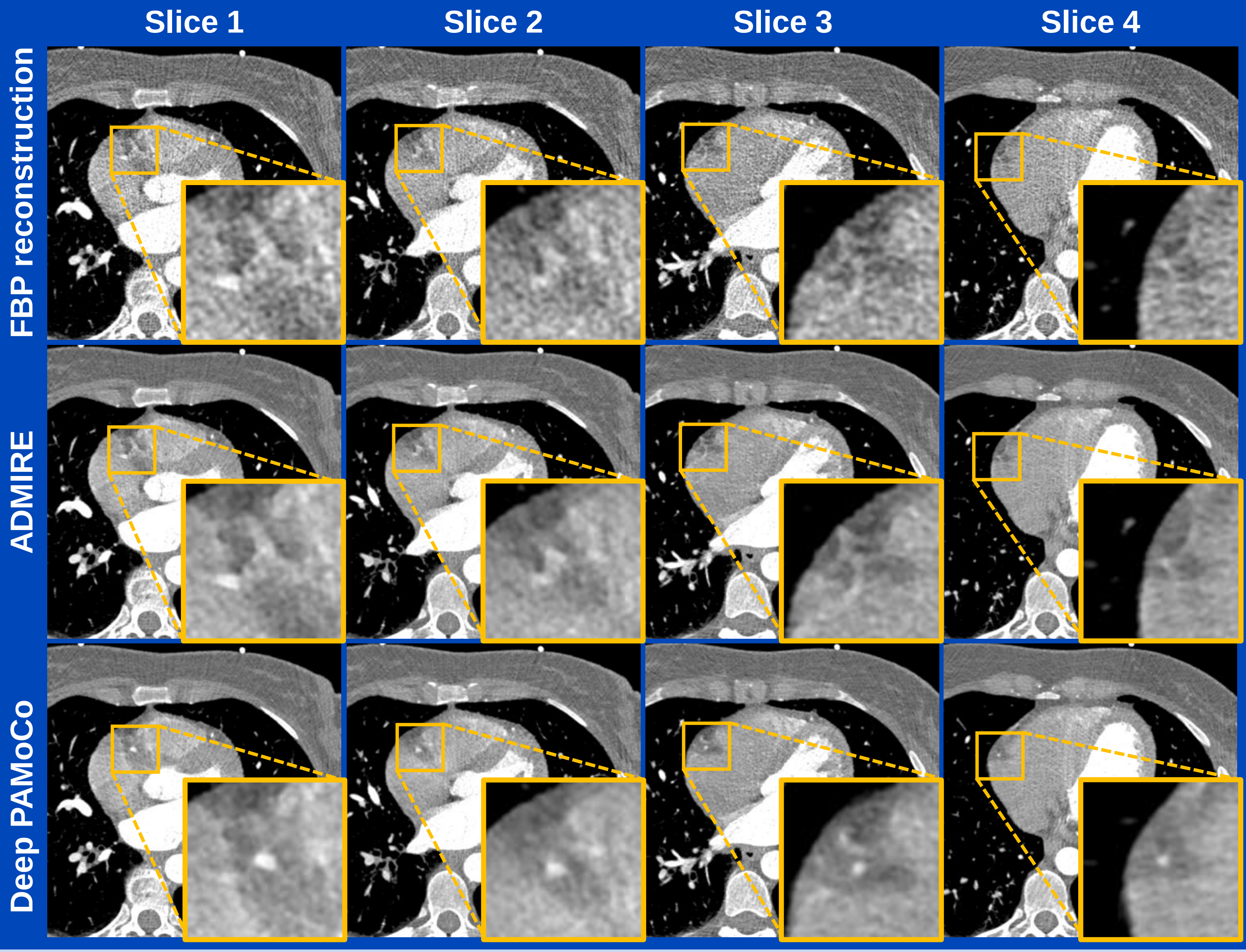

C = 0 HU, W = 1200 HU

Results

Measurements at a Siemens Somatom AS, patient 3

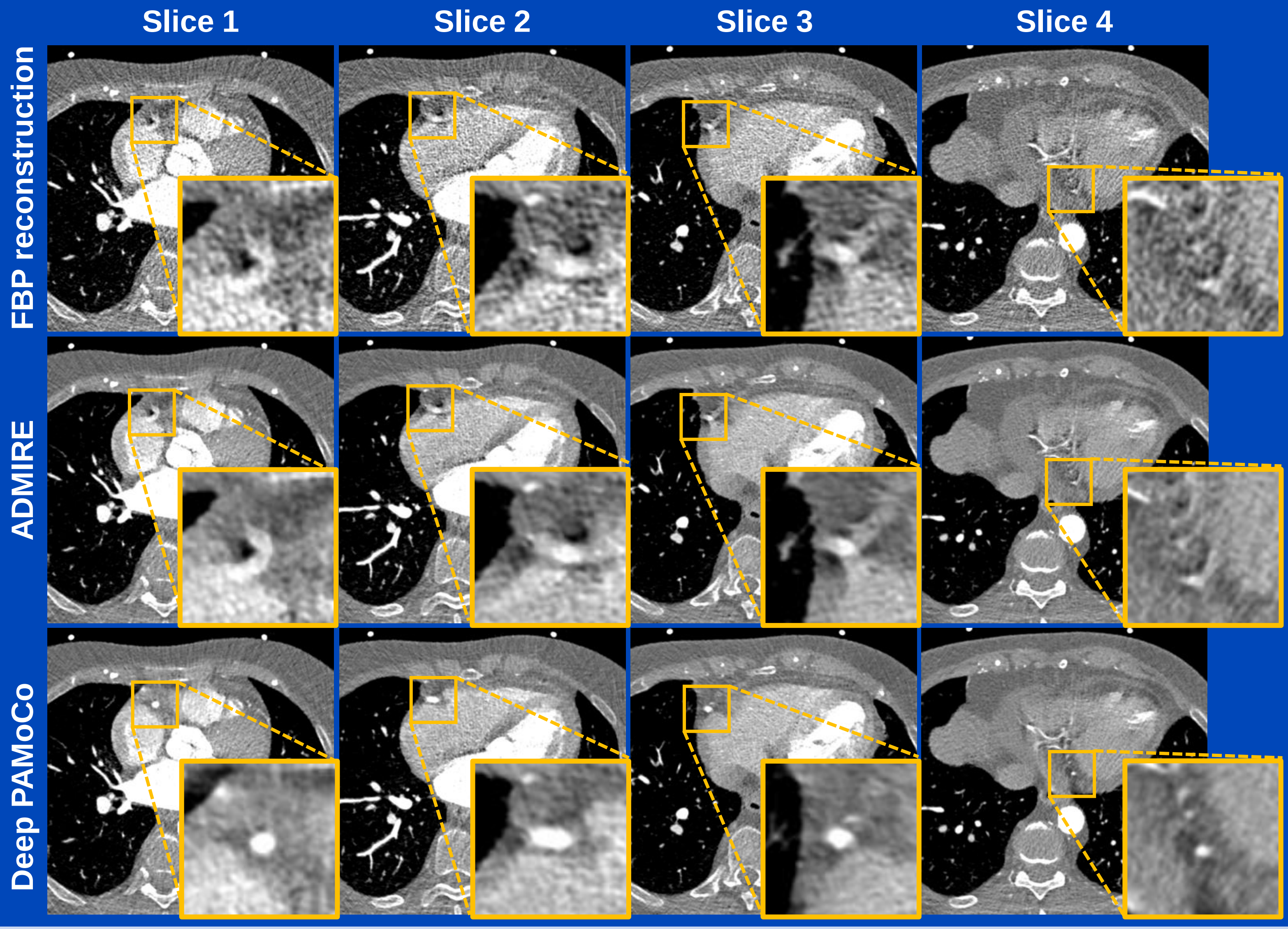

C = 0 HU, W = 1400 HU

dkfz.

Thank You!

This presentation will soon be available at www.dkfz.de/ct.

Job opportunities through DKFZ's international PhD programs or through marc.kachelriess@dkfz.de.

Parts of the reconstruction software were provided by RayConStruct® GmbH, Nürnberg, Germany.